# METAL OXIDES MODIFIED MULTIWALLED CARBON NANOTUBES BASED BIOSENSOR FOR DETERMINATION OF HYPOXANTHINE

**By**

**THOLE DINA**

**DISSERTATION**
**Submitted in fulfilment of the requirements for the degree of**
**MASTER OF SCIENCE**

**In**

**CHEMISTRY**
**in the**

**FACULTY OF SCIENCE AND AGRICULTURE**
**(School of Physical and Mineral Sciences)**
**at the**

**UNIVERSITY OF LIMPOPO**
**SUPERVISOR: PROF T MAGADZU**
**CO-SUPERVISOR: DR SC TSHIDINO (UNIVEN)**

**2021**

## DEDICATION

I dedicate this work to my family and friends. A special feeling of gratitude to my loving mother Leah and uncle, Johannes Thole whose words of encouragement and push for perseverance ring in my ears.

## DECLARATION BY CANDIDATE

I declare that **METAL OXIDES MODIFIED MULTI-WALLED CARBON NANOTUBES BASED BIOSENSOR FOR THE DETRMINATION OF HYPOXANTHINE** is my own work and that all the sources that I have used or quoted have been indicated and acknowledged by means of complete references and that this work has not been submitted before for any other degree at any other institution.

Full Names: Dina Thole

Signature: D. Thole Date: 28-September-2021

## ACKNOWLEDGEMENT

A special thanks to Prof T Magadzu, my supervisor for his countless hours of reflecting, reading, encouraging, and most of all patience throughout the entire process.

Special thanks again go to Dr SC Tshidino for the additional reading, reflecting, correcting, and teaching with her patience throughout the research project.

I would also like to express my sincere gratitude to Prof Motaung and Ms Popoti Maake at CSIR for carrying out TGA, XRD, and SEM for this study.

I would like to acknowledge and thank the University of Limpopo, Department of Chemistry for allowing me to conduct my research and providing any assistance requested.

A very special thank you to my Sasol mentor Dr Matthew Coombes for his advice and support as well as NRF Sasol Inzalo foundation for financial support.

A very special thank you again goes to my family (Johannes, Leah, and Thabiso Thole) and friends for their support and words of encouragement.

## ABSTRACT

Heart and Stroke Foundation South Africa (HSFSA) reports that about 17.3% of deaths in the country are associated with heart-related diseases and this rate is expected to increase to 41% by the year 2030. This severe increase in death cases is related to diseases caused by consumption of meat (i.e., pork, fish, red meat, and poultry) with high levels of hypoxanthine. Therefore, this raises the need to investigate and detect hypoxanthine levels in the meat. This study aimed at developing a highly stable and sensitive biosensor for the detection of hypoxanthine in fish meat using the glassy carbon electrode (GCE) modified with carbon nanocomposites materials (consisting of metal oxides doped multi-walled carbon nanotubes (MO-MWCNTs) that are treated with amine groups) and an enzyme, xanthine oxidase (XOD) as a catalyst.

The sol gel method was used to prepare the metal oxides including zinc oxide (ZnO), zirconium dioxide ($ZrO_2$), manganese ($MnO_2$), cobalt oxide ($Co_3O_4$), and titanium dioxide ($TiO_2$). The *in-situ* method of functionalisation of MWCNTs was employed to increase their current outputs/sensitivity using selected amines, namely, methylenediamine, hydrazine, ethylenediamine (EDA), and triethylenetetramine (TETA). The electrochemical properties of the metal oxides and amine functionalised MWCNTs were studied using both cyclic and differential pulse voltammetry. Fourier-transform infrared spectroscopy (FTIR) confirmed the presence of carboxyl (COOH), hydroxyl (OH), and amino ($NH_2$) groups on the surface of the modified MWCNTs; as well as formation of stretching vibrations which appear at lower wavelengths due to the metallic species within the nanocomposite. Thermal gravimetric analyser (TGA) was employed to determine the thermal stability of the nanocomposite. Scanning electron microscopy (SEM) was used to confirm the composite structure and correct deposition of the metal oxides on the walls of MWCNTs. XRD was used to confirm correct structure formation, the crystallinity, and the purity of the nanocomposite. Optimum conditions of the developed biosensor were determined, and the application of the developed biosensor was undertaken on fish meat bought at the local supermarket using the Cyclic and Differential pulse voltammetric techniques.

Two highly electrochemical metal oxides among others were $TiO_2$ and $Co_3O_4$. The modified MWCNTs containing TETA possess good electrochemical properties with improved sensitivity and selectivity towards hypoxanthine. The presence of metal oxides on MWCNTs and their treatments with amines as confirmed by techniques such as TGA, SEM, XRD, and FTIR have provided a suitable matrix for the immobilisation of the enzyme, namely, xanthine oxidase at 0.5 unit (U). TGA results showed that the unmodified MWCNTs decompose at around 600 $^0$C, but when they are modified with acids and amine decomposition starts at 230 $^0$C, proving that functionalisation of MWCNTs tempers with their thermal stability. Based on the SEM morphological results, attachment of the amines and metal oxides on MWCNTs was seen at x60 000 magnification. Morphology of acid treated MWCNTs appeared thinner, revealing that acids tends to deteriorate the MWCNTs, while the amino treated MWCNTs appeared well modified with less damage on the MWCNTs. XRD confirmed the successful purification of MWCNTs with the intense diffraction peak at $26^0$ that can be assigned to the (002) reflection of graphite. The strong diffraction peak at $25^0$ and a broad peak at $45^0$ indicate that the titania nanoparticles are pure and in the anatase phase. They also show successful deposition of the titanium dioxide onto the surface of the MWCNTs. However, on the formation of cobalt oxide two phases were observed which were CoO, and $Co_3O_4$, and on bimetallic nanocomposite (cobalt titanium oxide) also two phases were observed which were $CoTiO_3$, and $Co_2TiO_4$. It was found that the sensor performs better at 25 $^o$C at a pH of 7.5 in a phosphate buffer at concentration of 5 mM. The limit of detection of the biosensor was found to be 0.16 nM. The highly electroconductive electrode was XOD/3%$Co_2TiO_4$-MWCNTs-TETA/GCE, which was selected for analysis of fish meat. The biosensor has shown low interfering values with high stability, good reusability retaining 73.4% of its initial performance after 50 days of continuous study. The excellent results were obtained on fish meat analysis using cyclic and differential pulse voltammetry revealed that even meat which is deep frozen can also deteriorate as time passes by. Altogether, the findings from this study suggest that the developed biosensor is a reliable analytical tool for the determination of freshness of fish meat using hypoxanthine levels as a marker.

TABLE OF CONTENTS

## LIST OF FIGURES

## LIST OF ABBREVIATIONS

| | |
|---|---|
| CNTs | Carbon nanotubes |
| SWCNT | Single-Walled Carbon Nanotubes |
| MWCNT | Multi-Walled Carbon Nanotubes |
| ZnO | Zinc oxide |
| ZrO | Zirconium oxide |
| MnO | Manganese oxide |
| $TiO_2$ | Titanium oxide |
| MO | Metal oxide |
| $Co_3O_4$ | Cobalt oxide |
| HPLC | High-Performance Liquid Chromatography |
| BASI | Bioanalytical system |
| pH | Potential of hydrogen |
| pt | Platinum |
| GCE | Gassy carbon electrode |
| Ag/AgCl | Siver-silver chloride |
| COOH | Carboxylic acid |
| Hx | Hypoxanthine |
| G | Glucose |
| UA | Uric acid |
| X | Xanthine |
| AA | Ascorbic acid |
| $Mn(NO_3)_2 \cdot 6H_2O$ | Manganese nitrate hexahydrate |
| $Co(NO_3)_2.6H_2O$ | Cobalt (II) nitrate hexahydrate |
| TTIP | Titanium isopropoxide |

| | |
|---|---|
| $H_2SO_4$ | Sulfuric acid |
| $HNO_3$ | Nitric acid |
| PBS | Phosphate buffer |
| DMF | *N, N*-Dimethylformamide- |
| $N_2H_4$ | Hydrazine |
| XOD | Xanthine oxidase |
| EDA | Ethylenediamine |
| TETA | Triethylenetetramine |
| TEM | Transmission Electron Microscopy |
| SEM | Scanning Electron Microscopy |
| XRD | X-Ray Diffraction |

# CHAPTER ONE

# 1. INTRODUCTION

## 1.1 Background

The developments of various biosensors for the detection of hypoxanthine (Hx) have increased over the past decades due to a rise in the number of diseases that are associated with the quality of food around the society. This includes diseases like heart failure, stroke, hypertension, and gout [1]. Health hazards brought by unhealthy eating of food with a high level of Hypoxanthine are a risk to the global community.

Hypoxanthine ($C_5N_4OH_4$) is one of the organic molecules which belongs to a family of heterocycles and their structures consist of pyrimidine rings fused to azolic moieties [2,3]. It is catalysed to xanthine during purine catabolism reaction as a product of the enzymatic reaction of xanthine oxidase (XOD) as shown in figure 1.1 [4]. The Increase in concentrations of hypoxanthine generally shows a problem, i.e., higher concentrations of hypoxanthine found in meat during analysis simply imply that the meat is not healthy for human consumption. It also brings about the bitter taste in most of the meat we consume [5].

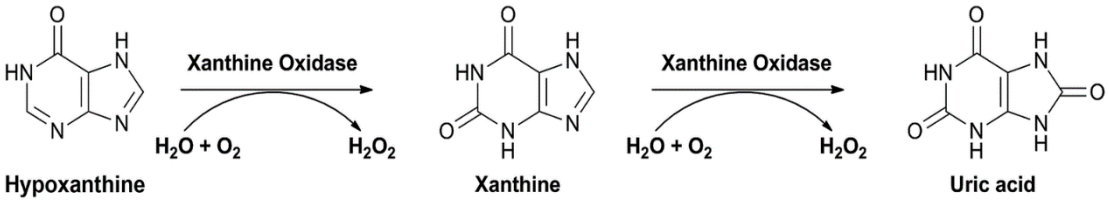


Figure 1.1: Hypoxanthine reaction catalysed by xanthine oxidase

The increase in the population at first was the major concern to food safety and security but recently the COVID-19 pandemic has elevated the threat of food supply and security [6]. Because of that, the urge for long-term storage and maintenance of food is the major concern for human well-being [7]. This pandemic has brought the necessity to evolve new and cheaper techniques, which could display and retain

food freshness and protection during the duration of its shelf-life to decrease food insecurity [8].

The use of the sensors for the determination of food quality and safety is recognised by most scientists due to their ease to use, fast response time, and high specificity and sensitivity [9]. The field of research on sensors is foreseeing the use of smart sensors in the future, for example, the smart sensors and tags that may be connected with packaging will represent the generation of smart packaging and fast detection of food spoilage [10].

These can provide qualitative information about the current condition, estimated spoilage date of the product on the shelf, as well as the nutritional information of the product [11]. These can be indicators of freshness and quality of the food products by measuring changes in temperature, moisture, and smell. Additional skills can be added to offer shielding functions, for example, packaging with a coat that can act as an oxygen blockade to prevent spoilage, in view that oxygen is one of the compounds, which increase the degree of spoilage [12].

These techniques can replace high-priced strategies that are currently being used to display food products. This may also increase the economy of the country, since the shelf time for products would increase instead of the need to want more of the same products, because of the high deterioration rate which is caused by their storage and incorrect packaging [13]. Improvement in advanced nanotechnology and the conservatory of innovative various sensors with various chemical composites for modifications has been a regulating key venture inside the fabrication and improvement of very steady efficient sensors [8].

Nanotechnology is a new discipline of scientific research focusing on the synthesis of nanoparticles (NPs) and nanocomposite carbon nanomaterials for their application in diverse fields such as electrochemistry, catalysis, and sensors [13]. The main reason for using nanotechnology in a variety of fields is its distinctive ability to magnify the efficiency of the system and giving the highest possible results [14]. In nanotechnology, the most important thing is the size of the nanoparticles, which tends to give the characteristics and the reactivity/properties of the material [15].

These nanoparticles are the group of atoms bonded together with the smallest sizes possible. The attractive part of nanoparticles is their large surface area which makes them more efficient to react with solvent molecules [16]. Accompanying this, the most significant properties of nanomaterials such as carbon-based materials and metal oxides are their good electrical conductivity and thermal properties [17]. These carbon nanomaterials enhance the sensitivity of the sensors that suffer from poor sensitivity and low detection limits [9].

### 1.2 Problem statement

Hypoxanthine (Hx) is one of the products of adenosine triphosphate (ATP) due to the low concentration of oxygen in the body cell [18]. Hence, its increase in concentration levels in food industries indicates food spoilage. Determination of Hx in food products is important to ensure quality control [19]. Several methods such as Gas Chromatography (GC) and High-Performance Liquid Chromatography (HPLC) have been proposed for the determination of trace amounts of Hx in food products. Although HPLC is highly recommended due to less time-consuming separation as compared to GC, it can be expensive, requiring large quantities of costly organics, a different array of modules, and column preparation [20]. GC requires sample incubation and preparation periods of about 6 months which is time-consuming [21].

Over the past two decades, different types of diagnostic tools that are rapid and sensitive towards a specific target have been developed [22-24]. Among those, electrochemical biosensors have attracted significant attention in recent years, due to their ease of fabrication and rapid detection. For example, previous studies have proven that carbon nanotubes modified materials improve Hx detection [25]. However, the study could not resolve the issue of interferences by ascorbic acid. Hence, the proposed study envisages that the sensitivity and selectivity of electrochemical biosensors can be improved by the combination of highly dispersed metal oxides on the surface of carbon nanomaterials such as carbon nanotubes.

## 1.3 Motivation

Carbon nanotubes (CNTs) represent an essential institution of nanomaterials that have attracted massive recognition in biosensor fabrication [26]. This is because they possess a large surface area, excellent mechanical strength, excessive electrical conductivity, and fine biocompatibility [27]. Carbon nanotubes primarily based biosensors have been found to be superior to traditional carbon electrode-based biosensors in terms of detection limit, sensitivity, and selectivity [28].

The utilisation of metal oxide nanoparticles in the construction of biosensors is also of great and profitable interest. This is because they exhibit excellent physical, chemical, and catalytic properties [29]. Metal oxides nanoparticles not only do they have a high surface area, chemical stability, low-toxicity, strong adsorption ability, and chemical stability, but they also have excellent electron transfer kinetics [30]. These properties make them good materials to be immobilised on the electrode surface for fast response time.

Multiwalled carbon nanotubes (MWCNTs) and metal oxide nanoparticles (MONPs) have been proven to be compatible materials for combination in preparing excessive overall best sensors which are highly sensitive and selective [31]. MWCNTs/MONPs nanocomposites are a new generation in nanotechnology with excellent properties that not only combine the properties MWCNTs and MONOPs but also hold new properties caused by the interaction between them. Previous research has proven that MWCNTs and MONPs nanocomposite resulted in a large electrochemical response, high surface area, and fast electron transfer for biosensor applications [32]. The proposed metal oxides for this study are zinc oxide (ZnO), manganese dioxide ($MnO_2$), zirconium dioxide ($ZrO_2$), cobalt oxide ($Co_3O_4$), and titanium oxide ($TiO_2$).

## 1.4. Aim and objectives

### 1.4.1. Aim

The aim of this study is to investigate the electrochemical behaviour and the detection mechanism of hypoxanthine using metal oxides modified multi-walled carbon nanotubes deposited on Glass Carbon Electrode (MO-MWCNTs/GCE).

### 1.4.2. Objectives

The objectives of the study are to:

i. prepare functionalised MWCNTs and metal oxides ($TiO_2$, ZnO, $ZrO_2$, $Co_3O_4$, and $MnO_2$) doped MWCNTs (MO-MWCNTs),
ii. characterise the prepared materials using techniques such as Scanning electron microscope (SEM), Transmission electron microscope (TEM), X-ray diffraction (XRD) and Fourier transform infrared spectroscopy (FTIR), and Thermalgravimetric analyzer (TGA).,
iii. immobilise xanthine oxidase on the surface of MO-MWCNTs composites and drop-dry the composite on the GCE surface,
iv. investigate the effects of metal oxides, pH of the environment, and temperature on the electrochemical response towards the detection of hypoxanthine and
v. uses the developed modified electrode for meat sample analysis.

## 1.5. Dissertation outline

The overall structure of the dissertation consists of the following 5 chapters

i. **Chapter 1**: Presents a general background of the study, problem statement, motivation, research aim, and objectives.

ii. **Chapter 2**: Describes the literature review of the electrochemical sensors, carbon nanotubes, and their role in electroconductivity on improving the sensitivity of biosensors. Hypoxanthine as the biomarker for food spoilage and other methods besides biosensing which are used for the detection of

hypoxanthine. Types of metal oxides and their role in electrochemistry in terms of increasing sensitivity of the electrodes. Finally, this chapter describes the types of electrochemical experiments in conjunction with nanomaterials for the detection of the analyte.

iii. **Chapter 3**: Focuses on the list of materials and chemicals used, the methodology followed including the oxidation of the MWCNTs and incorporation of metal oxides on MWCNTs to form composites, varying percentage of metal oxides (keeping the MWCNTs mass constant to study the effects of increasing metal oxides nanoparticles). The fabrication of the composite on the GCE surface for the detection of hypoxanthine. These was followed by the techniques used to study the characteristics of the nanocomposites, which includes Fourier-transform infrared spectroscopy (FTIR), Thermal gravimetric analysis (TGA), and Scanning electron microscopy (SEM). Finally, the descriptive method for determination of hypoxanthine in meat sample analysis.

iv. **Chapter 4**: The study firstly described in full details the characterisation of the metal oxides composites to confirm the correct structure formation using the techniques mentioned under methodology. The study also focused on the optimisation of the sensor concerning optimum temperature, time, pH, stability, concentration, and a scan rate of the electrode. These were followed by various investigations of effects of metal oxides and metal oxides doped multi-walled carbon nanotubes for detection of hypoxanthine using cyclic voltammetry and subsequently, the study reports the findings of the hypoxanthine detection in fish meat during real sample analysis. The study hoped at creating a sensitive biosensor for the detection of hypoxanthine even at the lowest of hypoxanthine concentrations using multiwalled carbon nanotubes doped metal oxides.

v. **Chapter 5:** This part of the dissertation consists of the conclusions of all the studies based on the results obtained, and the recommendations for future work related to the study of metal oxides modified multi-walled carbon nanotubes-based biosensor for detection of hypoxanthine.

## 1.6. ETHICAL CONSIDERATION

Ethical issues were not considered in the scope of this research, since in the real samples analysis study, investigations were accomplished using the processed meat purchased from the local supermarket

## 1.7. SCIENTIFIC CONTRIBUTION

The study will have an impact on the development of biosensors that could lead to early detection of the levels of hypoxanthine formed in relation to the freshness of meat. This could have a positive impact on the health of people since the degree of spoilage of food could be detected at an early stage, secondly, it could also benefit the economy of the country by producing cheap, easy to use and reusable biosensors for meat analysis against spoilage.

## 1.8. REFERENCES

[1] Chen, C. J., Lü, J. M., & Yao, Q. (2016). Hyperuricemia-related diseases and xanthine oxidoreductase (XOR) inhibitors: An overview. *Medical Science Monitor*, *22*, 2501–2512. https://doi.org/10.12659/MSM.899852

[2] Neethirajan, S., & Jayas, D. S. (2011). Nanotechnology for the food and bioprocessing industries. *Food and bioprocess technology*, *4*(1), 39-47.

[3]. Görgülü, M., Çete, S., Arslan, H., & Yaşar, A. (2013). Preparing a new biosensor for hypoxanthine determination by immobilization of xanthine oxidase and uricase in polypyrrole-polyvinyl sulphonate film. *Artificial cells, nanomedicine, and biotechnology*, *41*(5), 327-331.

[4]. Rodrigues, M. V. N., Correa, R. D. S., Vanzolini, K. L., Santos, D. S., Batista, A.A., & Cass, Q. B. (2015). Characterization and screening of tight binding inhibitors of xanthine oxidase: an on-flow assay. *Rsc Advances*, *5*(47), 37533-37538

[5]. Kumar, A.S. and Shanmugam, R., (2011). Simple method for simultaneous detection of uric acid, xanthine and hypoxanthine in fish samples using a glassy carbon electrode modified with as commercially received multiwalled carbon nanotubes. *Analytical Methods*, *3*(9), pp.2088-2094

[6] Mathew, M. R., Sam, S., Keerthi, K., & Kumar, K. G. (2020). Recent advances and challenges in electrochemical biosensors for emerging and re-emerging infectious diseases.*Journalof Electroanalytical Chemistry*, *878*, 114596.https://doi.org/10.1016/j. jelechem.2020.114596

[7]. Huss, M., Brander, M., Kassie, M., Ehlert, U., & Bernauer, T. (2021). Improved storage mitigates vulnerability to food-supply shocks in smallholder agriculture during theCOVID19pandemic.*GlobalFoodSecurity*,100468.https://doi.org/10.1016/j.gfs.2020.100468

[8]. Telukdarie, A., Munsamy, M., & Mohlala, P. (2020). Analysis of the impact of covid-19 on the food and beverages manufacturing sector. *Sustainability (Switzerland)*, *12*(22), 1–22. https://doi.org/10.3390/su12229331

[9]. Bunney, J., Williamson, S., Atkin, D., Jeanneret, M., Cozzolino, D., Chapman, J., Power, A., & Chandra, S. (2017). The use of electrochemical biosensors in food analysis. *Current Research in Nutrition and Food Science*, *5*(3), 183–195. https://doi.org/10.12944/CRNFSJ.5.3.02

[10]. Kuswandi, B., Wicaksono, Y., Jayus, Abdullah, A., Heng, L. Y., & Ahmad, M. (2011). Smart packaging: Sensors for monitoring of food quality and safety. *Sensing and Instrumentation for Food Quality and Safety*, *5*(3–4), 137–146. https://doi.org/10.1007/s11694-011-9120-x.

[11]. Khan, I., Saeed, K. and Khan, I., (2019. Nanoparticles: Properties, applications and toxicities. *Arabian journal of chemistry*, *12*(7), pp.908-931.

[12] Dolmacı, N., Çete, S., Arslan, F. and Yaşar, A., (2012). An amperometric biosensor for fish freshness detection from xanthine oxidase immobilized in polypyrrole-polyvinylsulphonate film. *Artificial Cells, Blood Substitutes, and Biotechnology*, *40*(4), pp.275-279.

[13] Bănică, Florinel-Gabriel (2012). Chemical Sensors and Biosensors: Fundamentals and Applications. Chichester, UK: John Wiley & Sons. p. 576. ISBN 9781118354230

[14] Turner, Anthony; Wilson, George; Kaube, Isao (1987). *Biosensors: Fundamentals and Applications. Oxford, UK: Oxford University Press*. p. 770. ISBN 978-0198547242

[15] Thiruvengadam, M., Rajakumar, G. and Chung, I.M., 2018. Nanotechnology: current uses and future applications in the food industry. *3 Biotech*, *8*(1), pp.1-13.

[16] Gupta, V. and Saleh, T.A., (2011). Syntheses of carbon nanotube-metal oxides composites; adsorption and photo-degradation. *Carbon Nanotubes-From Research to Applications*, *17*, pp.295-312.

[17] Manzetti, S. and Gabriel, J.C.P.,(2019). Methods for dispersing carbon nanotubes for nanotechnology applications: liquid nanocrystals, suspensions, polyelectrolytes, colloids and organization control. *International Nano Letters*, *9*(1), pp.31-49

[18] RoyChoudhury, S., Umasankar, Y., Bhushan, P., Hirt, P.A., MacQuhae, F.E., Borda, L.J., Lev-Tov, H.A., Kirsner, R. and Bhansali, S., (2019). Nanocomposite bienzymatic sensor for monitoring xanthine in wound diagnostics. *Journal of The Electrochemical Society*, *166*(9), p.B3295.

[19] Kumar, A., & Dixit, C. K. (2017). Methods for characterization of nanoparticles. In *Advances in nanomedicine for the delivery of therapeutic nucleic acids* (pp. 43-58).

[20] Kalimuthu, P., and Bernhardt, P. V., (2012) ‘Low-Potential Amperometric Enzyme Biosensor for Xanthine and Hypoxanthine’, pp. 10359–10365. doi: 10.1021/ac3025027.

[21] Pundir C.S., Rooma D, Jagriti N, Sandeep S, Jyoti N, Shweta C (2012) J Food Biochem 36:21–27 removal by combining the magnetic properties of iron oxide with adsorption properties of carbon nanotubes, *Water Research,* volume 45, (2011), pp 2207-2212.

[22] Torres, A., C., Ghica, M. E. and Brett, C. M. A. (2013) ‘Design of a new hypoxanthine biosensor : xanthine oxidase modified carbon film and multi-walled carbon nanotube / carbon film electrodes’, pp. 3813–3822. doi: 10.1007/s00216-012-6631-1.

[23] Wijemanne, N., Soysa, P., Wijesundara, S., & Perera, H. (2018). Development and validation of a simple high performance liquid chromatography/UV method for simultaneous determination of urinary uric acid, hypoxanthine, and creatinine in human urine. *International journal of analytical chemistry*, *2018*.

[24] Sharma, A.K., Pandey, S., Nerthigan, Y., Swaminathan,N., Wu, H.F. (2018) Nanostructure and performance of carbon nanotubes in the electrochemical hydrogen storage, *Digest Journal of Nanomaterial and Biostructure,* volume 9, pp 1331-1338.

[25] Wang,Q., Liu F., Yang, X., wang, K., Wang, H., Deng, X., Biosensor. Bioelectron. 64, 161-164 (2015) nanostructure and performance of carbon nanotubes in the electrochemical for the detection of hypoxanthine, *Digest Journal of Nanomaterial and Biostructure,* volume 9, pp 1331-1338.

[26] Albelda, J.A.V., Zuo, C.T., Seki, Y., Yamaji, K.A., and Shinoda A. (2017) “Simultaneous determination of creatinine, hypoxanthine and uric acid in biological samples by column-switching liquid chromatography with ultraviolet detection,” Journal of Pharmaceutical and Biomedical Analysis, vol.15, no.9-10, pp.1621–1626

[27] Zieglar, M., Alt, K., Paterson,B.M., Kanellaskis, P., Bobik, A., Donnelly, P.S., Hagemeyer, C.E., Peter, K., (2014) nanostructure and performance of carbon nanotubes in the electrochemical for detection of xanthine and uric acid, *Digest Journal of Nanomaterial and Biostructure,* volume 7 , pp 1441-1448.

[28] Pandey, P., & Dahiya, M. (2016). Carbon nanotubes: Types, methods of preparation and applications. *Carbon*, *1*(4), 15-21.

[29] Dalk, B., Erden, E. & Esma, K. (2017)Talanta Amperometric biosensors based on carboxylated multiwalled carbon composite for the determination of xanthine. **167**, 286–295.

[30] Ribeiro, B., Botelho, E. C., Costa, M. L., & Bandeira, C. F. (2017). Carbon nanotube buckypaper reinforced polymer composites: a review. *Polímeros*, *27*(3), 247-255.

[31] Moon, S. A., Salunke, B. K., Alkotaini, B., Sathiyamoorthi, E., & Kim, B. S. (2015). Biological synthesis of manganese dioxide nanoparticles by Kalopanax pictus plant extract. *IET nanobiotechnology*, *9*(4), 220-22

[32] Stankic, S., Suman, S., Haque, F., & Vidic, J. (2016). Pure and multi metal oxide nanoparticles: synthesis, antibacterial and cytotoxic properties. *Journal of nanobiotechnology*, *14*(1), 1-20.

[33] Kerdcharoen, T., & Wongchoosuk, C. (2013). Carbon nanotube and metal oxide hybrid materials for gas sensing. In *Semiconductor Gas Sensors* (pp. 386-407)

# CHAPTER 2

# 2. LITERATURE REVIEW

## 2.1 Biosensors for detection of food spoilage

Precise detecting of chemical or biological procedures for monitoring food quality remains important for medical and biological applications [1]. Electrochemical sensors can ideally satisfy that objective by converting a chemical or a biological response into a processable and quantifiable signal that can be investigated both quantitatively and qualitatively in response to the concentration of the analyte in question [2]. In the previous two decades, escalated innovative work and development of electrochemical sensors have allowed to fabricate different types of devices for the discovery of various biological samples [3].

The study by Agriopoulou and co-workers [4] has proven that biosensors can be used to determine the degree of food spoilage. Their study was focused on the detection of food spoilage caused by toxigenic fungi and mycotoxins, regarding concentrations and degree of spoilage in food. Other researchers reported the use of biosensors for the determination of xanthine, hypoxanthine, and dopamine [5-7]. These studies have confirmed that biosensors are emerging as the powerful research tools for the detection of many life-threatening compounds.

A biosensor is a material that recognises and quantifies physical and chemical objects and quantities into a signal or visual which could then be examined by another electronic tool [8] as shown in Figure 2.1 [9]. There are two kinds of biosensors, (a) Active biosensors that require an outside power supply to produce a signal, which yields the information about the sample being examined. (b) Passive biosensors do not require any external energy for the generation of an output signal [10]. However, both biosensors have a transducer that converts a signal from one form of energy to another form, which can be easily read and analysed by another instrument in correlation to the analyte in question [11].

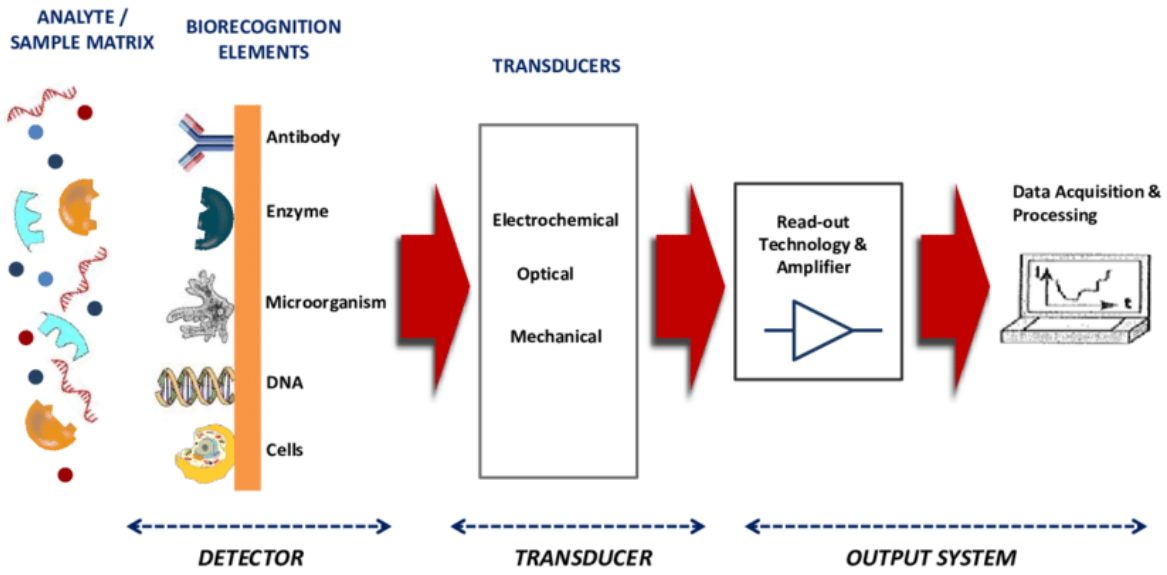


Figure 2.1 Simplified diagram of a biosensor [9].

### 2.1.1 Pre-requirements of a biosensors

To produce the functional biosensors, the following requirements are implemented during the construction of biosensors [12]:

**(a) Selectivity**: The biosensor should be highly selective towards the analyte and show less minimal interference effects on other compounds in the matrix that have a similar structure to the analyte. A biosensor that shows high interference values with other components cannot be trusted for quantitative analysis [13].

**(b) Quick response time**: Time is an important parameter used for analysis. Biosensors should respond faster and very accurately [14].

**(c) Stability and reusability**: Biosensors are used to analyse materials for both qualitative and quantitative., They must be highly stable at physiological conditions and reusable. Mostly stable biosensors tend to be also reusable [12].

(d) **Reproducibility of the results**: any analysis which was determined using a biosensor, with the same concentration of the analyte and conditions, the results should be reproduced when repeated for validation of the results [15].

(e) **Sensitivity**: The biosensor has to detect the lowest concentration of the analyte with high accuracy and precision [16].

### 2.1.2 Types of Biosensors

Four types of biosensors are documented in the literature.

#### 2.1.2.1. Electrochemical biosensors:

Electrochemical biosensors presently dominate the biosensing field of research with the most well-known approaches including

I. Amperometric: where the current produced is measured in relation to the concentration of the analyte [17].

II. Potentiometric: this includes measuring the electrical potential throughout the reaction which then the measured potential gives information about the analyte [18].

III. Conductometric: this technique relies on changes of electric conductivity of a material, of which the conductivity is affected by the analyte [19].

IV. impedimetric techniques are assembled by fabricating biological compounds onto an electrode surface which can catalyse the reaction, e.g., enzymes, it gives information, through measurements of the catalytic reaction, and the targeted analyte by the output of an electrical impedance signal made proportional to analyte activity [20].

#### 2.1.2.2. Calorimetric biosensors

This type of biosensor measures the change in temperature during sample analysis. Since most enzymes are exothermic, the temperature change is measured in conjunction with the analyte being investigated [21]. According to the literature, most

of these biosensors are not mostly used, this is because these biosensors do not offer qualitative information of the analyte [22].

#### 2.1.2.3. Optical biosensor

This is a compact analytical device composing of a biorecognition detecting component integrated with an optical transducer system [23]. Optical biosensors offer incredible preferences over most analytical techniques since they give immediate response results with high accuracy and precision for many biological and chemical substances. Their good characteristics include high specificity, sensitivity, small size (easy to handle), and cost-effectiveness [24].

#### 2.1.2.4. Gravimetric biosensors

This type of biosensors measures the change in mass which is proportional to the analyte. Many gravimetric biosensors utilise thin piezoelectric quartz gems, as resonating crystals alternatively as mass/surface devices [25,26].

Studies have shown that research regarding biosensors is focusing more on the detection of biomarkers in food for the determination of the freshness of the food we consume [27]. Hypoxanthine is one of the biomarkers which indicate the level of food spoilage. This is because it has been documented that the increase in many diseases such as heart diseases and gout affecting many individuals is mediated by consumption of food with high levels of hypoxanthine [28-30].

### 2.2 Analysis of meat and storage

The temperature and the time at which food is stored play a crucial role in the development of hypoxanthine concentration built-up [31]. Frozen storage is a significant technique for the protection of food spoilage. It is normally utilised in fish meat and other animal protein-based industries. This is because under low temperatures the quality of food is maintained for a long period. In addition, this technique has numerous advantages such as negligible changes in the product regarding product colour, flavour, and texture, and low decomposition rate [32]. However, the loss of quality of fish cannot be avoided when stored in a frozen state

[33]. The alteration in fish muscle fibres, lipids proteins, and textural properties through frozen storage has been investigated for numerous decades due to their economic importance [34]. The genuine storage temperature of fish relies on the freezing properties of various fish species. This should be sustained to have a good impact on the quality of fish. Alterations in the quality and freshness of the fish flesh rely on the temperature and extent of the storage period [35].

People choose different freezing techniques to maintain the quality of meat [36]. On a commercial scale, the freezing of fish meat is done at -50 $^0$C to -60 $^0$C. If the whole water content in the meat is frozen, the fish can be kept for a longer duration and nearly remains fresh [37]. In quick or freezing deep techniques the fish is frozen at -20 $^0$C and it maintains its physical properties and nutritive values [38]. Freeze drying is an adjusted deep-freezing technique that terminates all chances of denaturation. Separately from this, there are other techniques, used by small-scale households and industries. For example, chilling and frozen storage methods using refrigerators [39].

Fish spoilage takes place immediately after harvesting. This procedure starts immediately within 10 hours of their grasp in the high surrounding temperatures of the tropics [40]. The amount of fish spoilage relies on numerous factors inclusive of the type of fish species; their fat index, shape and size; the season of their catch, and the nature of the fishing grounds [41]. Most of the fish species deteriorate because of digestive enzymes and lipases, microbial spoilage from surface bacteria. During fish deterioration, there is a breakdown of numerous components of the fish and the formation of new ones. These new compounds are accountable for the alterations of the flavour, odour, and texture of the fish meat [42].

Accumulation of hypoxanthine is caused by low oxygen levels in the body. Therefore, at the point when an animal dies including fish or any type of meat source, adenosine triphosphate (ATP); resulting in an increased level of hypoxanthine [43]. This process occurs when ATP which is stored in the muscles dephosphorylates and deaminates to form hypoxanthine (refer to figure 2.2). Recognition of hypoxanthine by xanthine oxidase is an important pathway for the determination of fish freshness in the industry. Thus, hypoxanthine is firstly oxidised to xanthine, and afterward to uric acid by xanthine oxidase. The rate of fish

decomposition mostly depends on the environmental temperature, moisture, and feeding habits [44,45].

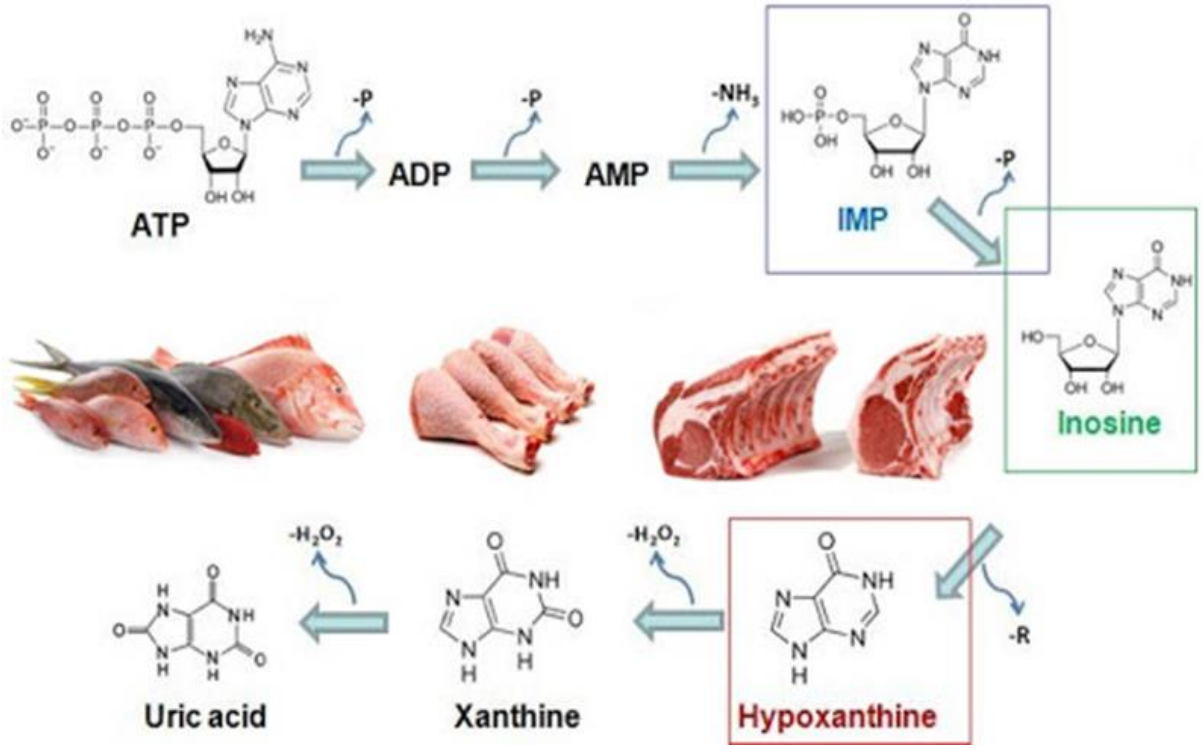


Figure 2.2. Degradation of meat. This diagram highlights the formation of hypoxanthine from ATP catabolites, followed by further degradation to uric acid by xanthine oxidase (Extracted from a poster of Novo CIB postmortem ATP catabolism in fish muscle by Dr Larissa Bala)

### 2.3 Methods used for determination of fish spoilage

Classical techniques that measure the degradation of food primarily based on hypoxanthine, include spectrophotometry, chemiluminescence, capillary electrophoresis, high-performance liquid chromatography, and gas chromatography, these have been applied in detecting Hypoxanthine [47]. However, these methods can be costly, laborious, extensive, often require sample preparation, and uses state of the art equipment which require trained personnel to operate. Specifically, chromatography methods regularly require analyte derivatisation, while spectrophotometry calls for tedious sample pre-treatment techniques, capillary

electrophoresis requires costly instruments and is prone to many interferences during analysis which can affect the final results [48]. While on the other hand, biosensors can provide easy-to-use, sensitive, cost-effective, and highly accurate detection.

Emphasis was made on the good properties of biosensors. For example, a report by Seki *et al*.,[49] clearly indicated that on the use of biosensors, these techniques cannot only detect analytes at low concentration due to their high sensitivity and selectivity, but they have also highlighted they can simultaneously detect many biological analytes. However, the study could not resolve the issue of interferences by ascorbic acid [50]. Hence, the proposed study envisages that the sensitivity and selectivity of electrochemical biosensors under interference studies can be improved by the combination of highly dispersed metal oxides on the surface of carbon nanomaterials such as carbon nanotubes to further increase their specificity per analyte.

Previously, enzyme-free electrochemical methods have been used for the detection of hypoxanthine, which has proved to yield satisfactory results in its determination. This is because these methods have simplicity, low cost, and are less time-consuming [50]. Even though numerous techniques have been studied to put together non-enzymatic electrodes, they lack selectivity, and also the oxidised species adsorbed on electrode surfaces after the reaction can lead to poor sensitivity and selectivity [51]. To overcome these problems, throughout the literature it is evident that different materials have been used to modify the bare electrodes, such as metal oxides, functionalisation of the multi-walled carbon nanotubes (MWCNTs), and the use of enzyme for direct specificity of the analyte.

## 2.4. Carbonanomaterials used in biosensors for the detection of hypoxanthine

### 2.4.1. Carbon nanotubes

Many researchers in the past have focused on the use of carbon nanotubes (CNTs) for the detection of hypoxanthine in food products such as fish [52]. CNTs are nanostructures attained from rolled graphene sheets (refer to figure 2.3). They are famous allotropes of carbon with both chemical and physical properties, making

them appreciably used in recent research studies [53]. The recognition of carbon nanotubes by Iijima in 1991 utilising High-Resolution Electron Microscopy (HREM) has motivated many researchers and theoretical studies on carbon nanotubes [54]. Carbon nanotubes have a small diameter, which leads to a high surface area. They are very conductive due to their metallic characteristics and high thermal stability. However, these nanomaterials are very insoluble in most of the solvents limiting their good properties [55].

Fortunately, studies by Abuilaiwi *et al* [56], and Michalska *et al* [57] demonstrated that modifications of these nanomaterials and other functional groups by attaching them to their walls can increase their solubility and conductivity [58]. The successive incorporation of compounds on the walls of the nanotubes is extremely easy since they possess a longer inner volume with respect to the diameter of nanotubes. The incorporation of other compounds also adds an advantage that they can be easily modified this is better illustrated by figure 2.4.

### 2.4.2. Types of carbon nanotubes (CNTs)

The carbon nanotubes are of two kinds namely: Single-walled carbon nanotubes (SWCNTs) and Multiple walled carbon nanotubes (MWCNTs). SWCNTs include a single cylindrical carbon layer that has a diameter of between 0.4-2 nm, relying on the temperature of their synthesis [60]. It was discovered that the higher the increase in temperature of their synthesis the bigger is the diameter of CNTs [61]. The SWCNTs possess an extremely high surface area as large as 1300 $m^2/g$, which provide an adequate surface area. This nanomaterial also shows a better electron conductance as compared to MWCNTs; this means that in SWCNTs all the electrons that enter one side of the conductor come out at the end of the conductor without scattering in the middle. While in the case MWCNTs this characteristic is slightly hindered due to the presents of multiple cylinders [60,61].

MWCNTs are made of countless coaxial cylinders, which are constructed from a single graphene sheet encircling a hollow core [62]. The outermost diameter of MWCNTs is ranging between 2-100 nm, whilst the interior diameter is within the range of 1-3 nm, together with their length is one to several micrometers [63]. These

nanotubes consist of a delocalized electron cloud next to the wall, which is created, and it is liable for the interconnections linking adjacent cylindrical layers in the tubes. These structures bond through $sp^2$ hybridisation [64], which is a consequence of much less flexible and extra structural defects. This increases the reactivity of MWCNTs with other compounds which includes depositing nanoparticles on the MWCNTs walls or ends, interacting through physical and chemical bonds with the potential applications in many fields such as catalysis, magnetic data storage, biosensors, biomedical, and electronic devices [65]. Figures 2.3 and 2.4 below show structure of both single and multi-walled carbon nanotubes and the deposition of nanomaterials on the walls of carbon nanotubes and, respectively. While figure 2.5 shows a pictorial version of CNTs, their colour, and texture

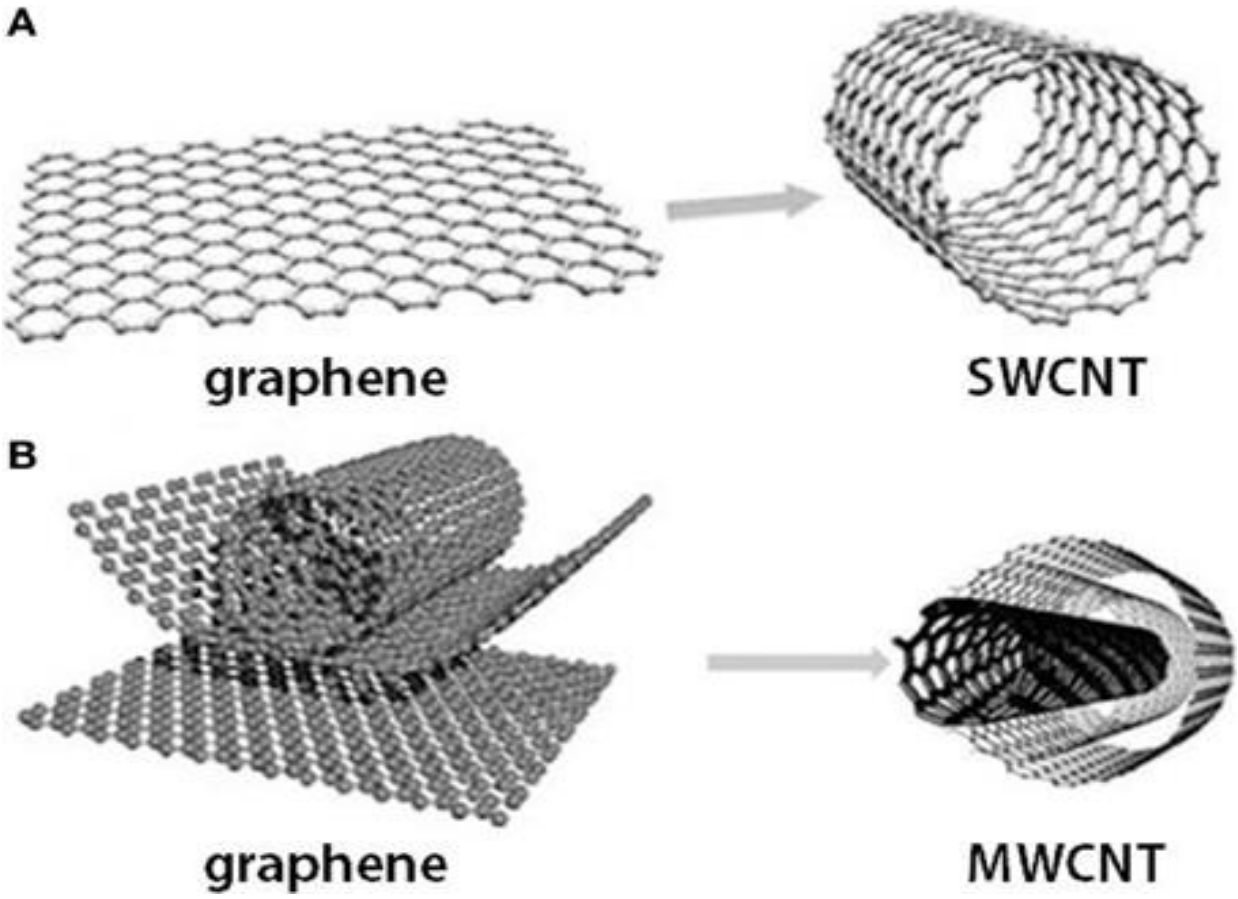


Figure 2.3: A typical structures of SWCNTs and MWCNTs with layers of graphene. (A) SWCNTs and (B) MWCNTs [66]

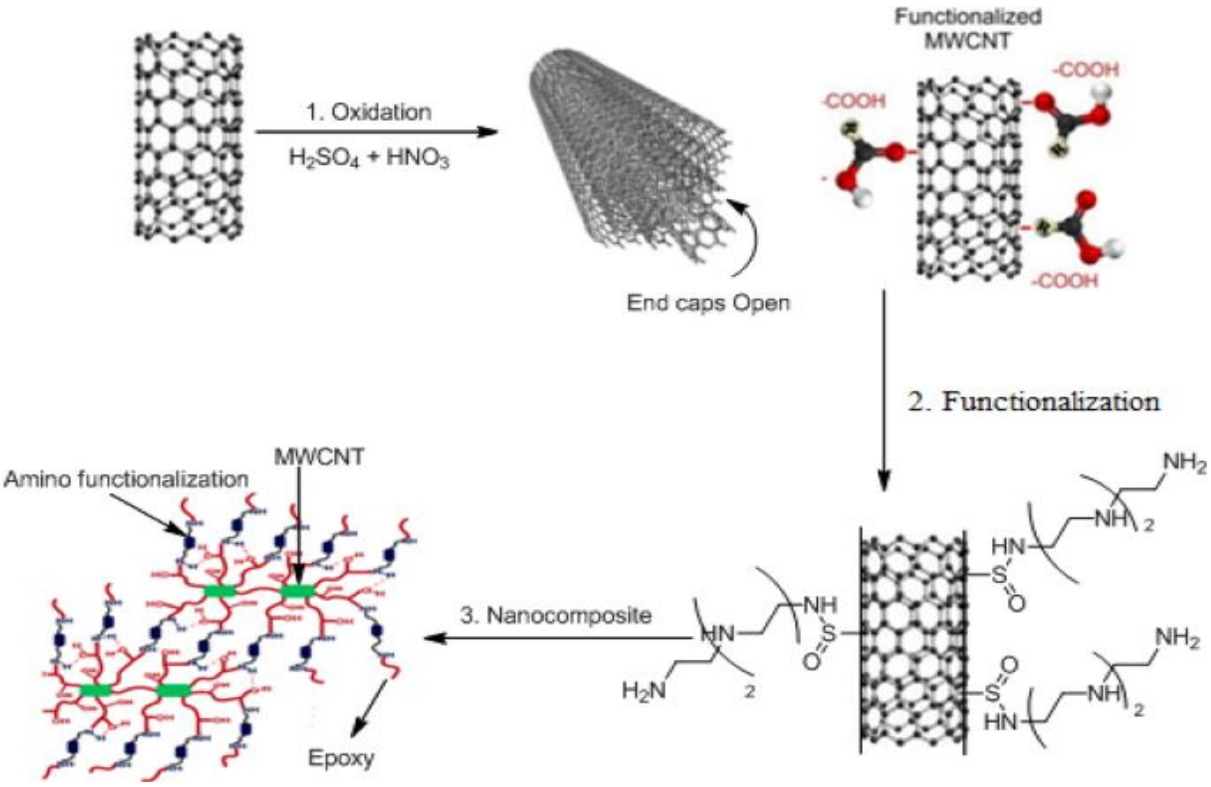


Figure 2.4. A typical modification of CNTs for increasing surface interaction [59].

Figure 2.5. The typical pictorial version of the carbon nanotubes, their colour, texture, and composition [67]

## 2.5 Methods used for the modification of CNTs with other compounds

### 2.5.1 *In-situ* method

Extensive research has focused on *in-situ* method for functionalisation of the CNTs. This method involves covalent interaction between the nanoparticles and CNTs; by depositing a precursor and forming a product onto the walls of the CNTs. The ability to create covalent interaction directly onto the walls of the CNTs is an added advantage for using this method because it prevents agglomeration while maintaining a good distribution of the deposited material The disadvantage of this method is that any precursor that did not react and attach to the walls might influence the final product [68].

### 2.5.2 *Ex-situ* method

The other important method for the synthesis of the nanocomposites is directly mixing the prepared nanomaterials with the CNTs. According to the literature, this method is not widely used and not highly recommended, because it leads to agglomeration of nanomaterials, which tends to decrease the surface area and the reactivity of the final product. However, this problem is recently solved by sonication methods to improve the dispersion of the MWCNTs [69].

## 2.6 Properties of metal oxides

Few studies have used metal oxides as nanomaterials that can be deposited on the surface of CNTs. This gap got the attention of this study by using metal oxides as compounds to be deposited on the walls of the CNTs to further improve their characteristics.

Studies have proven that metal oxides possess good electrochemical characteristics that can be used in biosensors for the detection of hypoxanthine [70,71]. Metal oxide nanoparticles have attracted a vast interest in electroanalysis for the identification of biomolecules [72]. The extensive gain of interest in research of metal oxide nanoparticles is due to their structural changes that permit the modification of lattice symmetry and cell parameters; an improvement in electrochemical characteristics because of the quantum confinement effect, and alteration in surface properties

directing to a decrease in the bandgap. This increases the conductivity and the chemical activity of the nanoparticles [73]. In addition, the significant property of the metal oxides is their low toxicity regarding the immobilisation of enzymes by increasing the selectivity and sensing of biomolecules [74]. Among various metal oxides the following were selected for this study are zinc Oxide (ZnO), cobalt Oxide ($Co_3O_4$), zirconium dioxide ($ZrO_2$), titanium dioxide ($TiO_2$), and manganese dioxide ($MnO_2$).

### 2.6.1 Zinc oxide

Zinc oxide (ZnO), specifically nano-scale ZnO has obtained substantial significance in the past few years because of its large variety of functions in various fields of science [75]. In addition, ZnO is an environmentally safe compound, and various physical and chemical techniques were used to acquire ZnO nanoparticles with various morphology [76]. Many techniques including hydrothermal, electrochemical, vapor deposition, and sol-gel have been used to synthesis of ZnO nanomaterials [77]. These nanomaterials have been seen as one of the most promising materials because of their important advantages such as low cost, abundance and electrochemical activity [78,79]

### 2.6.2 Cobalt oxide.

The undivided attention for using cobalt oxide ($Co_3O_4$) as an electrode coating component started in the late 1970s [80]. Complex metal oxides with spinel structure have been discovered to be very promising for a whole lot of functions because they are not only active but also less expensive and thermodynamically stable, typically in alkaline media [81]. Among these oxides, $Co_3O_4$ and other different cobalt-based oxides progress to stimulate interest in research, together with their feasible use in various fields, including, energy storage, and electrocatalysis are well-substantiated [82]. A series of studies further examined the composition, morphology, and chemical behaviour of $Co_3O_4$ coatings during the first half of the 1980s. It was once concluded that the high activity of $Co_3O_4$ coatings was primarily ruled by their large active surface area [83].

### 2.6.3 Zirconium oxide

Zirconium oxide ($ZrO_2$) has outstanding chemical stability, low toxicity and can be a possible potential to exhibit electrochemical properties in biosensors [84]. They are semiconductors with many oxygen vacancies on their surface, together with their high ion-exchange magnitude and redox activities, they make these nanoparticles effective in many electrochemical processes [85]. Furthermore, because of their best mechanical strength and outstanding thermal along with optical properties, $ZrO_2$ nanoparticles were also used in different other fields like the dental industry, and ceramics [86].

Specifically, cubic $ZrO_2$ displays up to standard electrochemical properties because of its outstanding properties like good electrical along with surface charges, high mechanical strength, most appropriate chemical and thermal stability, and biocompatibility. As a result, it has obtained outstanding attention as a transducer in the fabrication of chemicals and biosensors [87]. Although, electrochemical applications of $ZrO_2$ have been critically hindered because of its average redox behaviour and low electrochemical active surface area [88]. In the light of the study, by Yazdi *et al* [89] they have critically evaluated and discovered that materials with high surface areas and excellent electrical conductivity can be potentially used to upgrade the electrochemical properties of $ZrO_2$. In this regard, this study is aiming at filling that gap with the improvement of the incorporation of the $ZrO_2$ nanoparticles with the carbon nanotubes.

### 2.6.4 Titanium dioxide

Titanium dioxide ($TiO_2$) nanoparticles are the most substantial studied semiconductors [90]. This aforementioned metal oxide is a good semiconductor commonly utilised as a photocatalyst due to its good photocatalytic characteristics, to add to that it is also non-toxic, chemically stable, and readily available [91]. The photoactivity comes from the semiconductor nature, mainly from the power of the light quantum absorption accompanied by the charge carrier generation. $TiO_2$ in the crystallographic form of anatase has begun to be an interesting candidate as an n-type photoanode because of its outstanding effectiveness to produce electron-hole pairs and high electron conductivity [92]. Recently many researchers used $TiO_2$ as a

modifier of the electron in biosensors and have reported that $TiO_2$ was found useful [93,94].

### 2.6.5. Manganese oxide.

According to the literature few researchers have reported on the use of manganese oxide as a modifier for enhancing electroconductivity for detection of the analytes. The interesting part of manganese oxide nanoparticles lies within the possible formation of numerous structures primarily based on specific preparations of the basic building. Structure of manganese oxide, which is $MnO_6$ octahedral [95]. This is a structure in which $O^{2-}$ ions are octahedrally coordinated to the central $Mn^{4+}$ ion. A structure with many rooms for the incorporation of electrolyte ions provides higher charge storage capacity and consequently leads to high electroconductivity [96]. These nanoparticles are mostly used to manufacture batteries due to their good conductivity. Because of that, these nanomaterials have the potential to be used in biosensors for the determination of the biological analyte. However, the formation of the structure of $MnO_2$ is reported to have poor electronic transfer properties which hinder the good properties of these nanoparticles. Fortunately, the study by Vimuna *et al* [97] has enlightened that this type of structure can be improved by incorporation with CNTs.

## 2.7. Photoactivity of the metal oxides and multi-walled carbon nanotubes

Recently many researchers have focused their attention on the photocatalytic activity of metal oxides [98]99][100]. But few have considered the effect of doping the metal oxides with MWCNTs to check the effect of combining these nanomaterials towards photoactivity. In the light of the study by Leary and co-worker [101] they have shown that CNTs have the potential to be used as templates to assembly the metal oxides and they were found to enhance the photocatalytic activity of metal oxide by the retardation of electron-hole recombination. A hole is better explained as a positive charge carrier and the process of electron-hole recombination is when the electron and hole interact and recombine, and the energy of their interaction is not lost through heat or thermal energy. Instead, the energy is transferred to excite the electrons for photoactivity [102].

## 2.8 A review of electrochemistry, principle, and applications in biosensors

Historically, the part of electrochemistry which is presently called voltammetry created from the revelation of polarography in 1922 by the Czech chemist Jaroslav Heyrovsky, for which he got the 1959 Nobel Prize in chemistry [103]. The early voltammetric methods experienced many challenges, making them not exactly perfect for routine investigative use. Nevertheless, in the 1960s and 1970s, noteworthy advances were made in every aspect of voltammetry (hypothesis, approach, and instrumentation), which extended the collection of diagnostic methods in all areas of voltammetry. Which upgraded the affectability and extended the collection of diagnostic methods to magnify the sensitivity and expanded the present analytical methods [104]. These advances enabled for minimal effort operational and additionally encouraged the fast analysis of results, with high accuracy and precision using the modest instrumentation. The regular trait of all voltammetric methods is that they include the utilisation potential to an electrode followed by observing of the subsequent current [105].

### 2.8.1 Electroanalytical system

The essential components of a present-time electroanalytical system for voltammetry include a potentiostat, electrochemical cell and the computer [106].

#### 2.8.1.1. The potentiostat

This is an instrument used to apply current to the electrode while measuring the potential voltage difference between the working and the reference electrode. The work of applying a known potential and checking the present current falls under the technique of potentiostat. Precise and adaptable control of the applied potential is a basic function of the potentiostat. The most generally used potentiostats in the present time contain electronic hardware and software that enables for analysis of three electrodes in an electrochemical cell [107].

#### 2.8.1.2. The electrochemical cell

A representative of an electrochemical cell accommodates the sample dissolved in a solvent, an ionic electrolyte, and three or two electrodes [108]. Cells that are sample holders are differentiated by shapes sizes, and materials. The type utilised relies upon the quantity and type of sample, the procedure, and the investigative data to be obtained [109]. The material of the cell (polyethylene, glass, and teflon) is chosen to limit reaction with the sample [110]. Systematically the reference electrode has to be put in close proximity to the working electrode, to avoid voltage drop [111].

### 2.8.2 Electrodes used in electrochemistry

The reference electrode by definition according to the literature it is the electrode that has a well-known and stable electrode potential [112]. Constant concentration with a redox system is used to reach the highest stability of the electrode. The most frequently utilised reference electrodes for aqueous solutions are the calomel electrode and silver-silver electrode. These electrodes are obtainable in different sizes and shapes [113].

Counter electrodes are the electrodes that are used to close the current circuit in an electrochemical cell. They are utilised nearly in all the voltametric techniques. The investigation reactions which take place at the electrode surfaces occur over an extremely short time and hardly ever give rise to any considerable alterations in the bulk concentrations. As a result, the separation of the counter electrode from the sample is not necessary. Most typically the counter electrode comprises of a thin Pt wire.

Working electrodes this is the electrode where the electrochemical reaction occurs. frequently utilised in electrochemistry are carbon electrodes specifically the pyrolytic graphite and glassy carbon [114]. They had long been recognised as adaptable and supporting materials, for electrocatalysis and electrochemical sensing [115]. They all have many advantages, for example, low cost, chemical stability and inertness, and wide potential window in most electrolyte solutions of which they are better than the expensive metal electrodes such as platinum, gold, aluminium, silver, and copper [116].

### 2.8.3 Cyclic Voltammetry (CV)

This technique has recently got the attention of many researchers as an electrochemical technique in various applications [117]. However, it is hardly ever for quantitative investigations, yet it is extensively used for studies related to redox processes under various chemical reactions, including the presence of intermediates, oxidation and reduction reactions, and the reversibility and the irreversibility of the chemical reactions. The fundamental procedure of this technique consists of the applied potential in both forward and reverse directions using a particular scan rate while current is measured. This technique is used to study thermodynamics, reaction mechanism, and kinetics of the analyte [118].

The current is primarily measured between the counter and the reference electrode while the voltage is measured between the working and the reference electrode [119]. The acquired results are plotted as current *vs.* voltage, also called voltammogram. The current increase as the voltage is raised in the direction of the electrochemical reduction potential of the analyte [120]. The final shape of the voltammogram varies from analyte to analyte. This graph is highly affected by the presence or absence of enzymes. Reactions that are catalysed by enzymes show a high peak current as compared to non-catalysed reactions. Secondly, it is affected by scan rate, by increasing the scan rate of the reaction, this results in the increase in peak current.

### 2.8.4 Pulse methods under voltammetry

#### 2.8.4.1. Normal Pulse Voltammetry

The Normal Pulse Voltammetry (NPV) technique is normally done in solids electrodes in an unstarred solution. It utilises a sequence of potential pulses of increasing amplitude [121]. The current is measured per pulse at a particular potential and time. The time of the pulse is, normally 1 to 100 msec, and the pulse period is 0.1 to 5 sec. The final results of this type of analysis are represented by the voltammogram which consists of the current on the y axis versus the potential on the x-axis [122]. This technique shows high sensitivity, and it is used to study

quantitative information about the analyte, including kinetics and thermodynamics studies of the reaction

#### 2.8.4.2. Differential Pulse Voltammetry

The Differential Pulse Voltammetry (DPV) is the technique which is often used to investigate the electrochemical properties of most analytes. It consists of patterns, which have small pulses superimposed upon a staircase waveform [123]. The current is measure at two points for each pulse, before the application of each pulse and at the end of each pulse. This technique provides quantitative information about the analyte, reaction mechanism, kinetics, and thermodynamics. It also provides improved sensitivity as compared to CV, because it uses relatively short pulse time, increases measured currents and its differential nature discriminates against background processes. The results are represented by a voltammogram of current versus potential [124].

#### 2.8.4.3. Square-Wave Voltammetry

The Square-Wave Voltammetry (SWV) technique is mostly used in the electrochemical detection of analytes, due to its high sensitivity. This is considered as a form of linear potential sweep voltammetry that uses the combination of the square wave and staircase potential applied to the stationary electrode. It consists of applying symmetric square wave potential to the working electrode which is superimposed on a base staircase potential [125]. A full square wave corresponds to the duration of one step in the staircase waveform. Current is sampled twice during each square wave cycle, one at the end of the forward pulse ($I_F$) and the one at the end of the reverse pulse ($I_R$). This results in square wave modulation; reverse pulses cause the reverse reaction of any product that formed from the forward pulse [126]. SWV has numerous advantages among these are the rejection of background currents and its incredible sensitivity towards analytes [127]. It is found in numerous applications including medicinal and various sensing research-related studies [128]. The results from this technique are presented as current versus potential.

## 2.9. Modification of the electrodes.

In biosensors development, the type of components which are used to modify the electrode and the technique for electrode modification, as well as the detection strategy are all significant [129]. Biosensors use biological components and the method by which it is fabricated on the electrode will determine the overall performance of the sensor. Through a thorough search on the literature the following techniques for the fabrication of the biological component on the electrode have been described (inclusive of 'adsorption'), through which the biological unit is directly adsorbed onto appropriate surface [130]. Secondly the entrapment in this procedure the biological unit is confined inside the matrix [131]. Thirdly microencapsulation herein the biological unit is confined in the between two membranes [132]. Lastly cross-linking', where the biological unit is chemically attached to the surface of the sensor either directly or rather through the binding agent [133]. Electrode modification methods that can be used to modify working electrodes include; Electrodeposition, electropolymerisation, and dip-dry, [134].

### 2.9.1. Electrodeposition

This is the form of plating technique that uses current from the external source like the battery and the conducting electrolyte that consist of the analyte solution with ions and the anode and the cathode electrodes in the cell. The analyte ions attract the electrode of opposite charge by the electrostatic force of attraction [135].

### 2.9.2. Electropolymerisation

This is the most well-structured technique of depositing polymer films on electrodes. The procedure includes using a cathode electrode and the electrolyte with the organic analyte dissolved inside [136]. The organic analyte transfers an electron to the cathode, and it is left with cations monomers and solutions, that will share electron and bond with each other to form a polymer, and the polymer binds to the electrode through electrostatic force of attraction

### 2.9.3. Dip-dry

This method requires the insertion of an electrode in the solution of a modified composite for a specified period to permit the surface adsorption of the material [137]. The electrode is then withdrawn and the solvent with the composite is allowed to dry [138]. Throughout this method, the electrode is then modified by placing a few drops of the catalyst onto the surface which consists of the dried composite, and the solvent is allowed to dry off [139].

## 2.10 Mass transport

Mass transport procedure in the electrochemical cell is a process that controls the net motion of all the ions [140]. The three mass transport processes are as follows:

### 2.10.1. Diffusion

Diffusion is a voluntary motion due to the effect of the concentration gradient. The procedure where there is the motion of an analyte from an area of high concentration to an area of low concentration [141].

### 2.10.2. Migration

Migration is the kind of charge movement which includes the movement of charged particles down the electrical field. The movement of the ions in the electrolyte is towards an electrode of opposite charge [142].

### 2.10.3. Convection

Convection is the transportation of analyte to the electrode by dissolving the analyte in the electrolyte. For instance, convection by mechanical means where the analyte is carried to the electrode by stirring the solution either by magnetic stirrer or other methods including rotating the electrode and incorporating the electrode into a flow cell. The influence is terminated by sustaining the cell under quiet and stable conditions [143].

## 2.11. Recent findings on the detection of Hypoxanthine using various nanomaterials

The study by Luo *et al* [145] have used sulfonic groups functionalised nitrogen-doped graphene to check the simultaneous detection of hypoxanthine, xanthine, and uric acid. Based on their findings they indicated an increase in conductivity and dispersity of the graphene nanoparticles after they were functionalised as compared to raw graphene nanoparticles. They have also indicated the low detection limit of 0.0838 μM. They have indicated the reusability of the electrode for 15 days with 86.4% of remained sensitivity after being used. They concluded that the fuctionalised graphene nanoparticles have the potential to be used in human serum.

The analysis by Borisova *et al* [146] have used reduced graphene oxide-carboxymethyl cellulose layered with platinum nanoparticles, Poly(amidoamine) dendrimer and magnetic nanoparticles hybrids for hypoxanthine detection. The biosensor showed excellent electrochemical properties with the detection limit of 13 nM, it has also retained 94% of its initial activity after 1 week of reusability studies. They have concluded that this developed sensitive biosensor has the potential to be employed for the accurate determination of fish freshness.

The investigations by Wen *et al* [147] used nanocomposite of palygorskite and nitrogen doped graphene nanoparticles for the hypoxanthine, xanthine and uric acid. They have indicated an improvement of the sensors capabilities after doping with palygorkite and nitrogen. They have recorded a limit of detection of 0.4 μM for hypoxanthine detection and good reproducibility without giving specific values. However, the results showed poor interferences of hypoxanthine with other purines which need further developments. Nevertheless, they have concluded that the biosensor showed satisfactory results for the detection and analysis of hypoxanthine in chicken and bovine serum samples.

The research by Hu *et al*. [148] reported the use of amino-functionalised metal organic frame work nanosheet with peroxidase and fluorescence properties for the development of the biosensor. They have shown the improvement of the sensor with excellent results and detection limit of 3.93 μM. No results reported for the reusability

of the biosensor. However, they have noted that the sensor showed good potential to be used for fish analysis and it is promising for analysis of variety of food against spoilage.

The study by Yazdanparast *et al.* [149] used poly(L-aspartic acid)-multi-walled carbon nanotubes (MWCNTs) bio-nanocomposite for hypoxanthine detection. They have indicated good electrochemical results with the detection limit of $3.5\times10^{-4}$ μM, and they have noted drastic improvement in the sensitivity of the electrode upon functionalisation of MWCNTs. They have concluded that their biosensor has good potential for quality assessment of the meat products.

The journal by Chen *et al* [150] reported on the use of fluorescent biosensor based on catalytic activity of platinum nanoparticles for freshness evaluation of aquatic products. The results show the importance of platinum nanoparticles after being polished on the electrode which showed an in increase in the overall performance of the biosensor with limit of detection of 2.88 μM. They report 9% decrease in activity of the biosensor after 3 cycles. Their conclusion indicated that their results showed good selectivity for various potential interfering substances and could be used for detecting the hypoxanthine contents in real samples such as fish, shrimp, and squid with good recoveries.

Mustafa *et al* [151], reported on the detection of hypoxanthine using cerium oxide-based hypoxanthine biosensor for fish spoilage monitoring. The results showed that cerium oxide increases the sensitivity of electrode towards hypoxanthine detection. A detection limit of 15 μM was reported, with ~93% activity for the first 14 days, which then decreased gradually to ~86 % after 30 days of storage. They concluded that this biosensor immobilised with cerium oxide has good potential for determination of freshness of fish meat.

### 2.12. Concluding remarks

It is evident that the aforementioned properties of nanoparticles have good electrochemical characteristics that can be used by sensors for the determination of analytes. It is proven by the literature that CNTs and metal oxides have some drawbacks that hinder some of the good properties in electrochemistry. This study is

focused on synthesis metal oxides and fuctionalisation of CNTs and the formation of nanocomposites, i.e., combining these two nanomaterials together to further increase conductivity and hinder some of the disadvantages each nanomaterial experience individually. Additionally, a review by Pan *et al*. [144], highlighted that the metallic bond brought by nanomaterial increases the electron conductivity of the material. Therefore, this study is further aimed at combining the two metal oxides to increase the conductivity by bimetallic bonds, in creating a sensitive sensor for the determination of hypoxanthine at very low concentrations in fishes stored at selected temperatures.

Recent advances in nanotechnology intend new innovative applications in the food industry, specifically fish meat due to its high deterioration rates as compared to other types of meat. Biosensors are exposed to be efficient in determining the accurate results in freshness of meat. While nanomaterials, for example metal oxides and carbon nanotubes offers great potential benefits for analysis of spoilage of meat, they are emerging concerns in the interfering species during analysis. This can be combated with good selection of metal oxides and good product synthesis to avoid such throwbacks.

## 2.13 REFERENCES


[1] Tamura, T. (2016). Review of monitoring devices for food intake. *CICSJ Bulletin*, *34*(3), 73. https://doi.org/10.11546/cicsj.34.73

[2] Rovina, K., Merillyn, J., Nurul, S., & Xin, S. (2019). Sensing and Bio-Sensing Research Development of biodegradable hybrid polymer film for detection of formaldehyde in seafood products. *Sensing and Bio-Sensing Research*, *October*, 100310. https://doi.org/10.1016/j.sbsr.2019.100310100310, 2019, doi: 10.1016/j.sbsr.2019.100310.

[3] Turner, A. P. F. (2013). Biosensors: Sense and sensibility. *Chemical Society Reviews*, *42*(8), 3184–3196. https://doi.org/10.1039/c3cs35528d

[4] Agriopoulou, S., Stamatelopoulou, E., & Varzakas, T. (2020). Advances in analysis and detection of major mycotoxins in foods. *Foods*, *9*(4), 1–23. https://doi.org/10.3390/foods904051

[5] Khan, M. Z. H., Ahommed, M. S., & Daizy, M. (2020). Detection of xanthine in food samples with an electrochemical biosensor based on PEDOT:PSS and functionalized gold nanoparticles. *RSC Advances*, *10*(59), 36147–36154. https://doi.org/10.1039/d0ra06806c

[6] Liao, L., Xing, Y., Xiong, X., Gan, L., Hu, L., Zhao, F., Tong, Y., & Deng, S. (2020). An electrochemical biosensor for hypoxanthine detection in vitreous humor: A potential tool for estimating the post-mortem interval in forensic cases.*MicrochemicalJournal*,*155*(February),104760.https://doi.org/10.1016/j.microc.2020.104760

[7] Yang, C., Liu, M. M., Bai, F. Q., Guo, Z. Z., Liu, H., Zhong, G. X., Peng, H. P., Chen, W., Lin, X. H., Lei, Y., & Liu, A. L. (2019). An electrochemical biosensor for sensitive detection of nicotine-induced dopamine secreted by PC12 cells. Journal of Electroanalytical Chemistry, *832*217–224. https://doi.org/10.1016/j.jelechem.2018.10.018

[8] Cui, Y. E. (2017). Wireless Biological Electronic Sensors. Sensors, *17*(10), p.2289. https://doi.org/10.3390/s17102289

[9] Azura, N., Said, M., & Ogurtsov, V. I. (2014). 25.)Electrochemical biosensor based on microfabricated electrode electrochemical biosensor based on for life sciences applications A dissertation submitted for the degree of Doctor of Philosophy National University of Ireland April 2014 Supervisors Dr . V. April. https://doi.org/10.13140/RG.2.2.11066.49603

[10] Lugari, A. (2018). Active and passive remote sensing techniques and artificial

neural networks in support of buildings seismic vulnerability c ivil and c omputer e ngineering d ept . may. https://doi.org/10.13140/2.1.2200.7682

[11] Lichtenberg, J. Y., Ling, Y., & Kim, S. (2019). Non-specific adsorption reduction methods in biosensing .*Sensors (Switzerland)*, *19*(11),117.https: //doi.org/10.3390/s19112488

[12] Thakur, M. S., & Ragavan, K. V. (2013). Biosensors in food processing. *Journal of Food Science and Technology*, *50*(4), 625–641. https://doi.org/10.1007/s13197-012-0783-z

[13] Bhalla N, Jolly P, Formisano N, Estrela P. (2016). Introduction to biosensors. Essays Biochem.;60(1):1-8. doi: 10.1042/EBC20150001.

.

[14] Harrad, L. El, Bourais, I., Mohammadi, H., & Amine, A. (2018). Recent advances in electrochemical biosensors based on enzyme inhibition for clinical and pharmaceutical applications. *Sensors (Switzerland)*, *18*(1). https://doi.org/10.3390/s18010164

[15] Artigues, M., Abellà, J., & Colominas, S. (2017). Analytical parameters of an amperometric glucose biosensor for fast analysis in food samples. *Sensors (Switzerland)*, *17*(11). https://doi.org/10.3390/s17112620

[16] Chalklen, T., Jing, Q., & Kar-Narayan, S. (2020). Biosensors based on mechanical and electrical detection techniques. *Sensors (Switzerland)*, *20*(19), 26–37. https://doi.org/10.3390/s20195605

[17] Pilo, M., Farre, R., Lachowicz, J. I., Masolo, E., Panzanelli, A., Sanna, G., Senes, N., Sobral, A., & Spano, N. (2018). Design of Amperometric Biosensors for the Detection of Glucose Prepared by Immobilization of Glucose Oxidase on Conducting (Poly)Thiophene Films. *Journal of Analytical Methods in Chemistry*, *2018*. https://doi.org/10.1155/2018/1849439

[18] Ding, J., & Qin, W. (2020). Recent advances in potentiometric biosensors. TrACTrendsinAnalyticalChemistry,*124*,115803.https://doi.org/10.1016/j.trac.2019.115803

[19] Shetti, N. P., Nayak, D. S., Reddy, K. R., & Aminabhvi, T. M. (2019). Graphene Clay-Based Hybrid Nanostructures for Electrochemical Sensors and Biosensors. In *Graphene-Based Electrochemical Sensors for Biomolecules*. Elsevier Inc. https://doi.org/10.1016/B978-0-12-815394-9.00010-8

[20] Wang, T., Song, B., Qiao, K., Huang, Y., & Wang, L. (2018). Effect of dimensions and agglomerations of carbon nanotubes on synchronous enhancement of mechanical and damping properties of epoxy nanocomposites.*Nanomaterials*,*8*(12),https://doi.org/10.3390/nano8120996

[21] Zhang, Y., & Tadigadapa, S. (2004). Calorimetric biosensors with integrated microfluidic channels. *Biosensors and Bioelectronics*, *19*(12), 1733–1743. https://doi.org/10.1016/j.bios.2004.01.009

[22] Kangas, M. J., Burks, R. M., Atwater, J., Lukowicz, R. M., Williams, P., & Holmes, A. E. (2017). Colorimetric Sensor Arrays for the Detection and Identification of Chemical Weapons and Explosives. *Critical Reviews in AnalyticalChemistry*,*47*(2),https://doi.org/10.1080/10408347.2016.1233805

[23] Svitel, J., & Katrl, J. (2016). *Optical biosensors Pavel Damborsk y*. *June*, 91–100. https://doi.org/10.1042/EBC20150010

[24] Ahuja, D., & Parande, D. (2012). *Optical sensors and their applications*. *1*(November), 60–68.

[25] Girard, O., Millet, G., Slawinski, J., Racinais, S., & Micallef, J. (2010). Changes in leg-spring behavior during a 5000 m self-paced run in differently trained

athletes Modifications des caractéristiques du modèle masse-ressort lors d ' une. *Science et Sports*, *25*(2), 99–102. https://doi.org/10.1016/j.scispo.2009.10.001

[26] Rughoobur, G., Miguel-ramos, M. De, Escol, J., Iborra, E., & Flewitt, A. J. (2017). *Gravimetric sensors operating at 1 . 1 GHz based on inclined c - axis ZnO grown on textured Al electrodes*. *March*, 1–9. https://doi.org/10.1038/s41598-017-015452

[27] Mishra, G. K., Barfidokht, A., Tehrani, F., & Mishra, R. K. (2018). Food safety analysis using electrochemical biosensors. *Foods*, *7*(9). https://doi.org/10.3390/foods7090141

[28] Görgülü, M., Çete, S., Arslan, H., Yaşar, A., Görgülü, M., Çete, S., Arslan, H., & Yaşar, A. (2013). Preparing a new biosensor for hypoxanthine determination by immobilization of xanthine oxidase and uricase in polypyrrole-polyvinyl sulphonate film Preparing a new biosensor for hypoxanthine determination by immobilization of xanthine oxidase and uricase *1401*. https://doi.org/10. 3109/21691401.2012.744993

[29] Yildirim, E., & Cete, S. (2020). Construction of biosensor for hypoxanthine determination by immobilization of xanthine oxidase and uricase in polypyrrole-paratoluenesulfonate film. *Journal of Solid State Electrochemistry*, *24*(7), 1695–1707. https://doi.org/10.1007/s10008-020-04715-x

[30] Mustafa, F., & Andreescu, S. (2018). Chemical and biological sensors for food-quality monitoring and smart packaging. *Foods*, *7*(10). https://doi.org/10.3390/foods7100168

[31] Li, T., Ren, L., Wang, D., Song, M., Li, Q., & Li, J. (2019). Optimization of extraction conditions and determination of purine content in marine fish during boiling. *PeerJ*, *2019*(5), 1–23. https://doi.org/10.7717/peerj.6690

[32] Fernandes, P. (2016). Enzymes in fish and seafood processing. *Frontiers in Bioengineering and Biotechnology*, *4*(JUL), 1–14. https://doi.org/10.3389/fbioe.2016.00059

[33] Hicks, D. (2016). Seafood Safety and Quality: The Consumer's Role. *Foods*, *5*(4), 71. https://doi.org/10.3390/foods5040071

[34] Dawson, P., Al-Jeddawi, W., & Remington, N. (2018). Effect of Freezing on the Shelf Life of Salmon. *International Journal of Food Science*, *2018*. https://doi.org/10.1155/2018/1686121

.

[35] Attrey, D. P. (2017). Safety and quality of frozen foods. In *Food Safety in the 21st Century: Public Health Perspective*. Elsevier Inc. https://doi.org/10.1016/B978-0-12-801773-9.00044-3

[36] Gall, C. Bisogni, C. Stark, and C. Sperazza,(2018) "Seafood Health Facts : Making Smart choices Balancing the Benefits and Risks of Seafood Consumption Resources for Healthcare Providers and Consumers Description of Omega-3 ' s and Their Role in Human Health [ 1 ]," pp. 1–2,.

[37] Sampels, S. (2015). The Effects of Storage and Preservation Technologies on the Quality of Fish Products: A Review. *Journal of Food Processing and Preservation*, *39*(6), 1206–1215. https://doi.org/10.1111/jfpp.12337

[38] Amit, S. K., Uddin, M. M., Rahman, R., Islam, S. M. R., & Khan, M. S. (2017). A review on mechanisms and commercial aspects of food preservation and processing. *Agriculture and Food Security*, *6*(1), 1–22. https://doi.org/10.1186/s40066-017-0130-8

[39] Gonçalves, A. A., & Blaha, F. (2011). Cold chain in seafood industry. Refrigeration: Theory, Technology and Applications, 287–367.

[40] Getu, A., & Misganaw, K. (2015). Post-harvesting and Major Related Problems of Fish Production. Fisheries and Aquaculture Journal, 06(04). https://doi.org/10.4172/2150-3508.1000154

[41] Debbarma,J., Viji.,P.,. Kamei, G., Sreedhar, U., and Madhusudana, R., “Fishing gear engineering for increasing for inland fishing efficiency and improved smoking process for quality smoked fish product-Training Manual,” pp. 1–11, 2018,

[42] Doan, T., Nam, C., & Programme, D. (2019). Diversifying the seafood market of finland.,” J. Mater. Sci., vol. 53, no. 13, pp. 9598–9610, 2018, doi: 10.1007/s10853-018-2233-4.

[43] Dolmacı, N., Çete, S., Arslan, F., Yaşar, A., Dolmac, N., Servet, Ç., Arslan, F., & Ya, A. (2012). An amperometric biosensor for fish freshness detection from xanthine oxidase immobilized in polypyrrole-polyvinylsulphonate film An amperometr i c b i osensor for f i sh freshness detect i on from xanth i ne ox i daseimmobilizedinpolypyrrolepoly.199.https://doi.org/10.3109/10731199.2011.646410

[44] Nickerson, M., Yan, C., Cloutier, S., & Zhang, W. (2014). Protection and Masking of Omega-3 and -6 Oils via Microencapsulation. In Microencapsulation in the Food Industry. Elsevier Inc. https://doi.org/10.1016/b978-0-12-404568-2.00037-6

[45] Mustafa, F., & Andreescu, S. (2011). Nanotechnology for the Food and Bioprocessing Industries. Food and Bioprocess Technology, 4(1), 39–47. https://doi.org/10.1007/s11947-010-0328-2

[46] Villalonga R, Diez P, Gamella M, Reviejo J, Pingarrón J.M., Electroanalysis 23:1790–1796 nanostructure and performance of carbon nanotubes in the

electrochemical for setection of hypoxanthine by enzymatic reactions, *Digest Journal of Nanomaterial and Biostructure,* volume 9, (2011), pp 1331-1338.

[47] Cifuentes, A. (2012). Food Analysis: Present, Future, and Foodomics. *ISRN Analytical Chemistry*, *2012*, 1–16. https://doi.org/10.5402/2012/801607

[48] Wen, G., Zhang, Y., Shuang, S., Dong, C., & Choi, M. M. F. (2007). Application of a biosensor for monitoring of ethanol. *Biosensors and Bioelectronics*, *23*(1), 121–129. https://doi.org/10.1016/j.bios.2007.03.024

[49] Seki, T., Orita, Y., Yamaji, K., & Shinoda, A. (1997). Simultaneous determination of creatinine, hypoxanthine and uric acid in biological samples by column-switching liquid chromatography with ultraviolet detection. In *Journal of pharmaceutical and biomedical analysis* (Vol. 15). https://doi.org/10.1016/S0731-7085(97)00011-3

[50] Zhang, L., Li, S., Xin, J., Ma, H., Pang, H., Tan, L., & Wang, X. (2019). A non-enzymatic voltammetric xanthine sensor based on the use of platinum nanoparticles loaded with a metal-organic framework of type MIL-101(Cr). Application to simultaneous detection of dopamine, uric acid, xanthine and hypoxanthine. *Microchimica Acta*, *186*(1). https://doi.org/10.1007/s00604-018-3128-4

[51] Zhu, X., Gan, X., Wang, J., Chen, T., & Li, G. (2005). A new reduction route of hypoxanthine and its nonenzymatic detection based on silver nanoparticles. *Journal of Molecular Catalysis A: Chemical*, *239*(1–2), 201–204. https://doi.org/10.1016/j.molcata.2005.06.016

[52] Torres, A. C., Ghica, M. E., & Brett, C. M. A. (2013). Design of a new hypoxanthine biosensor: Xanthine oxidase modified carbon film and multi-walled carbon nanotube/carbon film electrodes. *Analytical and Bioanalytical Chemistry*, *405*(11), 3813–3822. https://doi.org/10.1007/s00216-012-6631-1

[53] Pandey, P., & Dahiya, M. (2016). Carbon nanotubes: Types, methods of preparation and applications. *Carbon*, *1*(4), 15-21.

[54] Torabi, M., Drahansky, M., Paridah, M. ., Moradbak, A., Mohamed, A. ., Owolabi, F. abdulwahab taiwo, Asniza, M., & Abdul Khalid, S. H. . (2016). We are IntechOpen , the world ' s leading publisher of Open Access books Built by scientists , for scientists TOP 1 %. *Intech*, *i*(tourism), 13. khttps://doi.org/http://dx.doi.org/10.5772/57353

[55] Geckeler, K. E., & Premkumar, T. (2011). Carbon nanotubes: Are they dispersed or dissolved in liquids? *Nanoscale Research Letters*, *6*(1), 2–4. https://doi.org/10.1186/1556-276X-6-136

[56] Abuilaiwi, F. A., Laoui, T., Al-Harthi, M., & Atieh, M. A. (2010). Modification and functionalization of multiwalled carbon nanotube (MWCNT) via fischer esterification. *Arabian Journal for Science and Engineering*, *35*(1 C), 37–48.

[57] Michalska, M., Andrzejczuk, M., Krawczyńska, A., Roguska, A., Nikiforow, K., Żurek, P., Sikora, A., & Peikertová, P. (2021). The effect of MWCNT modification on structural and morphological properties of Li4Ti5O12. *Diamond and Related Materials*,*113*https://doi.org/10.1016/j.diamond.2021.108276

[58] Kashyap, A., Singh, N. P., Arora, S., Singh, V., & Gupta, V. K. (2020). Effect of amino-functionalization of MWCNTs on the mechanical and thermal properties of MWCNTs/epoxy composites. *Bulletin of Materials Science*, *43*(1). https://doi.org/10.1007/s12034-019-2012-0

[59] Mehra, N. K., Jain, A. K., Lodhi, N., Raj, R., Dubey, V., Mishra, D., Nahar, M., & Jain, N. K. (2008). Challenges in the use of carbon nanotubes for biomedical applications. *Critical Reviews in Therapeutic Drug Carrier Systems*, *25*(2), 169–206. https://doi.org/10.1615/CritRevTherDrugCarrierSyst.v25.i2.20

[60] Xu, J., & Wang, L. (2019). Carbon Nanomaterials. In *Nano-Inspired Biosensors for Protein Assay with Clinical Applications*. Elsevier Inc. https://doi.org/10.1016/b978-0-12-815053-5.00001-5

[61] Ando, Y., Zhao, X., Sugai, T., & Kumar, M. (2004). Growing carbon nanotubes. *Materials Today*, *7*(9), 22–29. https://doi.org/10.1016/s1369-7021(04)00446-8

[62] Dumitrescu, I., Unwin, P. R. and MacPherson, J. V. (2009) 'Electrochemistry at carbon nanotubes: Perspective and issues', *Chemical Communications*, 7345(45), pp. 6886–6901. doi: 10.1039/b909734a.

[63] Rastogi, V., Yadav, P., Bhattacharya, S. S., Mishra, A. K., Verma, N., Verma, A., & Pandit, J. K. (2014). Carbon Nanotubes: An Emerging Drug Carrier for Targeting Cancer Cells. *Journal of Drug Delivery*, *2014*(April), 1–23. https://doi.org/10.1155/2014/670815

[64] Porwal, M. (2017). An Overview on Carbon Nanotubes. *MOJ Bioequivalence & Bioavailability*, *3*(5), 114–116. https://doi.org/10.15406/mojbb.2017.03.00045

[65] Manzetti, S., & Gabriel, J.-C. P. (2019). Methods for dispersing carbon nanotubes for nanotechnology applications: liquid nanocrystals, suspensions, polyelectrolytes, colloids and organization control. *International Nano Letters*, *9*(1), 31–49. https://doi.org/10.1007/s40089-018-0260-4

[66] Rafique, I., Kausar, A., Anwar, Z., & Muhammad, B. (2016). Exploration of Epoxy Resins, Hardening Systems, and Epoxy/Carbon Nanotube Composite Designed for High Performance Materials: A Review. *Polymer - Plastics TechnologyandEngineering*,*55*(3),https://doi.org/10.1080/03602559.2015.1070874

[67] Keita, K., Okafor, F., Nyochembeng, L., Overton, A., & Sripathi, V. R. (2018). Plant and microbial growth responses to multi-walled carbon nanotubes. J

Nanosci: 123, “Plant and,” *J. Nanosci. Curr. Res.*, vol. 03, no. 02, , doi: 10.4172/2572-0813.1000123.

[68] Guo, Q., Ghadiri, R., Weigel, T., Aumann, A., Gurevich, E. L., Esen, C., Medenbach, O., Cheng, W., Chichkov, B., & Ostendorf, A. (2014). Comparison of in situ and ex situ methods for synthesis of two-photon polymerization polymernanocomposites.*Polymers*,*6*(7). https://doi.org/10.3390/polym6072037

[69] Das, S. K., Das, A. R., Guha, A. K., Nagrale, D. T., Gaikwad, A. P., Sharma, L., Lilia Anghel, G. D., Marcin NOWICKI, Marzena NOWAKOWSKA, A. N., KOZIK, E. U., Mazumdar H., H. N., Rautaray, D., Sanyal, A., Adyanthaya, S. D., Ahmad, A., Sastry, M., Samuel, J. S., Abraham, S. S. and J., Gade, A., Ingle, A., … Ikram, S. (2013). A study on biosynthesis of iron nanoparticles by Pleurotus sp. *Vegetable Crops Research Bulletin*, *8*(1), 5–19. https://doi.org/10.1016/j.jare.2015.02.007

[70] Liu, B., & Liu, J. (2019). Trends in Analytical Chemistry Sensors and biosensors based on metal oxide nanomaterials. *Trends in Analytical Chemistry*, *121*, 115690. https://doi.org/10.1016/j.trac.2019.115690

[71] Shi, X., Gu, W., Li, B., & Chen, N. (2014). *Enzymatic biosensors based on the use of metal oxide nanoparticles*. 1–22. https://doi.org/10.1007/s00604-013-1069-5

[72] Immanuel, S., Aparna, T. K., & Sivasubramanian, R. (2019). Graphene–Metal Oxide Nanocomposite Modified Electrochemical Sensors. In *Graphene-Based Electrochemical Sensors for Biomolecules*. Elsevier Inc. https://doi.org/10.1016/b978-0-12-815394-9.00005-4

[73] Akin, S., & Sonmezoglu, S. (2018). Metal Oxide Nanoparticles as Electron Transport Layer for Highly Efficient Dye-Sensitized Solar Cells. In *Emerging Materials for Energy Conversion and Storage*. Elsevier Inc.

https://doi.org/10.1016/b978-0-12-813794-9.00002-8

[74] Kim, H., & Kwon, J. Y. (2017). Enzyme immobilization on metal oxide semiconductors exploiting amine functionalized layer. *RSC Advances*, *7*(32), 19656–19661. https://doi.org/10.1039/c7ra01615h

[75] Chavali, M. S., & Nikolova, M. P. (2019). Metal oxide nanoparticles and their applications in nanotechnology. In *SN Applied Sciences* (Vol. 1, Issue 6). Springer International Publishing. https://doi.org/10.1007/s42452-019-0592-3

[76] Farzana, R., Rajarao, R., Behera, P. R., Hassan, K., & Sahajwalla, V. (2018). Zinc oxide nanoparticles from waste Zn-C battery via thermal route: Characterization and properties. *Nanomaterials* ,*8*(9). https://doi.org /10.3390/nano8090717

[77] Kolodziejczak-Radzimska, A., & Jesionowski, T. (2014). Zinc oxide-from synthesis to application: A review. *Materials*, *7*(4), 2833–2881. https://doi.org/10.3390/ma7042833

[78] Selvakumar, M., Krishna Bhat, D., Manish Aggarwal, A., Prahladh Iyer, S., & Sravani, G. (2010). Nano ZnO-activated carbon composite electrodes for supercapacitors. *Physica B: Condensed Matter*, *405*(9), 2286–2289. https://doi.org/10.1016/j.physb.2010.02.028

[79] Barzinjy, A. A., & Azeez, H. H. (2020). Green synthesis and characterization of zinc oxide nanoparticles using Eucalyptus globulus Labill . leaf extract and zinc nitrate hexahydrate salt. *SN Applied Sciences*, *2*(5), 1–14. https://doi.org/10.1007/s42452-020-2813-1

[80] Sutrave, D. S. (2018). Properties of Stacked Cobalt: Ruthenium Oxide Thin Film. *International Journal for Research in Applied Science and Engineering Technology*, *7*(1), 437–441. https://doi.org/10.22214/ijraset.2019.1076

[81] Duan, X., Wei, W., Wang, S., & Ni, B. J. (2019). Recent advances in transition metal-based electrocatalysts for alkaline hydrogen evolution. *Journal of Material ChemistryA*, *7*(25), . https://doi.org/10.1039/c9ta03220g

[82] Spataru, T., Osiceanu, P., Munteanu, C., Spataru, N., & Fujishima, A. (2012). Electrochemical preparation and characterization of a cobalt oxide-platinum composite with promising capacitive and electrocatalytic features. *Journal of Solid State Electrochemistry*, *16*(12), 3897–3905. https://doi.org/10.1007/s10008-012-1836-y

[83] Hummelgård, C., Karlsson, R. K. B., Bäckström, J., Rahman, S. M. H., Cornell, A., Eriksson, S., & Olin, H. (2013). Physical and electrochemical properties of cobalt doped (Ti,Ru)O 2 electrode coatings. *Materials Science and Engineering B: Solid-State Materials for Advanced Technology*, *178*(20), 1515–1522. https://doi.org/10.1016/j.mseb.2013.08.018

[84] Shaik, M. R., Alam, M., Adil, S. F., Kuniyil, M., Al-Warthan, A., Siddiqui, M. R. H., Tahir, M. N., Labis, J. P., & Khan, M. (2019). Solvothermal preparation and electrochemical characterization of Cubic ZrO2 Nanoparticles/Highly Reduced Graphene (HRG) based nanocomposites. *Materials*, *12*(5). https://doi.org/10.3390/ma12050711

[85] Singh, A. K., & Nakate, U. T. (2014). Microwave synthesis, characterization, and photoluminescence properties of nanocrystalline zirconia. *The Scientific World Journal*, *2014*. https://doi.org/10.1155/2014/349457

[86] Ye, M., & Shi, B. (2018). Zirconia Nanoparticles-Induced Toxic Effects in Osteoblast-Like 3T3-E1 Cells. *Nanoscale Research Letters*, *13*. https://doi.org/10.1186/s11671-018-2747-3

[87] Ishihara, A., Nagai, T., Ukita, K., Arao, M., Matsumoto, M., Yu, L., Nakamura,

T., Sekizawa, O., Takagi, Y., Matsuzawa, K., Napporn, T. W., Mitsushima, S., Uruga, T., Yokoyama, T., Iwasawa, Y., Imai, H., & Ota, K. I. (2019). Emergence of Oxygen Reduction Activity in Zirconium Oxide-Based Compounds in Acidic Media: Creation of Active Sites for the Oxygen Reduction Reaction. *Journal of Physical Chemistry C*, *123*(30), 18150–18159. https://doi.org/10.1021/acs.jpcc.9b02393

[88] Mudila, H., Rana, S., & Zaidi, M. G. H. (2016). Electrochemical performance of zirconia/graphene oxide nanocomposites cathode designed for high power density supercapacitor. *Journal of Analytical Science and Technology*, *7*(1). https://doi.org/10.1186/s40543-016-0084-7

[89] Yazdi, M. N., Yamini, Y., & Asiabi, H. (2018). Multiwall carbon nanotube-zirconium oxide nanocomposite hollow fiber solid phase microextraction for determination of polyaromatic hydrocarbons in water, coffee and tea samples. *Journal of Chromatography A*, *1554*(May), 8–15. https://doi.org/10.1016/j.chroma.2018.04.040

[90] Morozova, M., Kluson, P., Krysa, J., Vesely, M., Dzik, P., & Solcova, O. (2012). Electrochemical properties of TiO2 electrode prepared by various methods. *Procedia Engineering*, *42*(August), 573–580. https://doi.org/10.1016/j.proeng.2012.07.450

[91] Tsang, C. H. A., Li, K., Zeng, Y., Zhao, W., Zhang, T., Zhan, Y., Xie, R., Leung, D. Y. C., & Huang, H. (2019). Titanium oxide based photocatalytic materials development and their role of in the air pollutants degradation: Overview and forecast. *Environment International*, *125*(February), 200–228. https://doi.org/10.1016/j.envint.2019.01.015

[92] Kang, X., Liu, S., Dai, Z., He, Y., Song, X., & Tan, Z. (2019). Titanium dioxide: From engineering to applications. In *Catalysts* (Vol. 9, Issue 2). https://doi.org/10.3390/catal9020191

[93] Yang, W., Xu, W., Wang, Y., Chen, D., Wang, X., Cao, Y., Wu, Q., Tu, J., & Zhen, C. (2020). Photoelectrochemical Glucose Biosensor Based on the Heterogeneous Facets of Nanocrystalline TiO 2 /Au/Glucose Oxidase Films . *ACS Applied Nano Materials*, *3*(3), 2723–2732. https://doi.org/10.1021/acsanm.0c00086

[94] Vadlamani, B. S., Uppal, T., Verma, S. C., & Misra, M. (2020). Functionalized TiO2 nanotube-based electrochemical biosensor for rapid detection of SARS-CoV-2. *MedRxiv*, 1–10. https://doi.org/10.1101/2020.09.07.20190173

[95] Liu, X., Chen, C., Zhao, Y., & Jia, B. (2013). A review on the synthesis of manganese oxide nanomaterials and their applications on lithium-ion batteries. *Journal of Nanomaterials*, *2013*. https://doi.org/10.1155/2013/736375

[96] An, C., Zhang, Y., Guo, H., & Wang, Y. (2019). Metal Oxide-based Supercapacitors: Progress and Prospective. *Nanoscale Advances*. https://doi.org/10.1039/c9na00543a

[97] Vimuna, V. M., Athira, A. R., & Xavier, T. S. (2018). Microwave assisted synthesis of graphene oxide - MnO2 nanocomposites for electrochemical supercapacitors. *AIP Conference Proceedings*, *1953*. https://doi.org/10.1063/1.5032471

[98] Khan, M. M., Adil, S. F., & Al-Mayouf, A. (2015). Metal oxides as photocatalysts. *Journal of Saudi Chemical Society*, *19*(5), 462–464. https://doi.org/10.1016/j.jscs.2015.04.003

[99] Raizada, P., Soni, V., Kumar, A., Singh, P., Parwaz Khan, A. A., Asiri, A. M., Thakur, V. K., & Nguyen, V. H. (2021). Surface defect engineering of metal oxides photocatalyst for energy application and water treatment. In *Journal of Materiomics* (Vol. 7, Issue 2). Elsevier Ltd.

https://doi.org/10.1016/j.jmat.2020.10.009

.

[100] Karimi-Maleh, H., Kumar, B. G., Rajendran, S., Qin, J., Vadivel, S., Durgalakshmi, D., Gracia, F., Soto-Moscoso, M., Orooji, Y., & Karimi, F. (2020). Tuning of metal oxides photocatalytic performance using Ag nanoparticles integration. *Journal of Molecular Liquids*, *314*, 113588. https://doi.org/10.1016/j.molliq.2020.113588

[101] Leary, R., & Westwood, A. (2011). Carbonaceous nanomaterials for the enhancement of TiO2 photocatalysis. *Carbon*, *49*(3), 741–772. https://doi.org/10.1016/j.carbon.2010.10.010

[102] Pesci, F. M., Wang, G., Klug, D. R., Li, Y., & Cowan, A. J. (2013). Efficient suppression of electron–hole recombination in oxygen-deficient hydrogen-treated TiO2 nanowires for photoelectrochemical water splitting. *The Journal of Physical Chemistry C*, *117*(48), 25837-25844.

[103] Mendoza, S., Bustos, E., Manríquez, J., & Godínez, L. A. (2015). Voltammetric Techniques. *Agricultural and Food Electroanalysis*, 21–48. https://doi.org/10.1002/9781118684030

[104] Wen-zhi, L., You-qin, L. and Guang-qi, H. (2010) 'Preparation of Manganese Dioxide Modified Glassy Carbon Electrode By a Novel Film Plating/Cyclic Voltammetry Method for H(2)0(2) Detection', *Journal of the Chilean Chemical Society*, 54(4), pp. 2–7. doi: 10.4067/s0717-97072009000400009.

[105] Gan, T., Shi, Z., Sun, J., & Liu, Y. (2014). Simple and novel electrochemical sensor for the determination of tetracycline based on iron/zinc cations-exchanged montmorillonite catalyst. *Talanta*, *121*(March), 187–193. https://doi.org/10.1016/j.talanta.2014.01.002

[106] Vytřas, K. (2000). Modern Electroanalytical Methods. In *Journal of Solid State*

*Electrochemistry* (Vol. 4, Issue 6). https://doi.org/10.1007/s100080050001

[107] Dryden, M. D. M., & Wheeler, A. R. (2015). DStat: A versatile, open-source potentiostat for electroanalysis and integration. *PLoS ONE*, *10*(10), 1–17. https://doi.org/10.1371/journal.pone.0140349

[108] Collins, J., Gourdin, G., & Qu, D. (2018). Modern Applications of Green Chemistry: Renewable Energy. In *Green Chemistry: An Inclusive Approach*. Elsevier Inc. https://doi.org/10.1016/B978-0-12-809270-5.00028-5

[109] Fattah, Z. A. (2013). *Applications of bipolar electrochemistry: from materials science to biological systems* (Doctoral dissertation, Université Sciences et Technologies-Bordeaux I).

[110] Chen, S. (2007). Practical electrochemical cells. In *Handbook of Electrochemistry*. Elsevier B.V. https://doi.org/10.1016/B978-044451958-0.50003-3

[111] Kahlert, H. (2010). Reference electrodes. In *Electroanalytical Methods: Guide to Experiments and Applications*. Elsevier B.V. https://doi.org/10.1007/978-3-642-02915-8_15

[112] Szabó, S., & Bakos, I. (2010). Reference electrodes in metal corrosion. *International Journal of Corrosion*, *2010*. https://doi.org/10.1155/2010/756950

[113] Rostami, B., Mirzaei, S. I., Zamani, A., Simchi, A., & Fardmanesh, M. (2019). Development of an enhanced porosity AgAgCl reference electrode with improved stability. *Engineering Research Express*, *1*(1), 015039. https://doi.org/10.1088/2631-8695/ab4544

[114] Rowley-Neale, S. J., Brownson, D. A. C., & Banks, C. E. (2016). Defining the origins of electron transfer at screen-printed graphene-like and graphite

electrodes: MoO2 nanowire fabrication on edge plane sites reveals electrochemical insights. *Nanoscale*, *8*(33), 15241–15251. https://doi.org/10.1039/c6nr04220a

[115] Gupta, S., Smith, T., Banaszak, A., & Boeckl, J. (2017). Graphene quantum dots electrochemistry and sensitive electrocatalytic glucose sensor development. *Nanomaterials*, *7*(10). https://doi.org/10.3390/nano7100301

[116] Holmberg, S., Ghazinejad, M., Cho, E. B., George, D., Pollack, B., Perebikovsky, A., Ragan, R., & Madou, M. (2018). Stress-activated pyrolytic carbon nanofibers for electrochemical platforms. *Electrochimica Acta*, *290*, 639–648. https://doi.org/10.1016/j.electacta.2018.09.013

[117] Sutrave, D. S. (2018). A Brief Study of Cyclic Voltammetry and Electrochemical Analysis. *International Journal of ChemTech Research*, *11*(9), 77–88. https://doi.org/10.20902/ijctr.2018.110911

[118] Y. Wang., (2012)“A highly sensitive and automated method for the determination of hypoxanthine based on lab-on-valve approach using Fe3O 4/MWCNTs/β-CD modified electrode,” *Talanta*, vol. 99, pp. 840–845, 2012, doi: 10.1016/j.talanta.2012.07.040.

[119] Zong, W., Rutao, L., Sun, F., Wang, M., Zhang, P., Liu, Y., & Tian, Y. (2010). Cyclic voltammetry: A new strategy for the evaluation of oxidative damage to bovine insulin. *Protein Science*, *19*(2), 263–268. https://doi.org/10.1002/pro.313

[120] Elgrishi, N., Rountree, K. J., McCarthy, B. D., Rountree, E. S., Eisenhart, T. T., & Dempsey, J. L. (2018). A Practical Beginner’s Guide to Cyclic Voltammetry. *Journal of Chemical Education*, *95*(2), 197–206. https://doi.org/10.1021/acs.jchemed.7b00361

[121] Bezerra Dos Santos, V., Fava, E. L., Pessoa-Neto, O. D., Bianchi, S. R., Faria, R. C., & Fatibello-Filho, O. (2014). A versatile and robust electrochemical flow cell with a boron-doped diamond electrode for simultaneous determination of Zn2+ and Pb2+ ions in water samples. *Analytical Methods*, *6*(21), 8526–8534. https://doi.org/10.1039/c4ay01811g

[122] Ozkan, S. A., Kauffmann, J.-M., & Zuman, P. (2015). Electroanalysis in Pharmaceutical Biomedical and Pharmaceutical Sciences. in monographs in electrochemistry. https://doi.org/10.1007/978-3-662-47138-8_1

[123] Madej, M., Kochana, J., & Baś, B. (2019). Determination of viloxazine by differential pulse voltammetry with boron-doped diamond electrode. *Monatshefte Fur Chemie*, *150*(9), 1655–1665. https://doi.org/10.1007/s00706-019-2380-6

[124] Matthew Siebritz, R., Baker, P., & Iwuoha, E. (2011). The preparation of an immunosensor for the detection of microcystins and nodularins by immobilisation of a labelled antibody onto a polymer modified electrode. November, 1–80.

[125] White, R., & Collette, T. W. (1990). Chromatography / Fourier Transform Infrared and its Applications. *Vibrational Spectroscopy*, *1*(1), 101–102. https://doi.org/10.1016/0924-2031(90)80012-s

[126] Sandford, C., Edwards, M. A., Klunder, K. J., Hickey, D. P., Li, M., Barman, K., Sigman, M. S., White, H. S., & Minteer, S. D. (2019). A synthetic chemist's guide to electroanalytical tools for studying reaction mechanisms. *Chemical Science*, *10*(26), 6404–6422. https://doi.org/10.1039/c9sc01545k

[127] Uslu, B. (2011). The Analytical Applications of Square Wave Voltammetry on Pharmaceutical Analysis. *The Open Chemical and Biomedical Methods Journal*, *3*(1), 56–73. https://doi.org/10.2174/1875038901003010056

[128] Batchelor-Mcauley, C., Kätelhön, E., Barnes, E. O., Compton, R. G., Laborda, E., & Molina, A. (2015). Recent Advances in Voltammetry. *ChemistryOpen*, *4*(3), 224–260. https://doi.org/10.1002/open.201500042

[129] Mittal, S., Kaur, H., Gautam, N., & Mantha, A. K. (2017). Biosensors for breast cancer diagnosis: A review of bioreceptors, biotransducers and signal amplification strategies. *Biosensors and Bioelectronics*, *88*, 217–231. https://doi.org/10.1016/j.bios.2016.08.028

[130] Jung, K. W., Jeong, T. U., Hwang, M. J., Kim, K., & Ahn, K. H. (2015). Phosphate adsorption ability of biochar/Mg-Al assembled nanocomposites prepared by aluminum-electrode based electro-assisted modification method with MgCl2 as electrolyte. *Bioresource Technology*, *198*, 603–610. https://doi.org/10.1016/j.biortech.2015.09.068

[131] Pinyou, P., Ruff, A., Pöller, S., Alsaoub, S., Leimkühler, S., Wollenberger, U., & Schuhmann, W. (2016). Wiring of the aldehyde oxidoreductase PaoABC to electrode surfaces via entrapment in low potential phenothiazine-modified redox polymers. *Bioelectrochemistry*, *109*, 24–30. https://doi.org/10.1016/j.bioelechem.2015.12.005

[132] Huang, L. jun, Wang, Y. xin, Tang, J. guo, Zhao, Y. chao, Liu, G. fei, Wang, Y., Liu, J. xian, Jiao, J. qing, Wang, W., Jin, B., Belfiore, L. A., & Kipper, M. J. (2017). Graphene/silver nanocomposites stabilize Mg-Ni-La electrode alloys and enhance electrochemical performance. *Journal of Alloys and Compounds*, *694*, 1140–1148. https://doi.org/10.1016/j.jallcom.2016.10.068

[133] Bai, H., Wang, C., Chen, J., Peng, J., & Cao, Q. (2015). A novel sensitive electrochemical sensor based on in-situ polymerized molecularly imprinted membranes at graphene modified electrode for artemisinin determination. *Biosensors and Bioelectronics*, *64*. https://doi.org/10.1016/j.bios.2014.09.034

[134] Kiio, L. K. (2017). *Fabrication and Characterization of Polyaniline-Carbon Modified Electrode (Cme) Biosensor for Analysis of Bisphenol a* (Doctoral dissertation, University of Nairobi).

[135] Lu, X., & Zhao, C. (2015). Electrodeposition of hierarchically structured three-dimensional nickel-iron electrodes for efficient oxygen evolution at high current densities. *Nature Communications*, *6*. https://doi.org/10.1038/ncomms7616

[136] Naoki, Ohira, M., NishiyaKoizumi, Y., Shidama, H., Tomita, I., & Inagi, S. (2016). Electropolymerization on wireless electrodes towards conducting polymer microfibre networks. *Nature Communications*, *7*, 1–6. https://doi.org/10.1038/ncomms10404

[137] Kaviyarasu, K., Maria Magdalane, C., Kanimozhi, K., Kennedy, J., Siddhardha, B., Subba Reddy, E., Rotte, N. K., Sharma, C. S., Thema, F. T., Letsholathebe, D., Mola, G. T., & Maaza, M. (2017). Elucidation of photocatalysis, photoluminescence and antibacterial studies of ZnO thin films by spin coating method. *Journal of Photochemistry and Photobiology B: Biology*, *173*(June), 466–475. https://doi.org/10.1016/j.jphotobiol.2017.06.026

[138] Tezel, N. S., Tezel, F. M., & Kariper, I. A. (2019). Surface and electro-optical properties of amorphous Sb 2 S 3 thin films. *Applied Physics A: Materials Science and Processing*, *125*(3), 1–16. https://doi.org/10.1007/s00339-019-2475-2

[139] Chipeture, A. T., Apath, D., Moyo, M., & Shumba, M. (2019). Multiwalled carbon nanotubes decorated with bismuth (III) oxide for electrochemical detection of an antipyretic and analgesic drug paracetamol in biological samples. *Journal of Analytical Science and Technology*, *10*(1). https://doi.org/10.1186/s40543-019-0181-5

[140] Karimi-Sibaki, E., Kharicha, A., Wu, M., Ludwig, A., & Bohacek, J. (2019). Modeling electrochemical transport of ions in the molten CaF 2 –FeO slag operating under a DC voltage. *Applied Mathematics and Computation*, *357*, 357–373. https://doi.org/10.1016/j.amc.2018.01.008

.

[141] Hakizimana, J. N., Gourich, B., Chafi, M., Stiriba, Y., Vial, C., Drogui, P., & Naja, J. (2017). Electrocoagulation process in water treatment: A review of electrocoagulation modeling approaches. *Desalination*, *404*, 1–21. https://doi.org/10.1016/j.desal.2016.10.011

[142] Shida, N., Zhou, Y., & Inagi, S. (2019). Bipolar Electrochemistry: A Powerful Tool for Electrifying Functional Material Synthesis. *Accounts of Chemical Research*, *52*(9),. https://doi.org/10.1021/acs.accounts.9b0033

[143] Perera, S. I. (2019). *Structure and composition of bismuth and silver bismuth films electrodeposited from deep eutectic solvents* (Doctoral dissertation, University of Leicester).

[144] Pan, M., Yang, J., Liu, K., Yin, Z., Ma, T., Liu, S., Xu, L., & Wang, S. (2020). Noble Metal Nanostructured Materials for Chemical and Biosensing Systems. *Nanomaterials*, *10*(2), 209. https://doi.org/10.3390/nano10020209

[145] Luo, A., Lian, Q., An, Z., Li, Z., Guo, Y., Zhang, D., Xue, Z., Zhou, X., & Lu, X. (2015). Simultaneous determination of uric acid , xanthine and hypoxanthine based on sulfonic groups functionalized nitrogen-doped graphene. *JEAC*, *756*, 22–29. https://doi.org/10.1016/j.jelechem.2015.08.008

[146] Borisova, B, Alfredo S, Sandra J, Miriam, M, Pedro S, Concepción, P, José M. Pingarrón, J, and Reynaldo Villalonga. (2016). “Reduced Graphene Oxide-Carboxymethylcellulose Layered with Platinum Nanoparticles/PAMAM Dendrimer/Magnetic Nanoparticles Hybrids. Application to the Preparation of

Enzyme Electrochemical Biosensors." *Sensors and Actuators, B: Chemical* 232: 84–90. https://doi.org/10.1016/j.snb.2016.02.106.

[147] Wen, Y, Juan C, Lanjiao, X, Xiaoning, L, Ling B, Yingdong, L, and Mingfang L. (2017). "Simultaneous Analysis of Uric Acid, Xanthine and Hypoxanthine Using Voltammetric Sensor Based on Nanocomposite of Palygorskite and Nitrogen Doped Graphene." *Journal of Electroanalytical Chemistry* 805 (159–70. https://doi.org/10.1016/j.jelechem.2017.09.053.

[148] Hu, S, Jingjing, Y, Xueming, H, Longhua, G, Zhenyu, L, Fang Luo, and Bin Q., (2018). "A Sensing Platform for Hypoxanthine Detection Based on Amino-Functionalized Metal Organic Framework Nanosheet with Peroxidase Mimic and Fluorescence Properties." *Sensors and Actuators, B: Chemical* 267 (May): 312–19. https://doi.org/10.1016/j.snb.2018.04.055.

[149] Yazdanparast, S, Ali, B, Saleheh, A, and Masoud, R. (2019). "Enzyme-Based Ultrasensitive Electrochemical Biosensor Using Poly(L-Aspartic Acid)/MWCNT Bio-Nanocomposite for Xanthine Detection: A Meat Freshness Marker." *Microchemical Journal* 149 (May): 104000. https://doi.org/10.1016/j.microc.2019.104000.

[150] Chen, J, Yi, L, Fen, Y, Yuanzi, W, and Zuquan, W. (2020). "A Fluorescent Biosensor Based on Catalytic Activity of Platinum Nanoparticles for Freshness Evaluation of Aquatic Products." *Food Chemistry* 310). https://doi.org/10.1016/j.foodchem.2019.125922

[151] Mustafa, F, Ali, O, and Silvana A,. (2021). "Cerium Oxide-Based Hypoxanthine Biosensor for Fish Spoilage Monitoring." *Sensors and Actuators, B: Chemical* 332 (September 2020): 129435. https://doi.org/10.1016/j.snb.2021.129435.

# CHAPTER 3

# 3. RESEARCH METHODOLOGY

## 3.1 Introduction

This chapter provides chemicals and reagents used in the study, which are followed by methodologies undertaken to prepare various metal oxides nanoparticles and metal oxide doped multi-walled carbon nanotubes. This are followed by the characterisation techniques. Lastly, this chapter describes in full details the procedure for using the prepared biosensors on fish meat samples.

## 3.2 Chemicals and reagents

All chemicals were generally of analytical grade and were utilised as received without further purification steps. Distilled water was used for all the preparations of materials in this study. Materials and analysis were done in duplicates throughout the study. Multi-walled carbon nanotubes (MWCNTs, > 98% purity and diameter of 110-170nm), manganese nitrate hexahydrate [$Mn(NO_3)_2{\cdot}6H_2O$], Zinc nitrate hexahydrate [$Zn(NO_3)_2{\cdot}6H_2O$], cobalt nitrate hexahydrate [$Co(NO_3)_2.6H_2O$], titanium isopropoxide (TTIP), Zirconyl chloride octahydrate, nafion, and aluminum oxide ($Al_2O_3$) nanopowder, sulfuric acid ($H_2SO_4$, 98%), nitric acid ($HNO_3$, 55%), hypoxanthine (Hx), phosphate buffer (PBS), *N, N*-dimethylformamide (DMF), hydrazine ($N_2H_4$), ethylenediamine (EDA), methylenediamine ($NH_2CH_2NH_2$), and triethylenetetramine (TETA**)** were purchased from Sigma Aldrich.

## 3.3 Research Methodology

### 3.3.1 Functionalisation of the MWCNTs using acids treatment.

Pure MWCNTs without any prior functionalisation, are insoluble and poorly electroactive. Briefly, about 2 g of MWCNTs was mixed with 50 ml of $H_2SO_4$ and $HNO_3$ (3:1, v/v) ratio. But before transferring the mixture to the reflux setup, it was ultrasonicated for 30 minutes to open the nanotubes to avoid agglomeration. The ultrasonicator bath (Bandelin sonorex, Germany) was at a frequency of 35 kHz and average sonic power of 320 W. It is equipped with a temperature control knob

because any unmonitored change of temperature caused by water vibrations can damage the MWCNTs and acids may evaporate. Therefore, the temperature was strictly kept at 25 $^0$C. A reflux setup was used for the functionalisation of the MWCNTs at 70 $^0$C for 30 minutes to prevent acid loss through evaporations [1]. The oxidized MWCNTs were washed several times with distilled water until the filtrate was at pH 7. Followed by drying in an oven at 80 $^0$C for 24h. The solid MWCNTs were crushed with pestle and mortar to give powder form of MWCNTs while being observant of not destroying the nanotubes. These were denoted as oxidised MWCNTs [2].

### 3.3 2. Functionalisation of the MWCNTs using amino groups.

#### 3.3.2.1. Preparation of acyl chloride MWCNTs.

About 1g of the obtained acid treated MWCNTs were used to prepare acyl chloride MWCNTs. This was achieved by mixing 100ml of thionyl chloride (SOCl) and 30ml tetrahydrofuran (THF). The mixture was sonicated for 30 minutes at room temperature. Followed by refluxing at 80$^0$C for 24h. This process was done to convert the carboxylic groups attached to the MWCNTs to acyl chloride groups. The MWCNTs were filtered using disc teflon membranes of 3µm pore size and washed with anhydrous THF and dried at 80$^0$C for 24h. These were denoted as Acyl chloride multi-walled carbon nanotubes (MWCNTs-COCl) [3].

#### 3.3.2 2. Preparation of the amino group-MWCNTs

About 0.1g of the obtained acyl chloride treated MWCNTs were ultrasonicated with *N, N*-dimethylformamide (DMF) as the solvent and the binder for 2h in separated beakers containing hydrazine ($N_2H_4$), methylenediamine $[CH_2(NH_2)]_2$**,** ethylenediamine (EDA), and triethylenetetramine (TETA) as the amino groups' donors. The mixtures were transferred in the round bottom flasks and refluxed for 72h at 80 $^0$C. This was done to allow amide linkage between the amino group donors and the MWCNTs. The suspension was filtered, and washed with acetone, and dried

in an oven at 80 $^0$C for 24h. These were denoted as amino-functionalised MWCNTs [4].

### 3.3.4. Preparation of Metal oxides

The sol-gel method was used for the preparation of metal oxides and the metal precursors were used for their synthesis. The metal oxides prepared were manganese oxide ($MnO_2$), zinc oxide (ZnO), cobalt oxide ($Co_3O_4$), and the metal precursors were manganese nitrate hexahydrate [$Mn(NO_3)_2{\cdot}6H_2O$], Zinc nitrate hexahydrate [$Zn(NO_3)_2{\cdot}6H_2O$], and cobalt nitrate hexahydrate [$Co(NO_3)_2.6H_2O$], respectively. The metal precursor was first dissolved in 70 ml of water and 2,5 ml of ammonia ($NH_3$) was added and the reacting solution was stirred for 1 h using a magnetic stirrer at room temperature. Followed by refluxing at 100 $^0$C for 6 h. The solution was cooled and filtered using a Whatman filter paper of pore size of 11 µm. The solids were then dried at 80 $^0$C for 24 h. Followed by calcining at 300 $^0$C for 2 h [5].

To synthesize titanium dioxide ($TiO_2$) [6], zirconium oxide ($ZrO_2$) [7], and cobalt titanium oxide ($Co_2TiO_4$) [8] similar procedure was followed.

### 3.3.5 Metal oxides incorporation with the MWCNTs

The basic preparation technique for $MnO_2$-MWCNTs, ZnO-MWCNTs, and $Co_3O_4$-MWCNTs composite followed the same procedure where the metal precursor of each metal oxide-MWCNTs was first dissolved in 70 ml of water, that followed by the addition of 2.5 ml of ammonia ($NH_3$), and the reacting solution was stirred for 1 hour. The metal precursors of the composites were manganese nitrate hexahydrate, Zinc nitrate hexahydrate, and cobalt nitrate hexahydrate for $MnO_2$-MWCNTs, ZnO-MWCNTs, and $Co_3O_4$-MWCNTs, respectively. The acid treated MWCNTs were added to the reaction solution and refluxed at 100°C for 6 hours. The reaction took place under a nitrogen environment. The solution was then cooled, filtered, and dried at 50°C overnight. The final step includes the calcination of the product at 300°C for 2 hours to form the above-mentioned nanocomposite [9].

A similar procedure was followed for the preparation of $TiO_2$-MWCNTs [10] and $ZrO_2$-MWCNTs [11].

### 3.3.6. Preparations of buffer solution

The buffer which was used throughout this study was 0.1 M phosphate buffer solution (PBS) this was prepared by using both sodium phosphate dibasic and sodium phosphate monobasic solution. The solutions were prepared by weighing accurately 7.1 g of sodium phosphate dibasic and mixing it in 500 ml of water to get 0.1 M of the solution. Subsequently 6.0 g of sodium phosphate monobasic was weighed and mixed with water to give a final volume of 500 ml at a concentration of 0.1 M. To get to 0.1M PBS, the solution of 0.1 M sodium phosphate monobasic solution was added to the 0.1 M sodium phosphate dibasic solution as much as needed until the desired pH of 7.5 was reached using a Metter Toledo FE20kit FiveEasy$^{TM}$ Benchtop pH meter [11]

### 3.3.7 Characterisation techniques

#### 3.3.7.1 Fourier transform infrared spectroscopy

To determine the successful modification of the MWCNTs by attachment of metal oxides and amine groups, Fourier transform infrared (FTIR) spectroscopy was employed. The FTIR spectroscopy (Agilent Cary 600 series) with a resolution of 10 $cm^{-1}$ and 20 scans per analysis was used to analyse the functional groups present in the wavelength range from 300 to 4000 wavenumber ($cm^{-1}$). The sample area of analysis was thoroughly cleaned with 98% ethanol. Approximately 1 mg of the sample deposited on the sample area with a spatula and compressed with a knob before analysis. The background check on the instrument was done and the samples were analysed. The data obtained was in a form of Agilent Cary spectrometer software, it was converted to excel for analysis.

### 3.3.7.2 Scanning electron microscopy

The surface morphology of the nanocomposites was investigated on the Supra 55 variable pressure field emission scanning electron microscope. Sample preparation using the K553 Scanning electron microscopy (SEM) sample preparation sputter coater. Approximately 2 mg of the solid nanomaterials were mounted onto the sample stubs using a double-sided carbon tape, they were followed by carbon coating of the sample. The sample was loaded onto the sample holder for analysis projecting the same sample at different magnifications ranging from x10 000 to x60 000. The images were captured using the SmartSEM® (Carl Zeiss, Germany) software.

### 3.3.7.3 X-ray diffraction

The crystallinity, particle size, and structure of the nanomaterials were determined by X-ray diffraction (XRD, Bruker focus D8 X-ray diffractometer). The sample was firstly finely ground by pestle and mortar to allow the x-ray beam to pass through. About 1 g of the sample was put on the XRD sample holder and pressed gently inside the sample holder using a glass slide to create a smooth upper surface of the sample. The sample was successfully loaded onto the x-ray machine and scanned at a rate of 0.02 $s^{-1}$ ranging from 5 to 65$^{o}$ 2-theta (2θ), in which θ is the diffraction angle onto the detector. The data was analysed by the D8 X-ray diffractometer software and converted to excel data before plotting in the origin 8.5 software for analysis.

### 3.3.7.4. Thermogravimetric analysis

The investigation of the thermal stability of the nanomaterials was done using the Simultaneous thermal analyzer (STA) 4000 PerkinElmer system. Approximately 10 mg of the sample was placed in a furnace pan and placed in an instrument. The temperature of the system was kept at 25 $^{0}$C initially and increased gradually to 900 $^{0}$C at 10 $^{0}$C/min, under the oxidative atmosphere of nitrogen gas at 50 mL/min. The informative data obtained from the TGA gives data regarding the thermal stability, purity of the composition of the nanocomposites.

### 3.3.8. Electrochemical studies

Electrochemical studies were carried out in a three-electrode cell, using the Basi Epsilon with the C3-cell stand. Silver-silver chloride (Ag/AgCl) electrode was used as a reference, platinum wire as the auxiliary electrode, and Glassy carbon electrode (GCE) as the working electrode.

#### 3.3.8.1 Fabrication of the electrode

The metal oxide-amine functionalized-MWCNTs nanocomposite (1mg) was dispersed in 5ml of ethanol and sonicated for 10 minutes to get a homogeneous suspension. Before surface modification of the GCE, the electrode was polished with 0.3mM of aluminum oxide nano powder slurry and rinsed with water. Then the electrode was sonicated in a mixture of ethanol and water in (1:1, v/v) ratio for 15 minutes to further remove any bound material on the surface of the electrode. The electrode was air-dried at room temperature before modifications. About 20 µL of the suspension was dropped onto the freshly polished electrode and dried for 30minutes at room temperature to get the metal oxide-amine functionalized-MWCNTs modified electrode. Then, 20 µL (0.5 U) of the enzyme, xanthine oxidase (XO) was dropped onto the electrode and was allowed to dry at room temperature for 2 h. To confirm the stable attachment of the nanocomposite onto the electrode, it was further coated with 5 µL of 5% Nafion. This electrode was stored at $5^0$C when not in use [13].

### 3.8.2. Preparation of electrodes and their electrochemical measurements

Electrochemical studies of fabricated electrodes were studied using a three-electrode system (BASi epsilon) at room temperature in a 5 mM ferrocyanide solution. Cyclic voltammetric (CV) measurements were carried out in a potential window of -200 to 1400 mV at a scan rate of 100 mV/s to determine the best metal oxides and determine the surface coverage and diffusion coefficient of the nanomaterials.

The experiments of hypoxanthine detection were carried out under the following conditions a 1mM of hypoxanthine concentration in phosphate buffer solution at pH

7.5. The analysis was carried out with CV and differential pulse voltammetry (DPV) all at the potential window of -200 to 1400 mV.

### 3.3.9. Fish meat analysis.

Three fishes of the same species named *Argyrozona Argyrozona* were purchased from the local market and analysed on their first day of arrival in the University laboratory. These fishes were kept at 3 different temperatures which were -15 $^0$C,5 $^0$C, and 25 $^0$C. The three fishes were analysed for seven days as follows: About 10 g of the fish meat was sliced, minced with a pestle and mortar, and mixed with 30 ml of PBS of pH 7.5. The solution was filtered with the Whatman filter paper with 11 µm pore size. The filtered solution was transferred onto a C3 cell stand and analysed using cyclic voltammetry (CV) and Differential pulse voltammetry (DPV) at a potential window of -200 to 1400 mV [14].

Figure 3.1. Presents 3 fishes of the same species named *Argyrozona Argyrozona* which were suspended at 3 different temperatures to study the hypoxanthine concentration using 3%$Co_2TiO_4$-MWCNTs-TETA.

## 3.4. REFERENCES


[1].Thi Mai Hoa, L. (2018) ‘Characterization of multi-walled carbon nanotubes functionalized by a mixture of HNO3/H2SO4’, *Diamond and Related Materials*. Elsevier, 89(May), pp. 43–51. doi: 10.1016/j.diamond.2018.08.008.

[2]. Jun, L. Y., Mubarak, N. M., Yon, L. S., Bing, C. H., Khalid, M., & Abdullah, E. C. (2018). Comparative study of acid functionalization of carbon nanotube via ultrasonic and reflux mechanism. *Journal of environmental chemical engineering*, *6*(5), 5889-5896..

[3] Soleimani, M., Ghahraman Afshar, M. & Sedghi, A.( 2013) Amino-Functionalization of Multiwall Carbon Nanotubes and Its Use for Solid Phase Extraction of Mercury Ions from Fish Sample. *ISRN Nanotechnology.*,1–8 (2013).

[4] Kashyap, A., Singh, N. P., Arora, S., Singh, V., & Gupta, V. K. (2020). Effect of amino-functionalization of MWCNTs on the mechanical and thermal properties of MWCNTs/epoxy composites. *Bulletin of Materials Science*, *43*(1). https://doi.org/10.1007/s12034-019-2012-0

[5] Mkhondo, N. B. and Magadzu, T. (2018) ‘Surface properties of metal oxides and their role on electrochemical hydrogen storage of carbon nanotubes’, *Digest Journal of Nanomaterials and Biostructures*, 13(4), pp. 921–929

[6] Ashkarran, A. A., Fakhari, M., Hamidinezhad, H., Haddadi, H. & Nourani, M. R. (2015) 'TiO2 nanoparticles immobilized on carbon nanotubes for enhanced visible-light photo-induced activity'. *J. Mater. Res. Technol.* **4**, 126–132. doi.org/10.1016/j.jmrt.2014.10.005.

[7]. Sigwadi, R. Dhlamini, M. (2019) ‘Preparation of a high surface area zirconium oxide for fuel cell application’, *International Journal of Mechanical and Materials Engineering*, 14(1). doi: 10.1186/s40712-019-0102-9.

[8]. Venegas, Constanza J., Fabiana A. Gutierrez, Marcos Egu, Jos F. Marco, Nik Reeves-mclaren, Gustavo A. Rivas, Domingo Ruiz-le, and Soledad Bollo. n.d. (2019) “Co 2 TiO 4 / Reduced Graphene Oxide Nanohybrids for Electrochemical Sensing Applications.” 1–18

[9] .Masipa, P. M., Magadzu, T. and Mkhondo, B. (2013) ‘Decoration of multi-walled carbon nanotubes by metal nanoparticles and metal oxides using chemical evaporation method’, *South African Journal of Chemistry*, 66, pp. 173–178.

[10]. Ashkarran, A. A., Fakhari, M., Hamidinezhad, H., Haddadi, H. & Nourani, M. R. (2015) 'TiO2 nanoparticles immobilized on carbon nanotubes for enhanced visible-light photo-induced activity'. *J. Mater. Res. Technol.* **4**, 126–132. doi.org/10.1016/j.jmrt.2014.10.005.

[11]. Wang, Z., Xia, J. (2013) 'Fabrication and characterization of a zirconia/multi-walled-carbon nanotube mesoporous composite'. *Mater. Sci. Eng. C* **33**, 3931–3934. DOI: 10.1016/j.msec.2013.05.031

[12]. Ganesh, K., Soumen, R. (2017) ‘Dynamic approach to predict pH profiles of biologically relevant buffers’, *Biochemistry and Biophysics Reports*, 9(November 2016), pp. 121–127. doi: 10.1016/j.bbrep.2016.11.017

[13]. Sokolov, A. N., Roberts, M. E. and Bao, Z. (2009) ‘Fabrication of low-cost electronic biosensors’, *Materials Today*. Elsevier Ltd, 12(9), pp. 12–20. doi: 10.1016/S1369-7021(09)70247-0.

[14]. Kumar, A. S. and Shanmugam, R. (2011) ‘Simple method for simultaneous detection of uric acid, xanthine and hypoxanthine in fish samples using a glassy carbon electrode modified with as commercially received multiwalled carbon nanotubes’, *Analytical Methods*, 3(9), pp. 2088–2094. doi: 10.1039/c1ay05065f.

# CHAPTER 4

# 4. Results and Discussion

## 4.1. Introduction.

This chapter consists of discussion of the results obtained while investigating the electrochemical behaviour and the detection mechanism of hypoxanthine using metal oxides modified multi-walled carbon nanotubes-based biosensor. The first part of the study has focused on functionalising MWCNTs with amine-containing agents from hydrazine, methylenediamine, ethylenediamine (EDA), and triethylenetetramine (TETA). The main aim of this study was to check the effect of increasing the organic length of the amine-containing agents on the current response in producing a highly sensitive biosensor for the determination of hypoxanthine (Hx). The second part deals with the comparative study of the metal oxides (MO) doped amine functionalised MWCNTs to further increase the stability and reusability of the biosensor. The MO-modified MWCNTs (MO = manganese dioxide ($MnO_2$), titanium dioxide ($TiO_2$), zirconium dioxide ($ZrO_2$), cobalt dioxide ($Co_3O_4$), and zinc oxide (ZnO)). While comparing metal oxides this work also include comparative of mono metallic and bi metallic biosensors towards the effect of metallic bond on the stability of the biosensor. The third part of this study focuses on the photocatalytic investigations of metal oxide doped amine functionalised MWCNTs. This work contributes to the new studies of photocatalytic studies of metal oxides and MWCNTs in improving sensitivity using light and increasing the organic length of amine containing agents towards the stability of the biosensor. The structure of prepared metal oxides amine functionalised MWCNTs were confirmed by Fourier-transform infrared spectroscopy (FTIR), Scanning electron microscope (SEM), Thermal gravimetric analysis (TGA), and X-ray diffraction (XRD.

## 4.2. Characterisation of the synthesised nanocomposites materials

### 4.2.1. Fourier-transform infrared spectroscopy

#### 4.2.1.1. FTIR of the raw, acid and amino functionalised MWCNTs

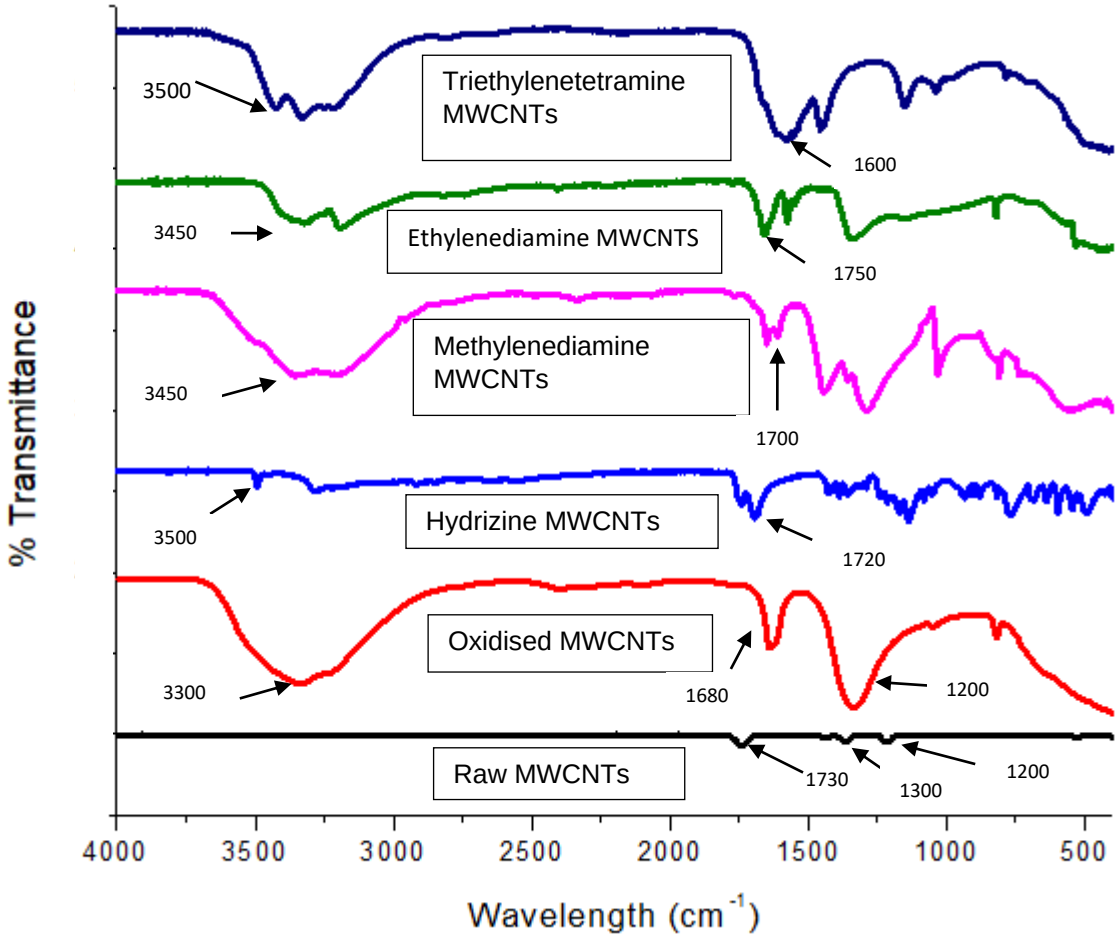


Figure 4 1. Presents surface functionalisation of the MWCNTs by acidic and amino groups from raw MWCNTs

The data in figure 4.1 shows FTIR profiles of raw-, oxidised-, hydrazine-, methylenediamine, ethylenediamine, and triethylenetetramine MWCNTs. The raw-MWCNTs have some weak stretching bands at around 1200, 1300, and 1730 $cm^{-1}$ which corresponds to =C-H and C=C respectively. They do not have many peaks presents which correspond with the fact that the raw MWCNTs are highly insoluble

due to the lack of functional group that increases their interaction with solvents [1]. The oxidised MWCNTs shows an increment in the intensity of the peaks. There is a broad peak at around 3300 $cm^{-1}$ which is caused by the vibrations of the hydroxyl group (OH) and the stretching band at around 1680 $cm^{-1}$ is reported to be that of the carbonyl carbon, this type of bands confirms the presence of carboxylic group (COOH) deposited by acid treatment [2]. Furthermore, there is a clear peak at around 1200 $cm^{-1}$ bands this is reported to be that of C=O vibrations at the different chemical environment, examples are ketones or aldehydes. [3]. The amino-functionalised MWCNTs (i.e., hydrazine, methylenediamine, ethylenediamine, and triethylenetetramine) shows a significant double stretch band that is appearing at 1600 $cm^{-1}$ to 1700 $cm^{-1}$, this is due to the amino ($NH_2$) deformation of hydrogen-bonded amine [4]. Furthermore, another peak appears at 3450 $cm^{-1}$ to 3500 $cm^{-1}$ which is associated with C-H stretching of $CH_2$-$NH_2$ groups. The presents of these bands confirm the successful deposition of the amino groups on the surface of MWCNTs [5].

#### 4.2.1.2. FTIR profiles of $TiO_2$, MWCNTs-TETA and 5% $TiO_2$-MWCNTs-TETA

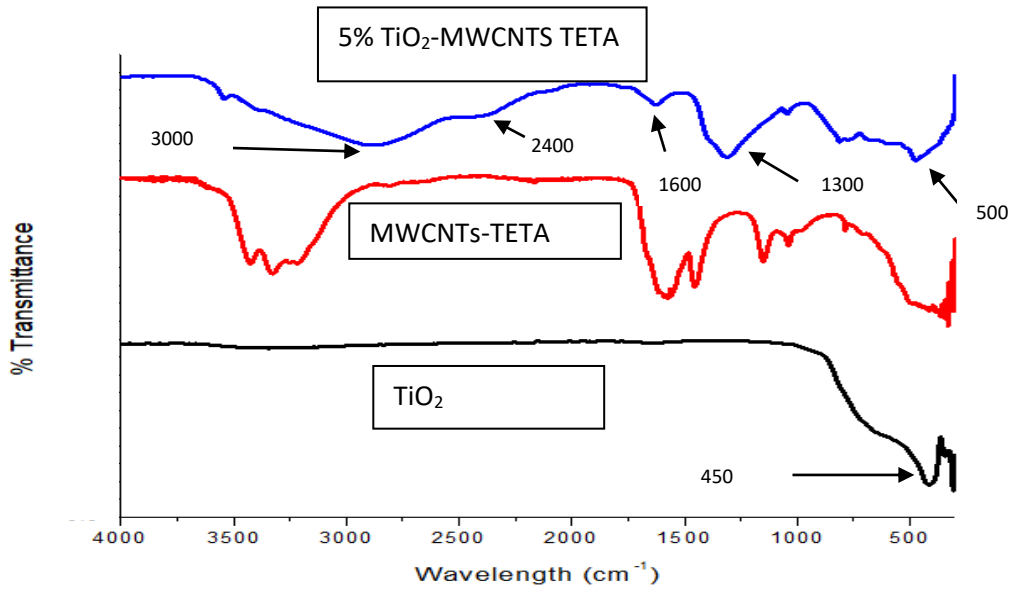


Figure 4 2. FTIR results of $TiO_2$, MWCNTs-TETA and 5% TiO2-MWCNTs-TETA

The FTIR spectra of the synthesised $TiO_2$, MWCNTs-TETA and 5% $TiO_2$ MWCNTs-TETA are shown in figure 4.2. The formation of nano $TiO_2$ was confirmed by the characteristic peak observed at 450 $cm^{-1}$ and this type of band is caused by the Ti-O stretching [6]. For the nanocomposite of 5% $TiO_2$-MWCNTs-TETA, the peaks at 1,300 and 1600 $cm^{-1}$ correspond to symmetric and asymmetric stretching vibrations of the adsorbed isopropanol, carboxylic group coordinating to titanium metal during their synthesis [7]. There is also a significant peak appearing at 500 $cm^{-1}$ on the nanocomposite. This confirms the successful deposition of the $TiO_2$ on the walls of MWCNTs. There is again the presence of a peak at 2400 $cm^{-1}$ which corresponds to the formation of metal-carbon bonding where the activated carbon or MWCNTs are functionalised with C=O functional groups before incorporating the metal oxide [8].

### 4.2.1.3. FTIR profile of $ZrO_2$, MWCNTs-TETA and 5% $ZrO_2$-MWCNTs-TETA

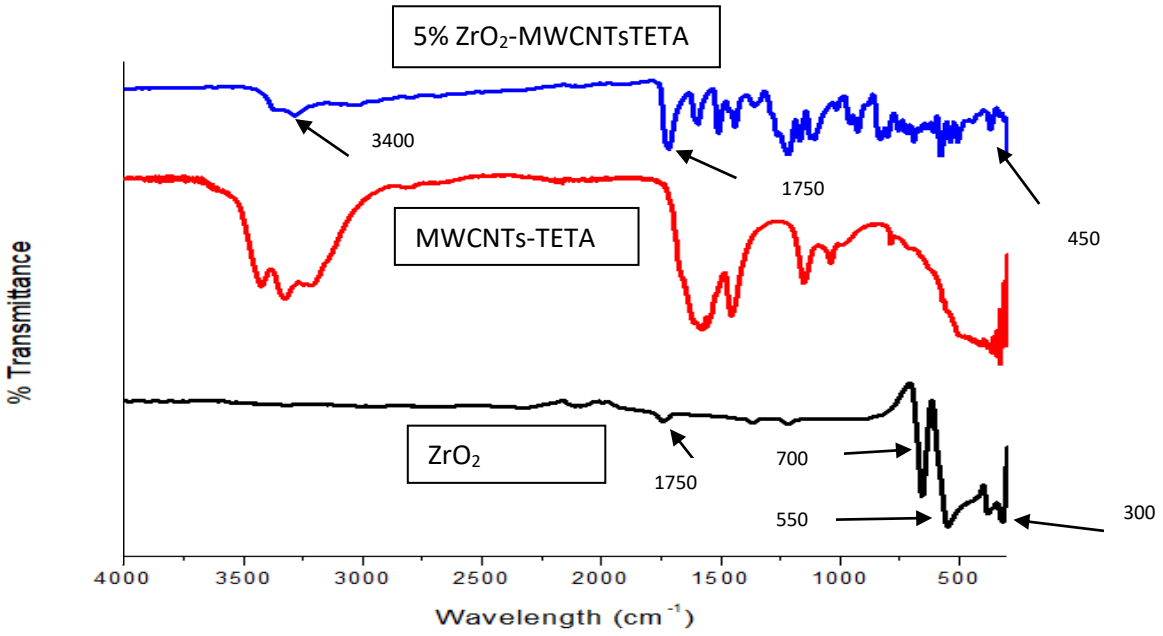


Figure 4 3. FTIR spectra of $ZrO_2$,MWCNTs-TETA and 5% $ZrO_2$-MWCNTs-TETA

The FTIR spectra of the as-synthesised inorganic/organic hybrid of zirconium dioxide ($ZrO_2$) nanoparticles, MWCNTs-TETA and 5% $ZrO_2$-MWCNTs-TETA are shown in Figure 4.3. The strong absorptions at 300, 550, and 700 $cm^{-1}$ on the $ZrO_2$ spectrum,

are designated to Zr-O vibrations. Whereas the less intense absorption band which appears at 1750 $cm^{-1}$ is characteristic of the bending vibration of water molecules. It is uncertain whether the water observed in these spectra reflects the composition of the surface resulting from the heating process or water which had rapidly attached to the surface during cooling [9]. On the 5% $ZrO_2$-MWCNTS-TETA, there is a presence of significant peak which appears at 450 $cm^{-1}$ due to the vibration of Zr-O on the walls of MWCNTs and confirms the successful modifications of the MWCNTs with $ZrO_2$

#### 4.2.1.4. FTIR profile of $MnO_2$, MWCNTs-TETA, and 5% $MnO_2$- MWCNTs-TETA

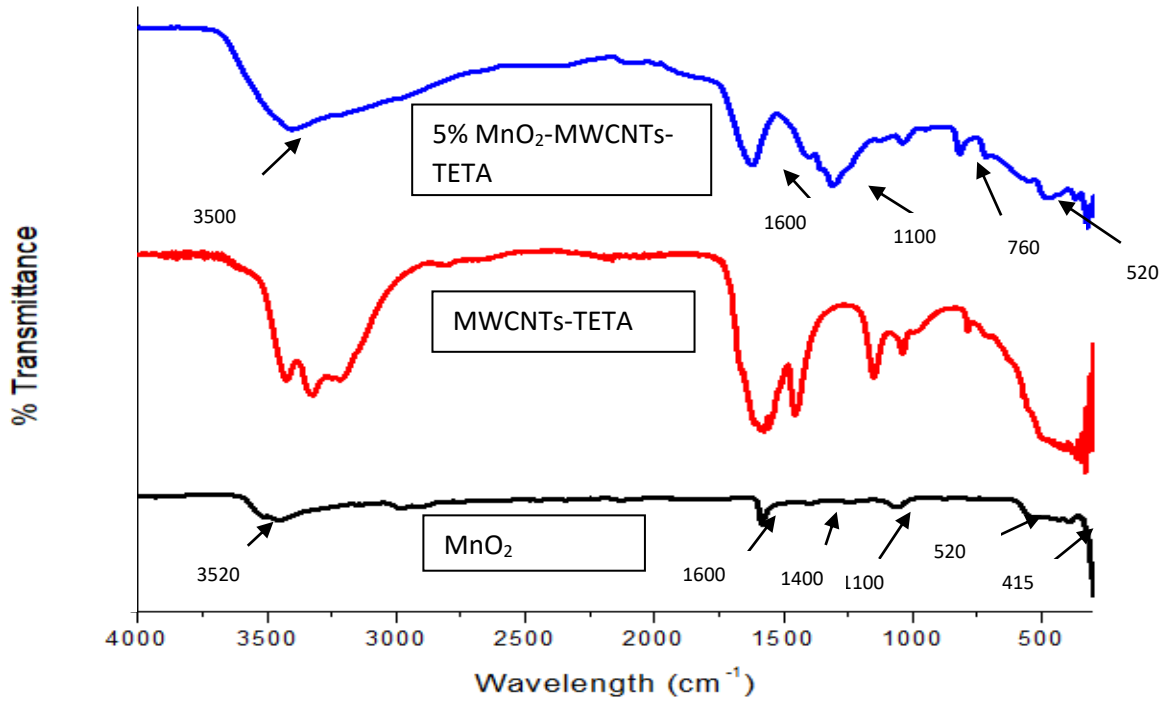


Figure 4.4: The FTIR results of manganese dioxide, MWCNTs-TETA and 5% $MnO_2$-MWCNTs-TETA

The FTIR data of the synthesised manganese oxide ($MnO_2$), MWCNTs-TETA and 5% $MnO_2$-MWCNTs-TETA nanocomposites are shown in figure 4.4. Low intense peaks at around 415 and 520 $cm^{-1}$ on the $MnO_2$ spectrum are observed; these are due to Mn–O vibrations and agrees with the literature data [10,11]. Mn–O stretching

modes occur in the higher wavenumber region and Mn–O bending vibrations in the lower wavenumber region [12]. The vibrational mode at 1100 $cm^{-1}$ corresponds to the stretching vibration of Mn–O bonds in $MnO_6$ octahedral along the double chain of $MnO_2$ [13]. The weak band observed at around 1400 $cm^{-1}$ is assigned to the vibration of the $Mn^{3+}$–O bond. This confirms the presence of $Mn^{3+}$ in the $MnO_2$ tunnel structure [14]. This FTIR analysis is consistent with the results reported in the literature [15]. The FTIR spectra help locate the presence of the OH groups as well as water molecules that may be present as bound water within the crystal structure. However, in the case of $MnO_2$ particles, they are three types of structures that bond differently to the OH group in the crystal structure of manganese dioxide, and these are α-$MnO_2$, β-$MnO_2$, and the γ-$MnO_2$. The α-$MnO_2$, exhibiting absorption around 3500 $cm^{-1}$, does not show an absorption band around 1620 $cm^{-1}$. This suggests that the OH groups are linked differently in the β-$MnO_2$ crystal whereby of β-$MnO_2$ samples, bands are visible at 3400 and 1620 $cm^{-1}$ and lastly, the absorption bands corresponding to the OH group are absent for γ-$MnO_2$ [16]. From this information, the conclusion was safely reached that the synthesised $MnO_2$ is the β-$MnO_2$ due to the presence of both peaks at 1600 and 3500 $cm^{-1}$. In addition, mineral structures such as $MnO_2$ have stronger bonds and weaker vibrations that decrease the peak intensity in FTIR results [16]. On the nanocomposite, the presence of a less intense peak at a lower wavelength around 450 $cm^{-1}$ corresponds to the $MnO_2$ attached to the walls of the MWCNTs.

### 4.2.1.5. FTIR results of $Co_3O_4$, MWCNTs-TETA, and 5% $Co_3O_4$- MWCNTs-TETA

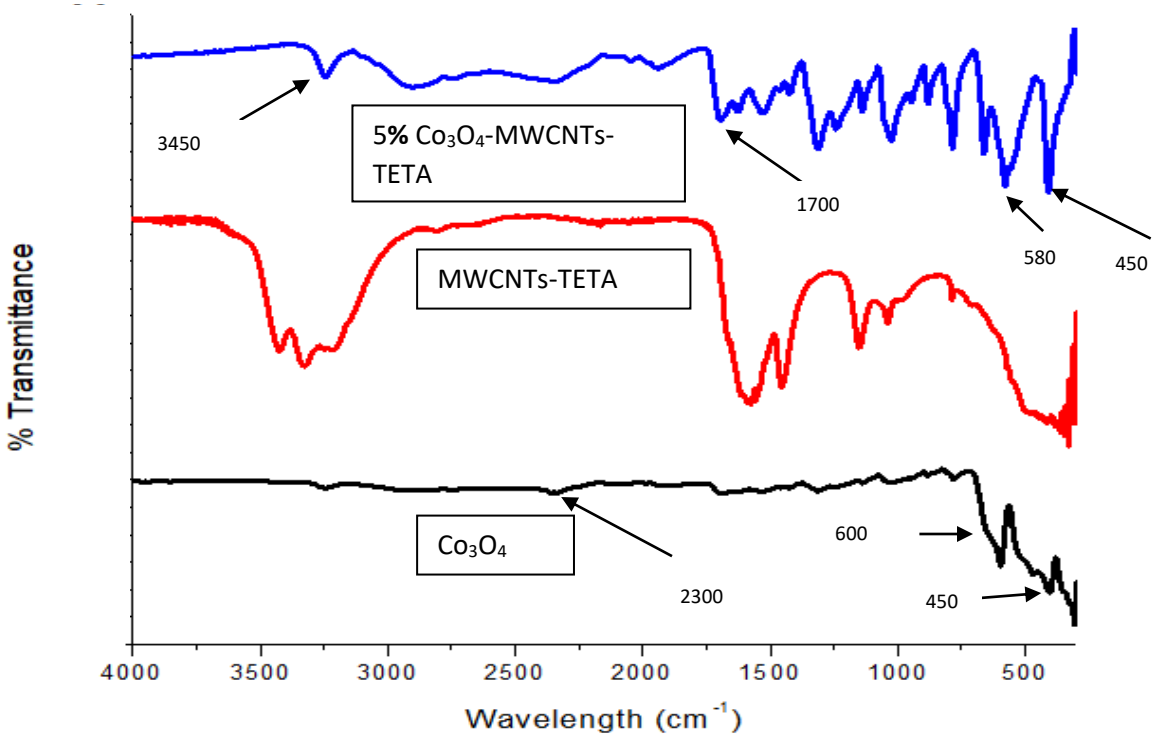


Figure 4 5. FTIR results of $Co_3O_4$, MWCNTs-TETA, and 5% $Co_3O_4$-MWCNTs-TETA

The FTIR spectroscopy was used to confirm the as-synthesised $Co_3O_4$, MWCNTs-TETA, and 5% $Co_3O_4$-MWCNTs-TETA composites as shown in figure 4.5. The appearance of two metal-oxygen vibration peaks at lower wavelength on the $Co_3O_4$ spectra corresponds to the formation of $Co_3O_4$ spinel lattice [17]. The band at 450 $cm^{-1}$ corresponds to the stretching peak of the $Co^{3+}$ and O bond where $Co^{3+}$ is present at the octahedral holes. The other band at 600 $cm^{-1}$ is attributed to the stretching vibration of $Co^{2+}$ and O bond where $Co^{2+}$ present at the tetrahedral hole of the spinel lattice [18]. There is the presence of a weak band at 2300 $cm^{-1}$ which is designated to be that of symmetric and anti-symmetric stretching of Co-O bond. Such bands correspond to the vibration of the C=O bond in the metal carbonyl compounds [18]. On the 5% $Co_3O_4$-MWCNTs-TETA spectra, the significant peaks at a lower wavelength around 450 and 580 $cm^{-1}$ are those of Co-O vibrations in the presence of the MWCNTs. This concludes that $Co_3O_4$ was successfully deposited on the MWCNTs.

### 4.2.1.6. FTIR profile of ZnO, MWCNTs-TETA, and 5% ZnO- MWCNTs-TETA

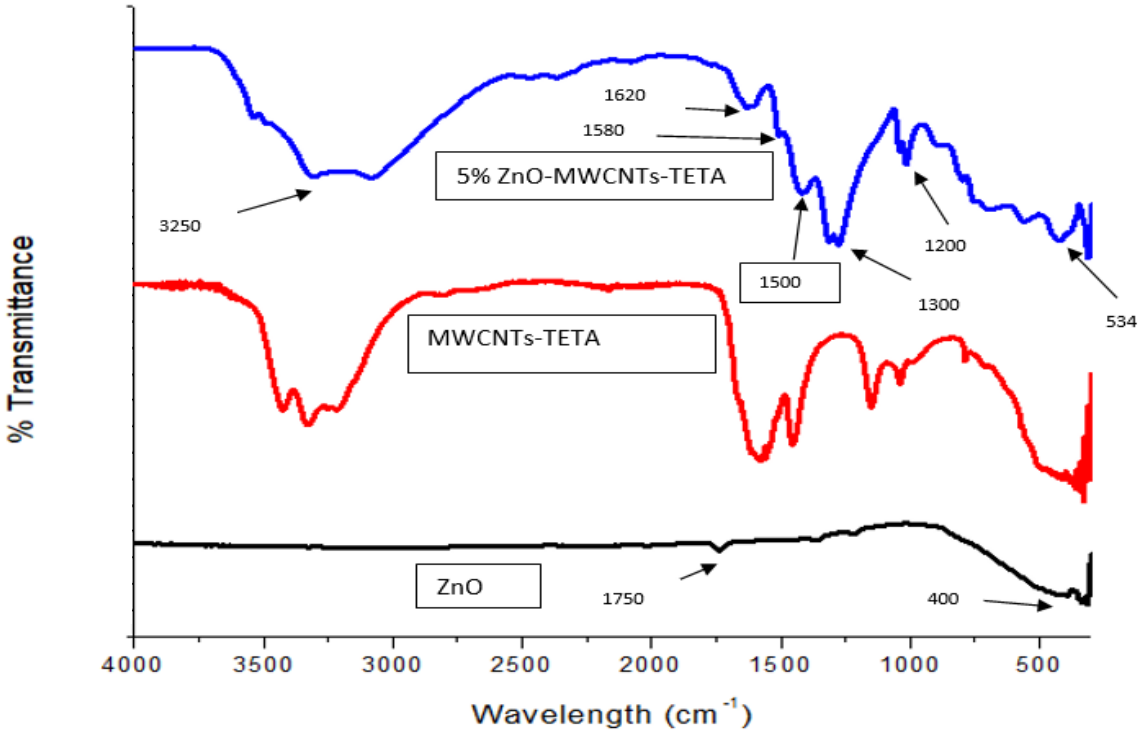


Figure 4 6: FTIR spectra of ZnO,MWCNTs-TETA, and 5% ZnO-MWCNTs-TETA

The spectrum of ZnO, MWCNTs-TETA, and 5% ZnO-MWCNTs-TETA are shown in figure 4.6. From the results of ZnO, the band at 400 $cm^{-1}$ is due to the Zn-O stretching mode, which indicates the formation of ZnO, it is also observed that there is an absence of the O-H group due to the drying process after their synthesis. This further confirms that the ZnO produced is pure with no adsorbed water molecules, and similar results were observed elsewhere [19]. On the 5% ZnO-MWCNTs-TETA, the peaks at 1200 and 1300 $cm^{-1}$ are due to nitrate ($NO_3^-$) bonding which might be due to the absorption of the TETA on the MWCNTs [20]. There are three bands with very low intensity at 1500, 1580 and 1620 $cm^{-1}$ corresponding to the C=C, C-O, and absorbed water, respectively, which appears on the surface of the molecule due to the oxidation of the MWCNTs before forming the composite with the zinc oxide [21]. There are also the weak bands at 534 $cm^{-1}$ on the 5% ZnO-MWCNTs-TETA and such bands are reported to be due to Zn-O stretching in the presence of MWCNTs [22]. Additional peaks which appear on the 5% ZnO-MWCNTs-TETA

nanocomposites, but absence in both the spectra of ZnO and MWCNTs-TETA are due to the effects of metal oxide doping on functionalised MWCNTs. These effects should owe to an interaction between ZnO and MWCNTs-TETA towards the formation of a new bond within the structure of ZnO-MWCNTs-TETA [23].

#### 4.2.1.7. FTIR profile of $Co_2TiO_4$, MWCNTs-TETA, and 3% $Co_2TiO_4$ - MWCNTs-TETA

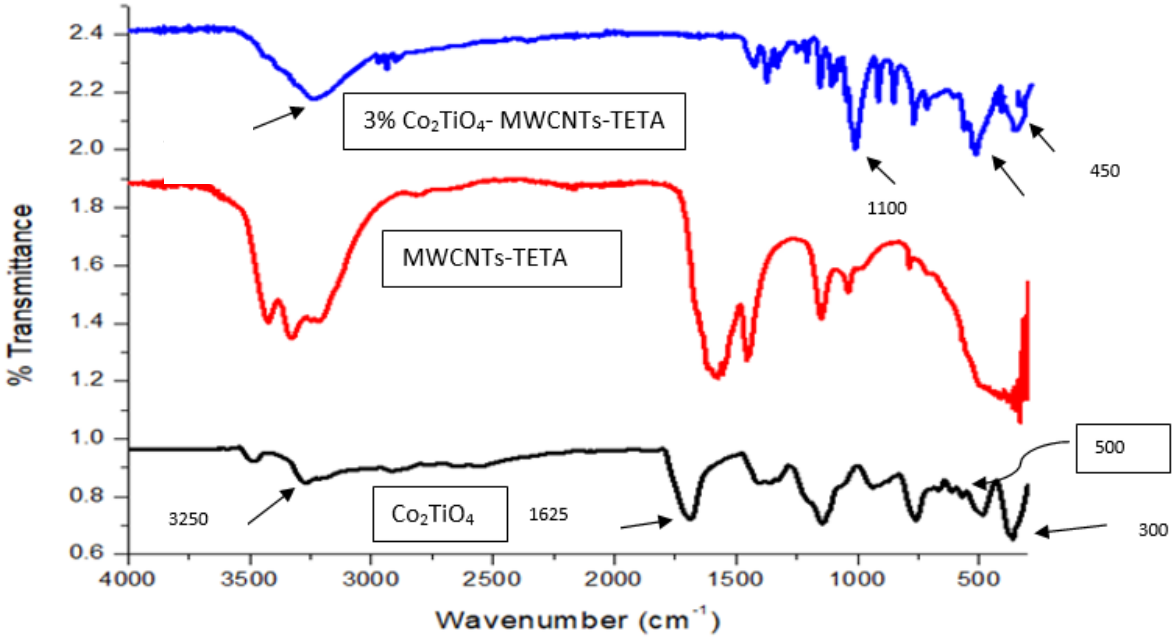


Figure 4 7: FTIR spectra of $Co_2TiO_4$, MWCNTs-TETA, and 3% $Co_2TiO_4$-MWCNTs-TETA

The analysis of the synthesised bimetallic nanoparticles, cobalt titanium oxide ($Co_2TiO_4$) and their nanocomposites (3% $Co_2TiO_4$-MWCNTs-TETA) were studied with FTIR as shown in figure 4.7. The results show the presence of both titanium and cobalt at 300 and 500 $cm^{-1}$. The is also the presence of hydroxyl group (OH) at 3250 $cm^{-1}$, this can be attributed to water molecules absorbed during their synthesis. On the spectrum of 3% $Co_2TiO_4$-MWCNTs-TETA the results show the presence of both titanium and cobalt at lower wavelengths, such band confirm successful deposition of the bimetallic nanoparticles onto the walls of the carbon nanotubes

### 4.2.2. X-ray diffraction analysis

#### 4.2.2.1. XRD patterns of $TiO_2$, MWCNTs-TETA, and $TiO_2$-MWCNTs-TETA

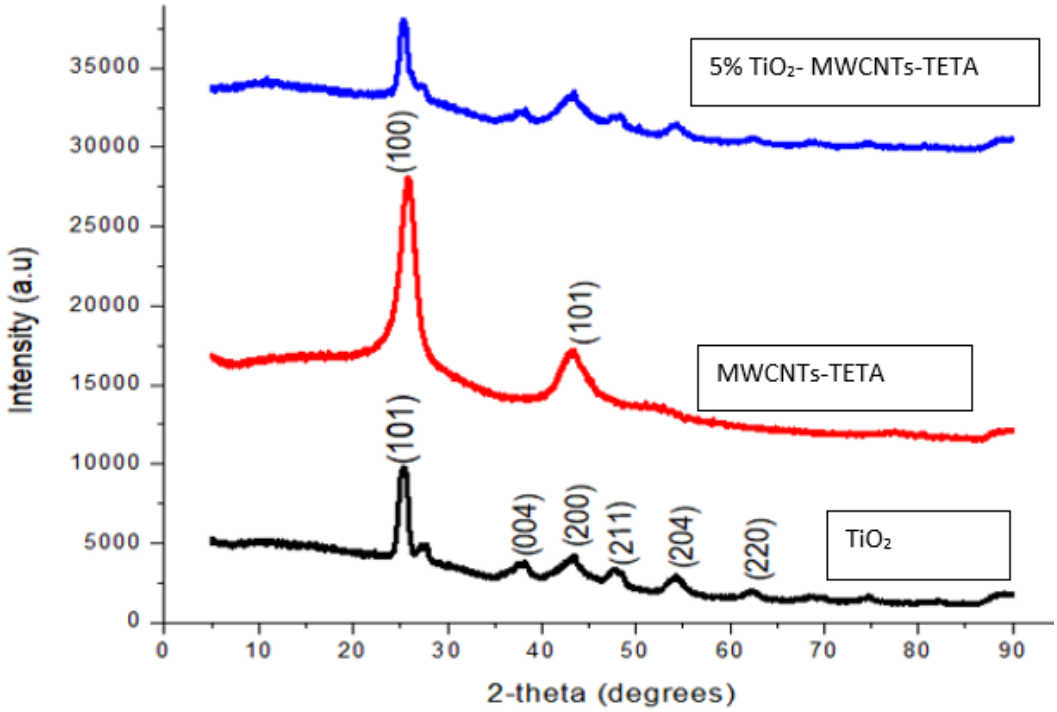


Figure 4.8. XRD patterns of $TiO_2$, MWCNTs-TETA, and 5% $TiO_2$-MWCNTs-TETA

The X-ray diffraction patterns of the synthesised titanium dioxide nanoparticles, MWCNTs-TETA, and 5% $TiO_2$-MWCNTs-TETA are showed in figure 4.8. The strong diffraction peak at 25° and a broad peak at 45° indicate that the titania nanoparticles are in the anatase phase. All the peaks are in agreement with the literature of diffraction pattern of titanium nanoparticles [24]. The literature has indicated that the diffraction peak intensity of titania nanoparticles increases with particles size. However, from the results this suggests that these nanoparticles compose of irregular polycrystalline structure. The low intensity peaks revealed the amorphous structure of the nanoparticles. Despite this the amorphous broadening of XRD peaks in nanosized materials is negligible [25]. The MWCNTs-TETA, data shows the first peak at 26° that can be assigned to the (002) reflection of graphite. The symmetric

diffraction peak at 43° is assigned to the (100) reflection of graphite, which is typically observed in MWCNTs [26]. The final results are that of the 5% $TiO_2$-MWCNTs-TETA, and the data show the presence of all peaks mentioned in the $TiO_2$ and MWCNTs-TETA, which confirms the successful preparation of the composite.

#### 4.2.2.2. XRD patterns of $Co_3O_4$, MWCNTs-TETA, and 5% $Co_3O_4$-MWCNTs-TETA

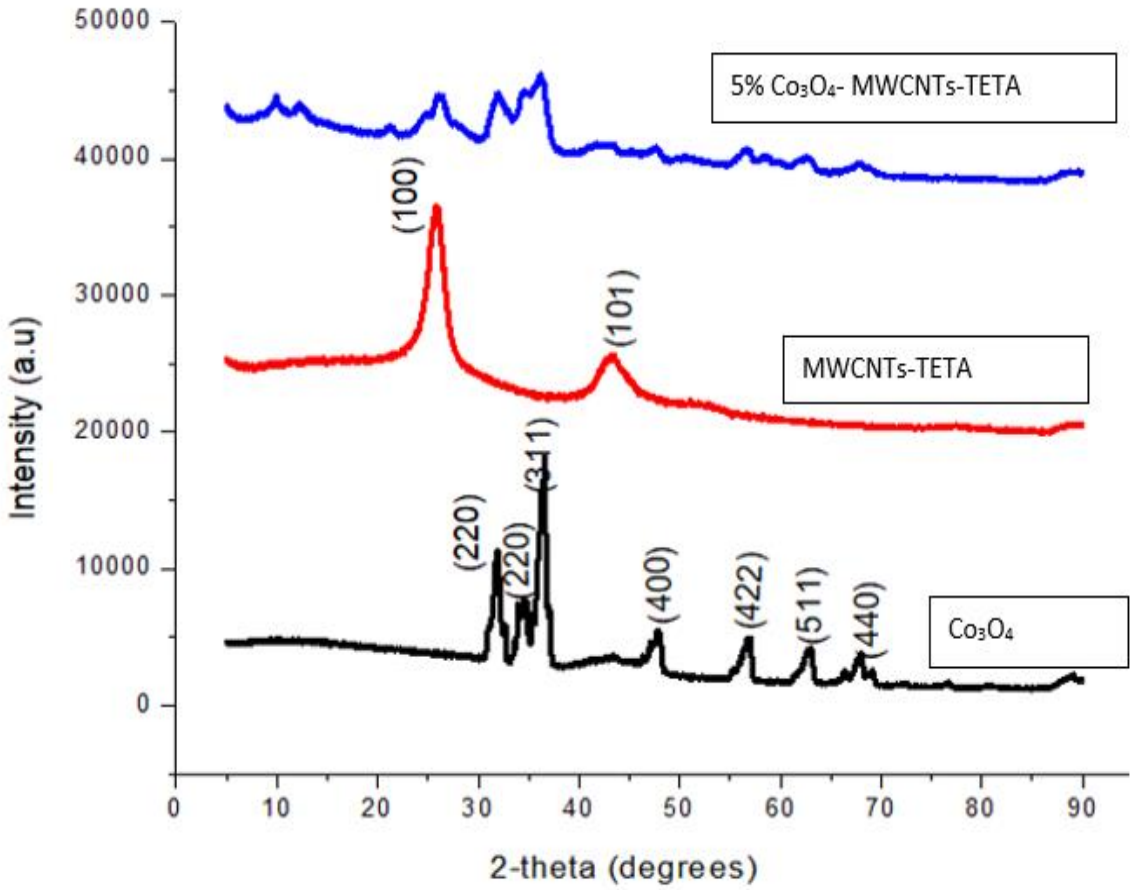


Figure 4 9. XRD patterns of $Co_3O_4$, MWCNTs-TETA, and 5% $Co_3O_4$-MWCNTs-TETA

The XRD pattern of the as synthesised cobalt oxide, MWCNTs-TETA, and 5% $Co_3O_4$-MWCNTs-TETA are shown in figure 4.9. The results demonstrate nanocomposite formation, which contained CoO and $Co_3O_4$. The profile shows a sequence of highly intense peaks at 31, 36 and 38° that are indexed to planes of (220), (311), and (222), respectively. Furthermore, these diffraction peaks can be indexed as typical cubic spinel structure of $Co_3O_4$ [27]. The second series of peaks

are observed on the cobalt oxide structure at 46, 56, 62 and 69° and are indexed planes of (400), (422), (511), and (440), respectively. These planes are similar to those reported for the CoO cubic structure [28]. From the results, no other phases were observed in the XRD patterns. These results suggested that the synthesised cobalt oxides particles consisted of the mixture of $Co_3O_4$ cubic spinel structure and CoO cubic structure. On the 5% $Co_3O_4$-MWCNTs-TETA composite the presence of all peaks confirms the successful deposition of the cobalt oxide nanoparticles on the walls of carbon nanotubes

#### 4.2.2.3. XRD patterns of 5%$Co_3O_4$-MWCNTs-TETA, 5% $TiO_2$-MWCNTs-TETA, and 3% $Co_2TiO_4$-MWCNTs-TETA

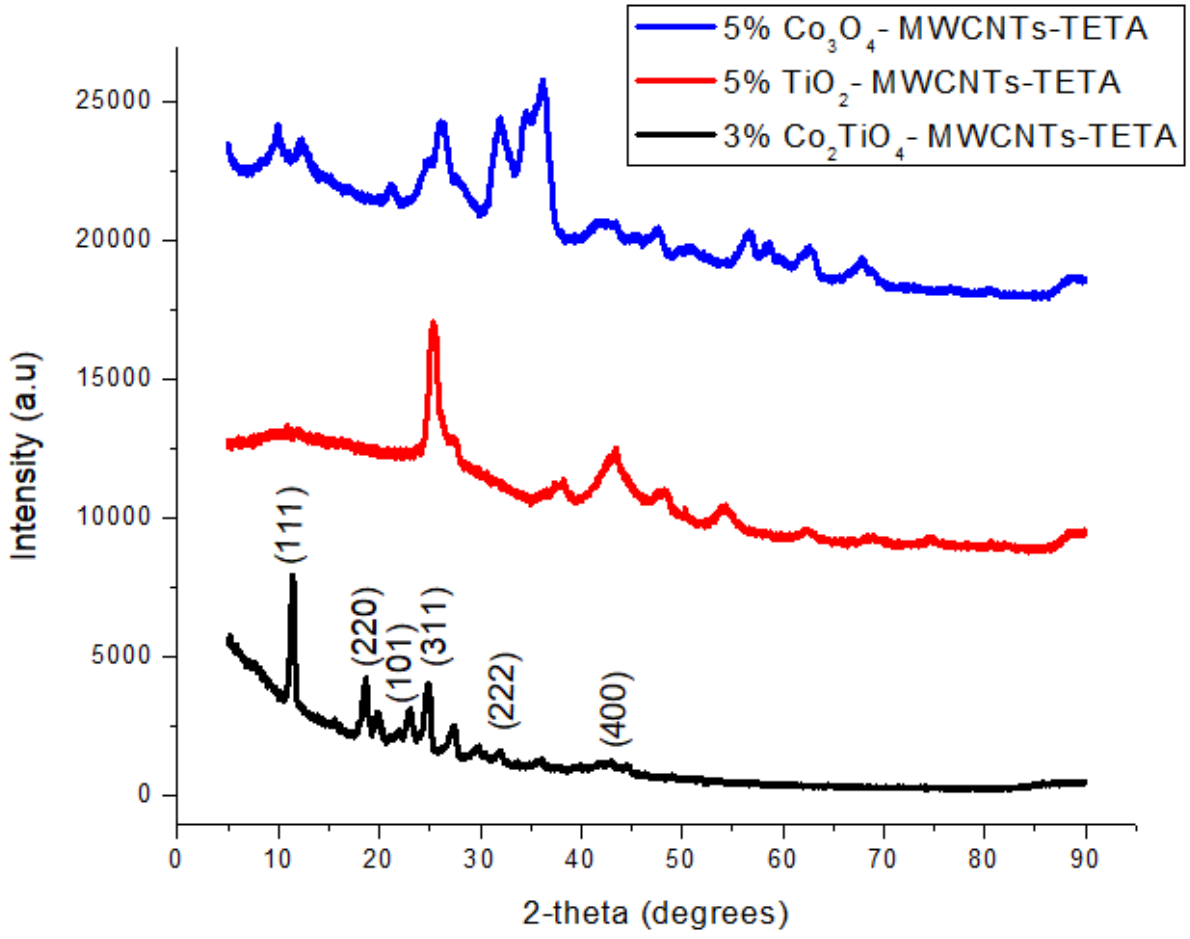


Figure 4.10: XRD patterns of $Co_3O_4$, MWCNTs-TETA, and 5% $Co_3O_4$-MWCNTs-TETA.

The phase formation of $Co_2TiO_4$ was analysed using the X-ray diffraction technique as shown in figure 4.10. XRD examination revealed that the as-prepared sample shows a multiphase composition consisting of $CoTiO_3$ and $Co_2TiO_4$ phases [28]. The diffraction peaks appearing at 20° to 30° correspond to the plane of low crystalline amorphous $Co_2TiO_4$ and $CoTiO_3$ [29]. However other planes completely disappear for phase identification of the bimetallic nanoparticles from 50°. It should be noted that the unit-cell parameters of $Co_2TiO_4$ could depend on the sintering conditions, such as temperature and pressure, and stoichiometry of the nanoparticles [30]. Therefore, it not clear as to which phase has been formed on the bimetallic structure of the nanoparticles. From the results it cannot be concluded that the synthesis of a single phase of $Co_2TiO_4$ is unlikely under the sol gel method. However, stoichiometry and synthetic temperature should be considered thoroughly during the synthesis. Interesting to note, on the XRD pattern of 3% $Co_2TiO_4$-MWCNTs-TETA the major phase obtained was $Co_2TiO_4$. This proves MWCNTs as good support material for deposition of cubic $Co_2TiO_4$ synthesis. To the best of our knowledge, there has been only one previous work reported on the yielding of the cubic $Co_2TiO_4$ as a single phase of which the synthesis method was co-precipitation followed by calcination at high temperature [31].

### 4.2.3. Thermal gravimetric analysis

#### 4.2.3.1. TGA profile of raw, oxidised, and amine modified MWCNTs

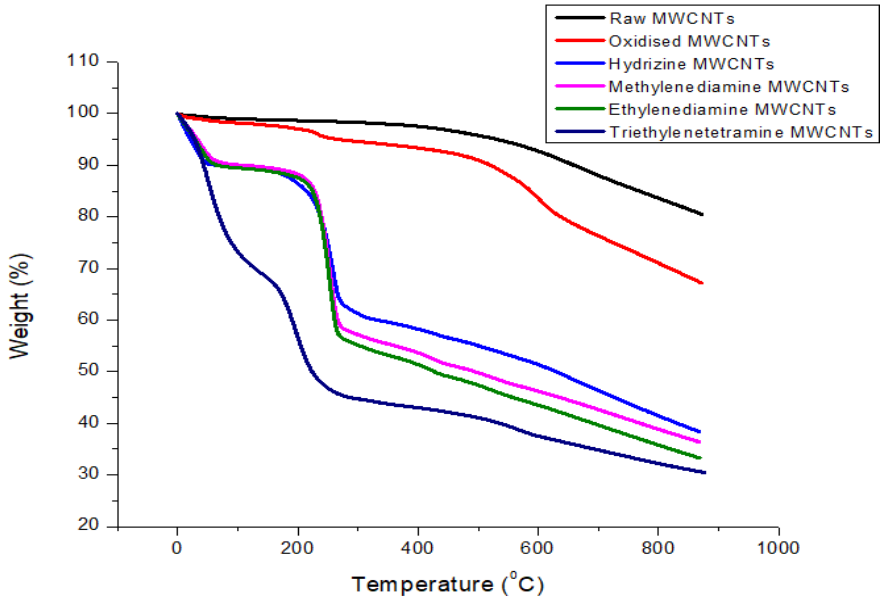


Figure 4.11. TGA profile of raw and amine functionalised MWCNTs

It is important to determine and compare the thermal stability of the raw, oxidised and amino functionalised MWCNTs because the step of functionalisation has an effect on the thermal stability of the MWCNTs [32]. The results are presented in figure 4.11 above. The raw and oxidised MWCNTs show similar trends. However raw MWCNTs showed high thermal stability as compared to oxidised MWCNTs. The oxidised MWCNTs showed the initial decomposition of the MWCNTs at 210 °C, this is due to defects on the nanotubes caused by acid treatment and the burning of the carboxyl group attached to the walls. The second decomposition is observed at 600 °C, this is the decomposition of the nanomaterials, this is proven by the same decomposition trend at 600 °C being observed on raw MWCNTs as reported elsewhere [33]. The amino functionalised MWCNTs by hydrazine, ethylenediamine, ethylenediamine, and triethylenetetramine show similar trends, the first decomposition at low temperatures of less than 100 °C is attributed to the loss of moisture absorbed both physically and chemically on the materials. There is a

thermal decomposition of 25, 30, 32, and 46% on hydrazine-, methylenediamine-, ethylenediamine (EDA), and triethylenetetramine (TETA)-MWCNTs, respectively. These results have proven that by increasing the organic length of the compound being attached on the material tempers with the thermal stability of the material. The results also highlight that by adding a step of functionalisation, the thermal stability of the MWCNTs decreases.

#### 4.2.3.2. The TGA profile of metal oxide doped MWCNTs

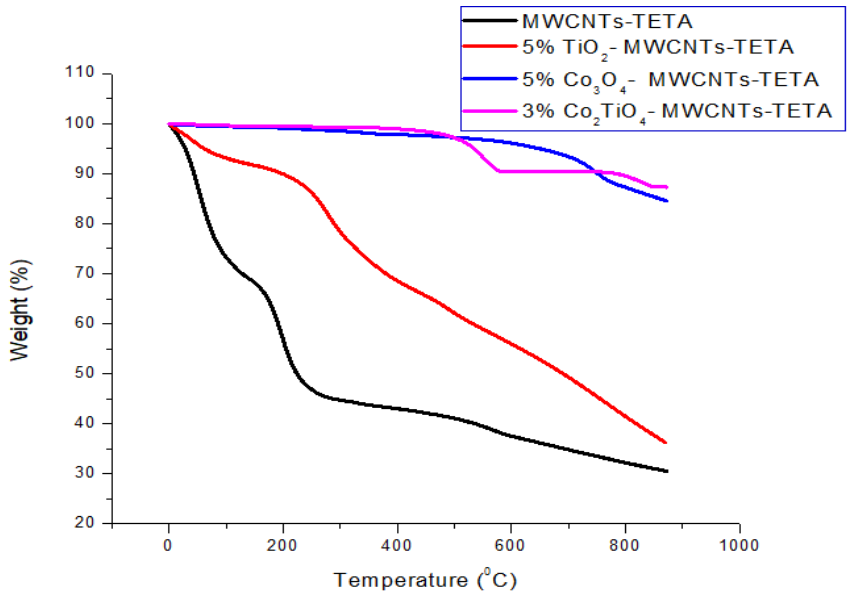


Figure 4 12. TGA profiles of metal oxide doped MWCNTs

The thermal stability of the metal oxides doped MWCNTs were investigated. The obtained results are presented in figure 4.12. The results showed that the $Co_3O_4$-MWCNTs have a higher stability as compared to $TiO_2$-MWCNTs. This is in agreement with the literature [34] It is also noteworthy to recognise that the thermal stability of the MWCNTs-TETA decomposition temperature was 150 $^0$C. However, when MWCNTs-TETA are doped with metal oxides, they showed a drastic improvement in thermal stability brought by metal oxides. Similar results have been reported by [35,36] where they have shown improvement in thermal stability of the MWCNTs after doping with titanium dioxide and cobalt oxide respectively.

### 4.2.4 Scanning electron microscope

#### 4.2.4.1. SEM of raw and modified MWCNTs by acids and amino groups

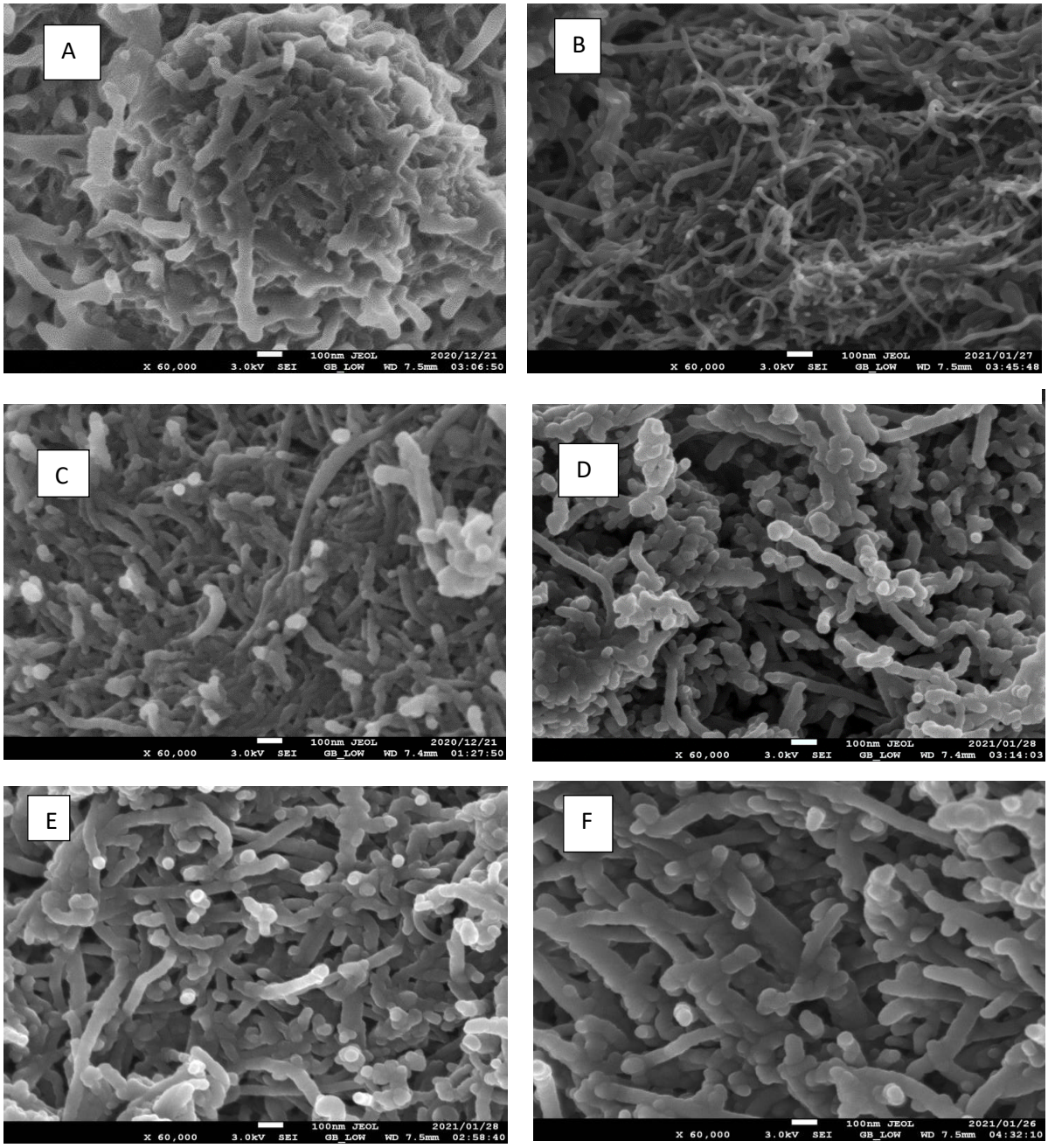


Figure 4.13: The SEM images of raw and modified MWCNTs, (A) raw MWCNTs. (B) MWCNTs-COOH, (C) MWCNTs-hydrazine, (D) MWCNTs-methylenediamine, (E) MWCNTs-ethylenediamine, (F) MWCNTs-triethylenetetramine

The Scanning electron microscopy (SEM) images in figure 4.13A-F shows the morphology before and after modification of the MWCNTs. The modification was done by introducing acidic and amine groups on the surface walls of the MWCNTs. The raw MWCNTs showed very agglomerated tubes that formed a spherical shape with reduced surface area (refer to figure 4.13A). This is in conjunction with the literature that raw MWCNTs are not reactive, and they need some modifications [37][38]. The second morphological results are those of the acid treated MWCNTs (Figure 4.13B), which confirmed that introducing acidic groups opens the tubes and increases the surface area and the reactivity of the MWCNTs. However, it cannot be ignored with the evidence that the tubes treated with acid appear thinner than the raw MWCNTs. This is because acids can deteriorate the walls of the MWCNTs [39,40]. The third results are one for modification of the MWCNTs using Hydrazine ($N_2H_4$) (Figure 4.13C). This morphological image showed an increase in diameter from the ones treated with acids, confirming the covalent attachment of the amino groups ($NH_2$). The fourth morphological results are that of the deposition of methylenediamine ($NH_2CH_2NH_2$) (Figure 4.13D), which was successfully attached as shown by the bumps on the MWCNTs. However, the length of the MWCNTs was diminished, while the agglomeration of the tubes seems to increase. The fifth morphological results are for the deposition of ethylenediamine ($NH_2CH_2CH_2NH_2$) (Figure 4.13E), revealing the successful deposition of this compound as shown by the bright field and the bumps on the walls of the MWCNTs. Introducing this material also showed a drastic improvement in the length and diameter ratio of the MWCNTs. This brings about the increase in surface area and reactivity of MWCNTs. The final morphological results are that of deposition of triethylenetetramine $[CH_2NHCH_2CH_2NH_2]_2$, (Figure 4.13F) which revealed successful attachment as shown by bumps on the MWCNTs accompanied by further improvement and fair distribution, showing less agglomeration. Altogether, these results show that by increasing the length of the organic moiety on modifications, the agglomeration sites tend to decrease [41,42].

### 4.2.4.2. SEM images of $TiO_2$ nanoparticles, and 5%$TiO_2$-MWCNTs-TETA

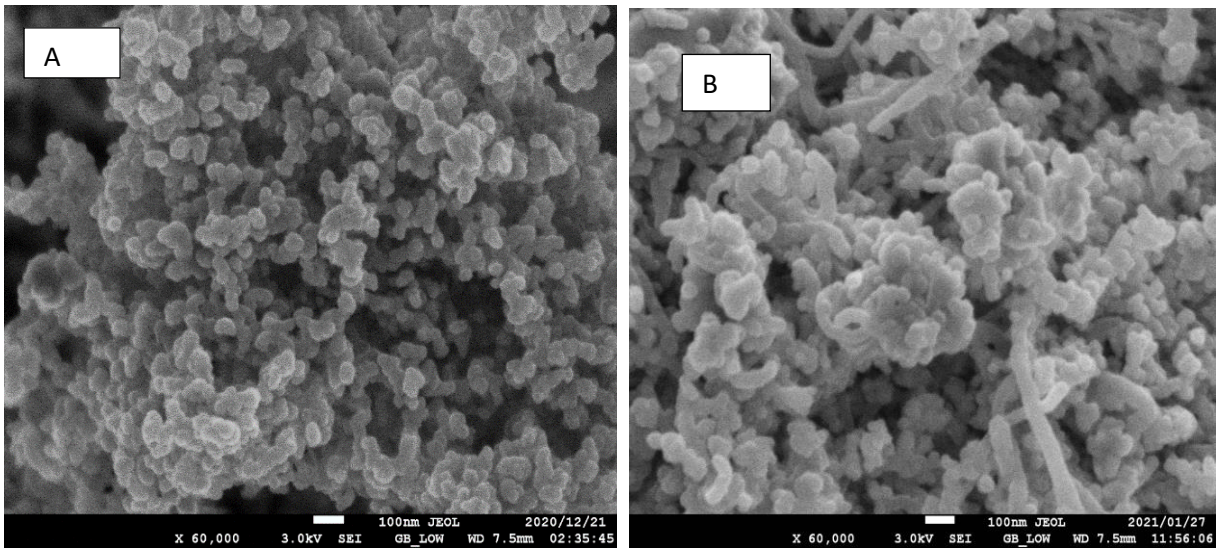


Figure 4.14. SEM images of $TiO_2$ nanoparticles (A) and 5% $TiO_2$-MWCNTs-TETA (B)

The SEM images of $TiO_2$ and 5% $TiO_2$-MWCNTs-TETA nanoparticles prepared by the sol-gel method shows uniform particles with small particles diameter as shown in figure 4.14, which results in high surface area of the nanoparticles as reported elsewhere [42]. The nanocomposite, 5%$TiO_2$-MWCNTs-TETA morphological results clearly show the successful deposition of the $TiO_2$ with a high dispersion rate. It is also observed that only 5% of $TiO_2$ covers most of the MWCNTs, this is because the quantity of the $TiO_2$ is more than that of MWCNTs. This results in the MWCNTs covered and hidden under $TiO_2$ particles. The entangles observed on the nanocomposite are caused by $TiO_2$ nanoparticles attaching to the MWCNTs with long lengths and strong van der Waal forces [43]. This type of aggregation of $TiO_2$ with the MWCNTs indicates the role of MWCNTs as good supporting materials for dispersion or the growth of $TiO_2$ on their surface [44].

### 4.2.4.3. SEM images of $ZrO_2$, and 5%$ZrO_2$-MWCNTs-TETA

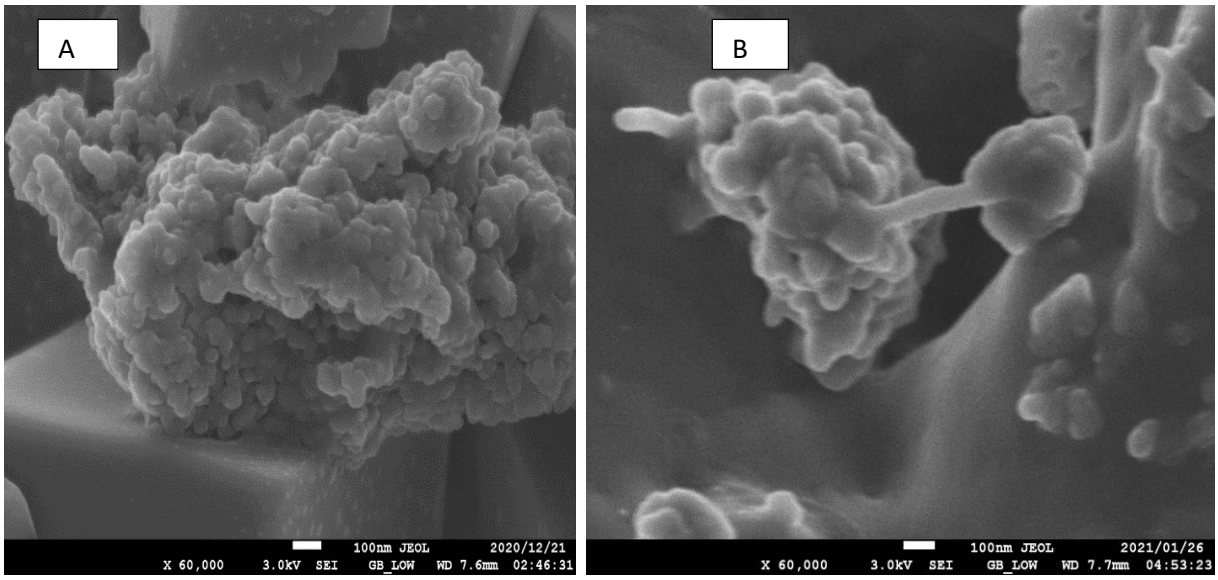


Figure 4.15. SEM results for $ZrO_2$ (A) and 5% $ZrO_2$-MWCNTs-TETA (B)

The SEM images of $ZrO_2$ and 5% $ZrO_2$-MWCNTs-TETA in figure 4.15 show the highly agglomerated nanocomposites that are sandwiched between two layers of cubic structures, and the interaction between agglomerates. It is argued that the hard agglomerates in the powder from the water-washed co-precipitates are formed by oxo-bridging between non-bridging hydroxyl groups present in the zirconium hydroxide structures due to the effect of hydrogen bonding in the aqueous system [44]. The Zirconia nanocomposites also show an amorphous layer of the nanocomposite with the agglomerated zirconium dioxide particles with the MWCNTs bridging between the agglomerated zirconium dioxide. This shows that in the case of zirconium oxide, MWCNTs did not improve the dispersion and deagglomeration of the nanoparticles. This type of bonds can be solved by ultrasonication with ethanol after washing during their synthesis [45,46].

### 4.2.4.4. SEM data of $MnO_2$, and 5%$MnO_2$-MWCNTs-TETA

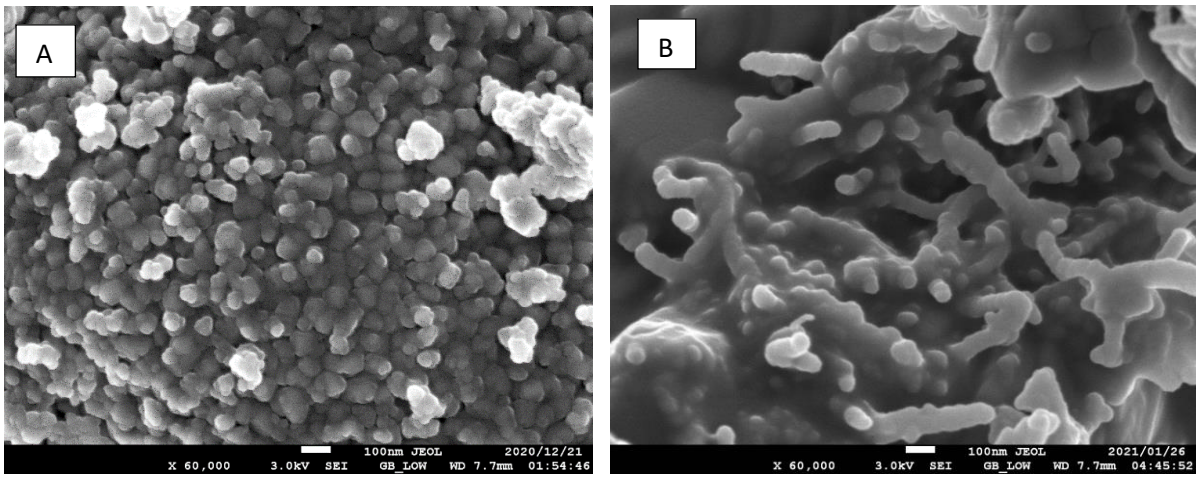


Figure 4.16. SEM images of $MnO_2$ (A) and 5% $MnO_2$-MWCNTs-TETA (B)

The results in figure 4.16 show the morphology of $MnO_2$ and 5% $MnO_2$-MWCNTs-TETA with uniform distribution of spherical particles on the $MnO_2$ observed. Similar results were reported on the literature [47,48]. The short space between the nanoparticles is associated with strong van deer wall forces of attraction between them. It cannot be ignored that there is a presence of some clusters that are caused by particles bonding together by strong van der walls forces, which hinders the surface area of the compounds. However, upon forming the composite with the MWCNTs, they change their morphology to become amorphous, this type of linkage is caused by the heating treatments and the type of metal precursor which was used for deposition of the $MnO_2$ on the walls of the MWCNTs [49,50].

### 4.2.4.5. SEM images of synthesised $Co_3O_4$, and 5% $Co_3O_4$-MWCNTs-TETA

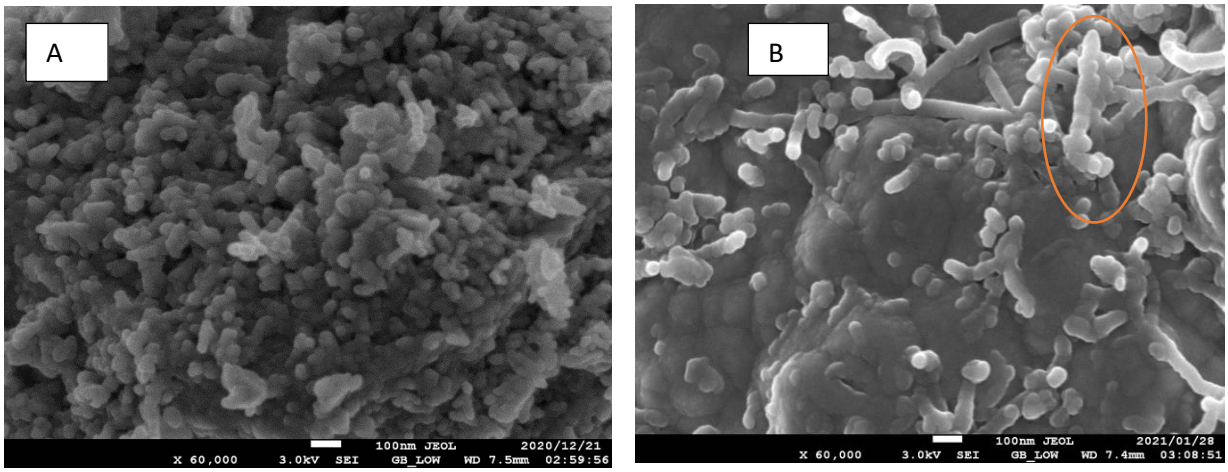


Figure 4.17. SEM images of synthesised $Co_3O_4$ (A) and 5% $Co_3O_4$-MWCNTs-TETA (B)

The results show the SEM images of $Co_3O_4$ and the composite of 5% $Co_3O_4$-MWCNTs-TETA prepared by the sol-gel method presented in figure 4.17. The results show small spherical particles of $Co_3O_4$ that are overlapping and with mild and partly agglomeration. This type of morphology is mostly presented by most researchers [51,52]. These types of structures can be attributed to the type of method and heating temperatures during their synthesis which causes the shape and the overall morphology of these nanoparticles [53]. These nanoparticles depict the rough surface and uniform distribution of the nanoparticles. These facilitate the formation of pores that helps with the introduction of electrolyte ions in the inner particles and these help in improving the faradic current [54]. However, these results also show amorphous structures of the $Co_3O_4$ particles with the MWCNTs, and a different morphology was observed when $Co_3O_4$ and MWCNTs are alone. This is due to pre-treatment temperature of synthesis which could have tempered with the structure of the nanocomposites. It is noteworthy to observe that despite that, successful deposition of the $Co_3O_4$ has been done due to the bumps which appear on the highlighted area of the 5% $Co_3O_4$-MWCNTs-TETA results (refer to figure 4.15 B).

### 4.2.4.6. SEM results for ZnO, and 5%ZnO-MWCNTs-TETA

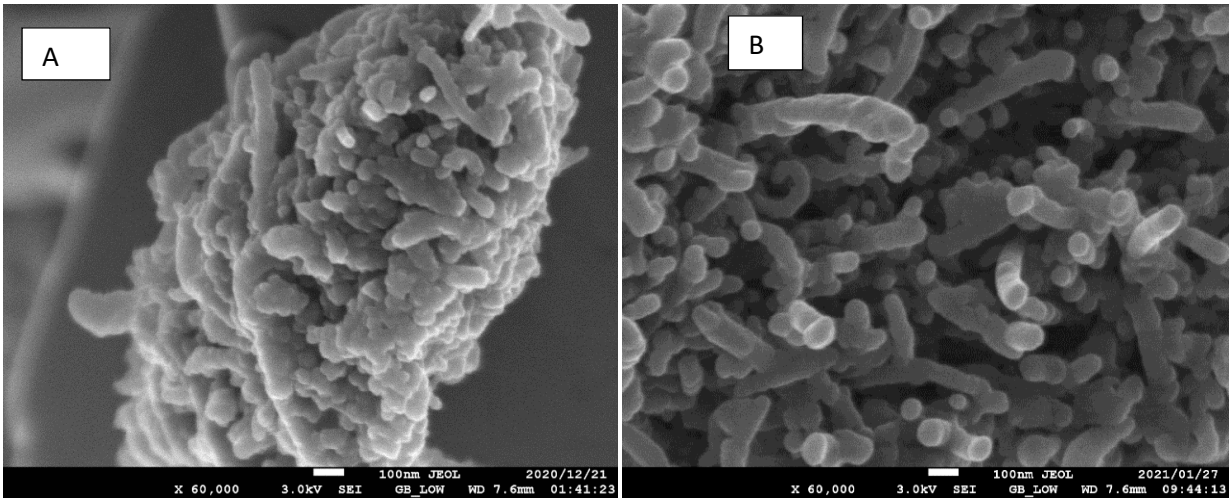


Figure 4.18. SEM results for ZnO (A) and 5% ZnO-MWCNTs-TETA (B)

The surface morphology of the ZnO particles and ZnO-MWCNTs-TETA are shown in figure 4.18 and it indicates the formation of ZnO nanorods which are highly agglomerated; this type of bonding between the ZnO nanoparticles is caused by the high surface energy of the nanoparticles [55]. These results hinder the channeling of electrons to the inner particles and decrease the faradic current of the nanoparticles. However, on the formation of the nanocomposite with MWCNTs, the results suggest that the presence of MWCNTs can be used as supporting material for the de-agglomeration of the ZnO particles. It is evident that the ZnO particles when they are grown on the MWCNTs they show fewer agglomerations as compared to when they were alone.

### 4.2.4.7. SEM images of 5%$Co_2TiO_4$-MWCNTs-TETA, 3%$Co_2TiO_4$-MWCNTs-TETA and 1%$Co_2TiO_4$-MWCNTs-TETA

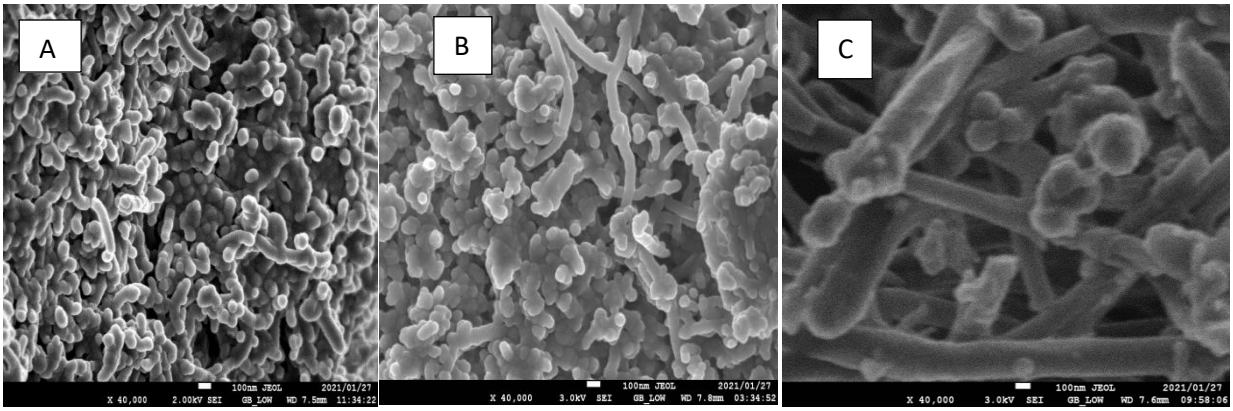


Figure 4.19. SEM images of 5% $Co_2TiO_4$-MWCNTs-TETA (A), 3% $Co_2TiO_4$-MWCNTs-TETA (B)1% $Co_2TiO_4$-MWCNTs-TETA (C)

The morphology of the nanocomposites of the bimetallic compounds between titanium dioxide and cobalt oxide was studied using scanning electron microscopy and it can be seen that the morphology of the nanocomposite is different from the morphology of the titanium dioxide and cobalt oxide results alone (refer to figure 4.19). This change is brought by the metal-metal bond between the nanoparticles [56]. The results of the 5% composition show, metal oxides have completely hindered the carbon nanotubes. This resulted in the decrease in faradic current as observed in the cyclic voltammetry experiment. This suggests that MWCNTs helps in channelling electrons for increasing the conductivity of the material. The 3% compositions MWCNTs on the surface of the MWCNTs with some partly agglomerated particles are caused by strong van der wall forces of attraction between atoms forming the nanocomposite. This resulted in increased faradic current observed under cyclic voltammetry [57]. The 1% composition shows successful attachment of the metal oxides on the walls of the MWCNTs, however, due to the low percentage of the metal oxide, this shows very low faradic current as compared with the 3% composition of the metal oxides. This highlighted a very important fact that metal oxides increase the electroconductivity of the material.

## 4.3. SOLUBILITY RESULTS

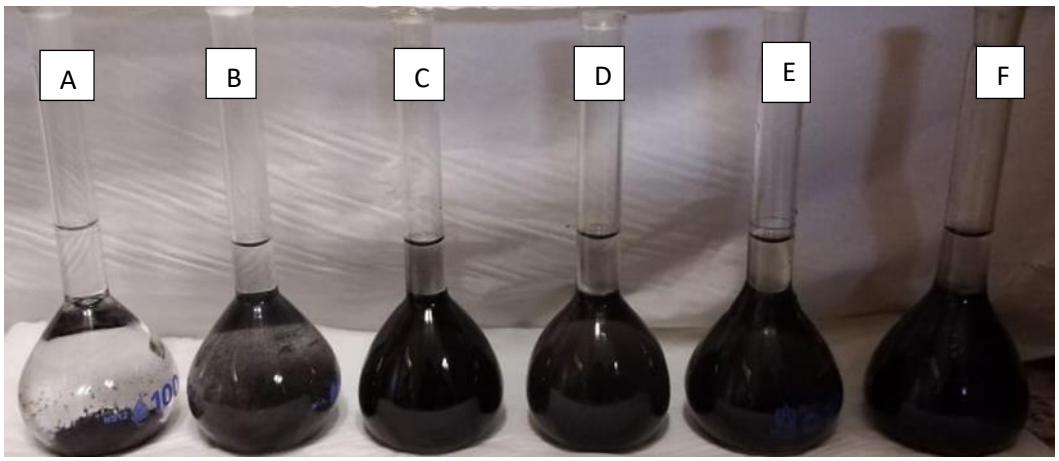


Figure 4.20. The solubility results of the functionalised MWCNTs. (A) Raw MWCNTs, (B) acid-treated, (C) Hydrazine MWCNTs, (D) Methylenediamine MWCNTs (E) Ethylenediamine MWCNTs, and (F) Triethylenetetramine MWCNTs

The image in figure 4.20 present the results of the study conducted to determine the solubility of the raw, oxidised and amino-functionalised MWCNTs. The study was conducted by checking the solubility of the MWCNTs inside phosphate buffer (PBS) since it is the electrolyte under electrochemical studies. The results were taken after leaving the samples for 24 h and it shows that raw MWCNTs are not interacting with the electrolyte. This hinders the raw MWCNTs from being used as a modifier for the biosensor since it shows no ionic conductivity with the electrolyte. The study by Cao *et al* [58] has reported the link between solubility and conductivity. To further support their findings this study has noted that as the MWCNTs are functionalised further their conductivity and solubility increases as compared to raw MWCNT. Similar findings are reported [59,60].

### 4.4. UV-VIS characterisation of MWCNTs, $TiO_2$, $Co_3O_4$, and 3% $Co_2TiO_4$-MWCNTs-TETA

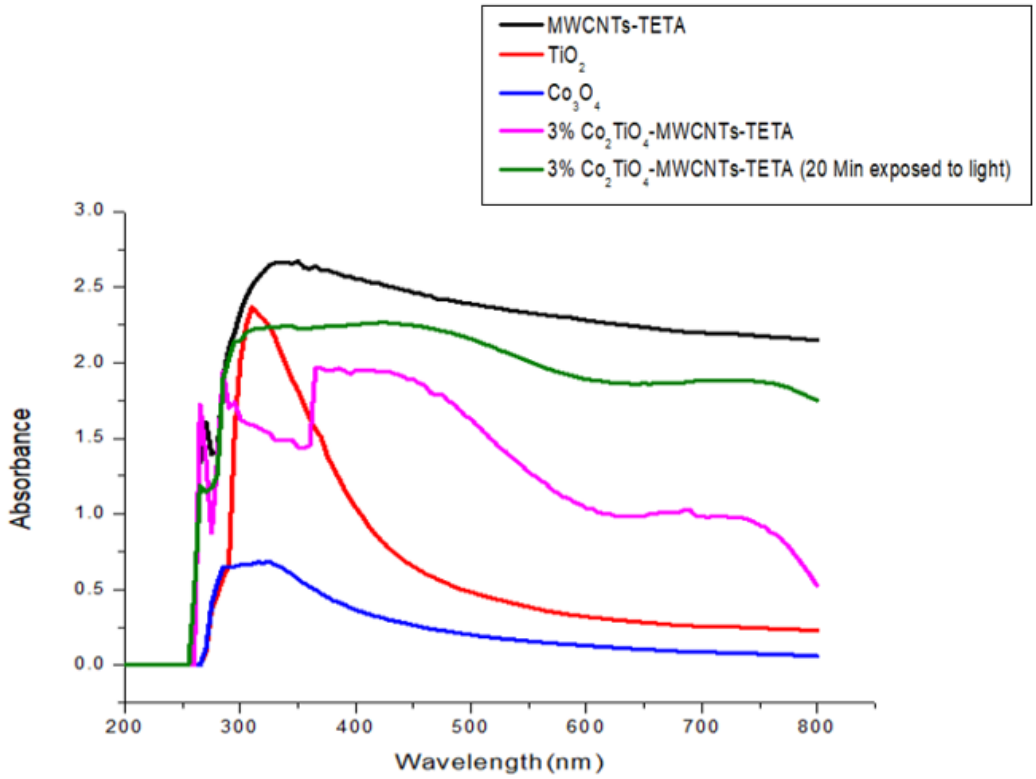


Figure 4.21. The UV-vis absorption spectra of MWCNTs-TETA, $TiO_2$, $Co_3O_4$, 3% $Co_2TiO_4$-MWCNTs-TETA, and 3% $Co_2TiO_4$-MWCNTs-TETA (20 minutes exposed to light).

The Uv-vis absorption spectroscopy can be used not only as a technique to quantify the dispersion of the nanomaterials in solvents but also as a tool to study the photocatalytic properties of the nanomaterials [61]. The photocatalytic study of the nanomaterials was studied, and the results are presented in figure 4.21. The oxidised MWCNTs showed maximum absorbance in the region of 200-800 nm, this is due to the sample black colour with high absorption capacity [62]. $TiO_2$ showed a very intense peak at around 350 nm while cobalt oxide ($Co_3O_4$) showed a broad absorption band at 290-400 nm. Interesting to note is that the 3%$Co_2TiO_4$-MWCNTs-TETA absorption has experienced a redshift at the higher wavelength at 350 to 530 nm this major shift is caused by the presence of metal-metal bond between titanium

and cobalt. The broad redshift is again observed when the 3% $Co_2TiO_4$-MWCNTs-TETA is irradiated with visible light for 20 minutes. This irradiation has brought the absorption of the nanocomposite to increase and to experience redshift again at broader wavelength. This is due to the excitation of the electrons of MWCNTs, $Co_3O_4$, and $TiO_2$ from the valence band to the conduction band [63]. It is noteworthy to observe that the presence of MWCNTs played a critical role as support materials for the metal oxides in the absorption of light.

## 4.5. Electrochemical Characterisation of metal oxides, modified MWCNTs, and metal doped MWCNTs in Potassium Ferricyanide by Using Cyclic Voltammetry

### 4.5.1. Effects of amine functionalisation on peak current response of MWCNTs

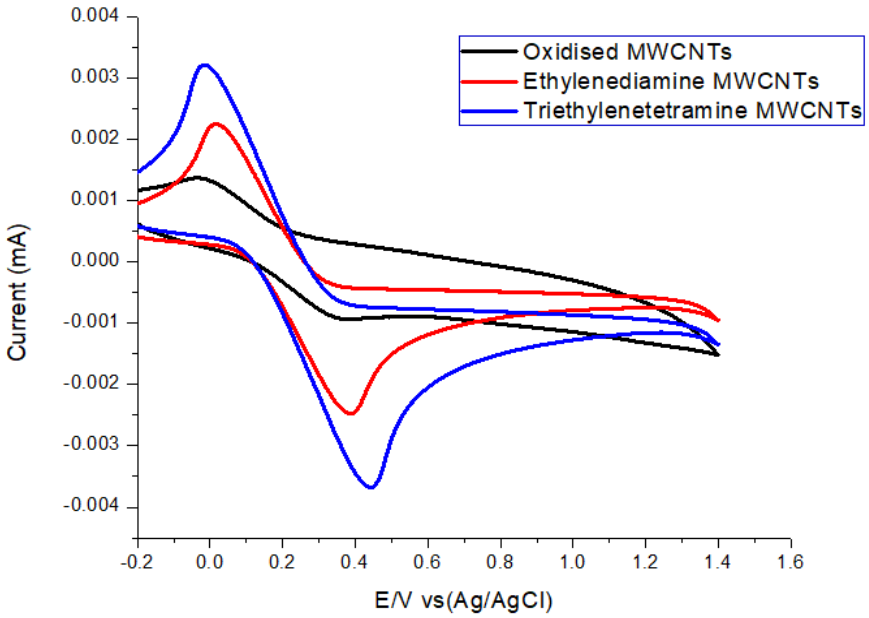


Figure 4.22: Cyclic voltammogram characterisation of raw, oxidised and amine functionalised MWCNTs in a phosphate buffer solution (0.1 M, pH 7.5) containing 5 mM $[Fe(CN)_6]^{-3/-4}$.

The results in figure 4.22 shows the cyclic voltammograms obtained when glassy carbon electrode (GCE) was polished with modified MWCNTs at a scan rate of 100

mV/s. The voltammogram obtained shows increase in oxidation and reduction peaks when the MWCNTs are modified with amino groups. This suggest that the electron transfer increases as the length of the organic moiety deposited on the MWCNTs increases. The increase in electron transfer (current response) followed this order: oxidised MWCNTs < hydrazine-MWCNTs < methylenediamine-MWCNTs < ethylenediamine-MWCNTs < triethylenetetramine-MWCNTs. Triethylenetetramine (TETA) modified MWCNTs were chosen for analysis and identification of hypoxanthine in this study due to high current response. This shows that MWCNTs-TETA has some interesting features which are confirmed by FTIR, SEM, and TGA. All comparative results containing all the modified MWCNTs is given in appendix 6.

### 4.5.2. Cyclic voltammograms for $Co_3O_4$, MWCNTs-TETA, and 5% $Co_3O_4$-MWCNTs-TETA

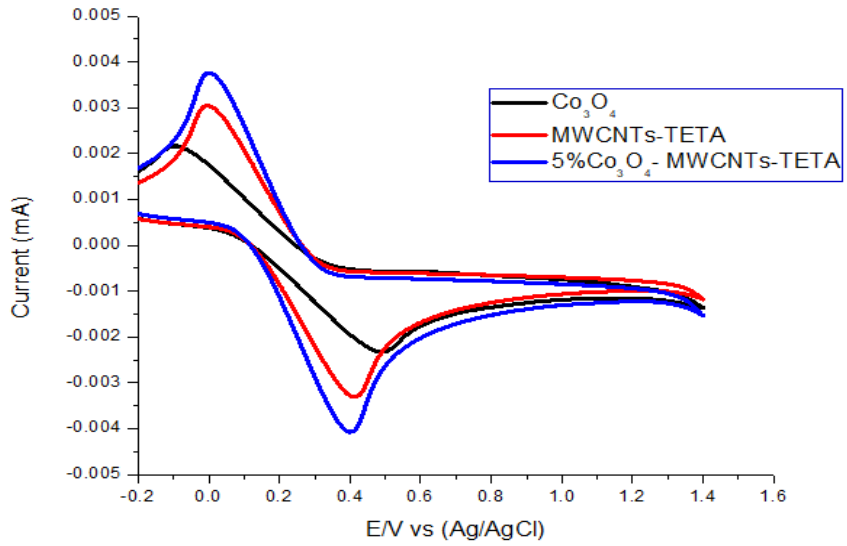


Figure 4.23: The cyclic voltammograms characterisations of cobalt oxide, MWCNTs-TETA, and their corresponding nanocomposites modified GCE in a phosphate buffer solution (0.1 M, pH 7.5) containing 5 mM $[Fe(CN)_6]^{-3/-4}$.

In order to investigate the catalytic performance of the metal oxides and their nanocomposite with MWCNTs, cyclic voltammetry experiments were conducted in 5 mM ferrocyanide solution at pH 7. The results in figure 4.23 shows that $Co_3O_4$ alone

gives low current levels. However, upon doping the MWCNTs, the is a drastic improvement in the overall current being produced. This shows that MWCNTs-TETA are very good support nanomaterials to be immobilised with $Co_3O_4$ for catalytic detection of hypoxanthine. Comparative study of all metal oxides is given in appendix 7

### 4.5.3. Cyclic voltammograms of $TiO_2$, MWCNTs-TETA, and 5% $TiO_2$-MWCNTs-TETA

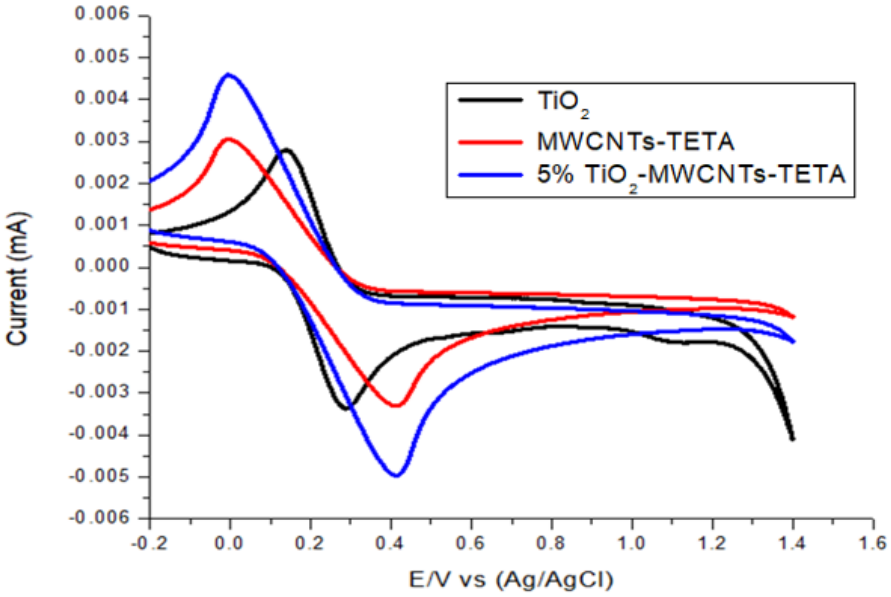


Figure 4.24: Cyclic voltammograms of $TiO_2$, MWCNTs-TETA, and 5% $TiO_2$-MWCNTs-TETA in 5 mM ferrocyanide solution at pH 7

The glassy carbon electrode (GCE) was used as a working electrode in the electrochemical characterisation of $TiO_2$, MWCNTs-TETA and 5% $TiO_2$ MWCNTs-TETA. All these nanomaterials show very good electrocatalytic response as shown in figure 4.24. However, by combining these nanomaterials in 5% $TiO_2$-MWCNTs-TETA, they show strong improvement in current response as compared when they are analysed individually. This shows that combinations of metal oxides with

MWCNTs have very interesting properties that lead to high current output. That is confirmed by FTIR, SEM, XRD, and TGA.

### 4.5.4. Comparative analysis of cobalt oxide, titanium dioxide and bimetallic nano compound of cobalt oxide-titanium dioxide nanocomposite

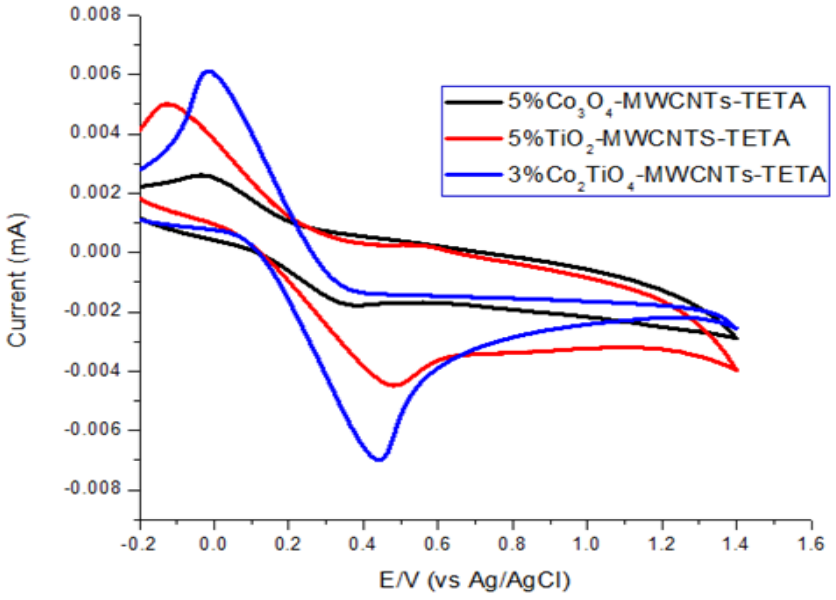


Figure 4.25: Cyclic voltammograms of nanocomposites of cobalt and titanium and their bimetallic nano compound in 5 mM ferrocyanide solution at pH 7

In order to further investigate the nanocomposites and their bimetallic nano composition. GCE was polished with 10 µL of each nanocomposite solution in dimethylformamide (DMF). Cyclic voltammogram experiment were conducted as shown in figure 4.25. The results show that the composite of titanium dioxide MWCNTs-TETA show best current response as compared to the nanocomposite of cobalt oxide MWCNTs-TETA. However, the bimetallic compound of cobalt-titanium oxide MWCNTs-TETA showed further improved current outputs as compared to when the metal oxides were treated individually. This highlighted the importance the metal-metal bond between cobalt and titanium. The bimetallic nanocomposite was selected and used throughout the study due to high current response.

### 4.6. Determination of diffusion coefficient and surface coverage for 5% $TiO_2$-MWCNTs-TETA, 5% $Co_3O_4$-MWCNTs-TETA, and 3%$Co_2TiO_4$-MWCNTs-TETA

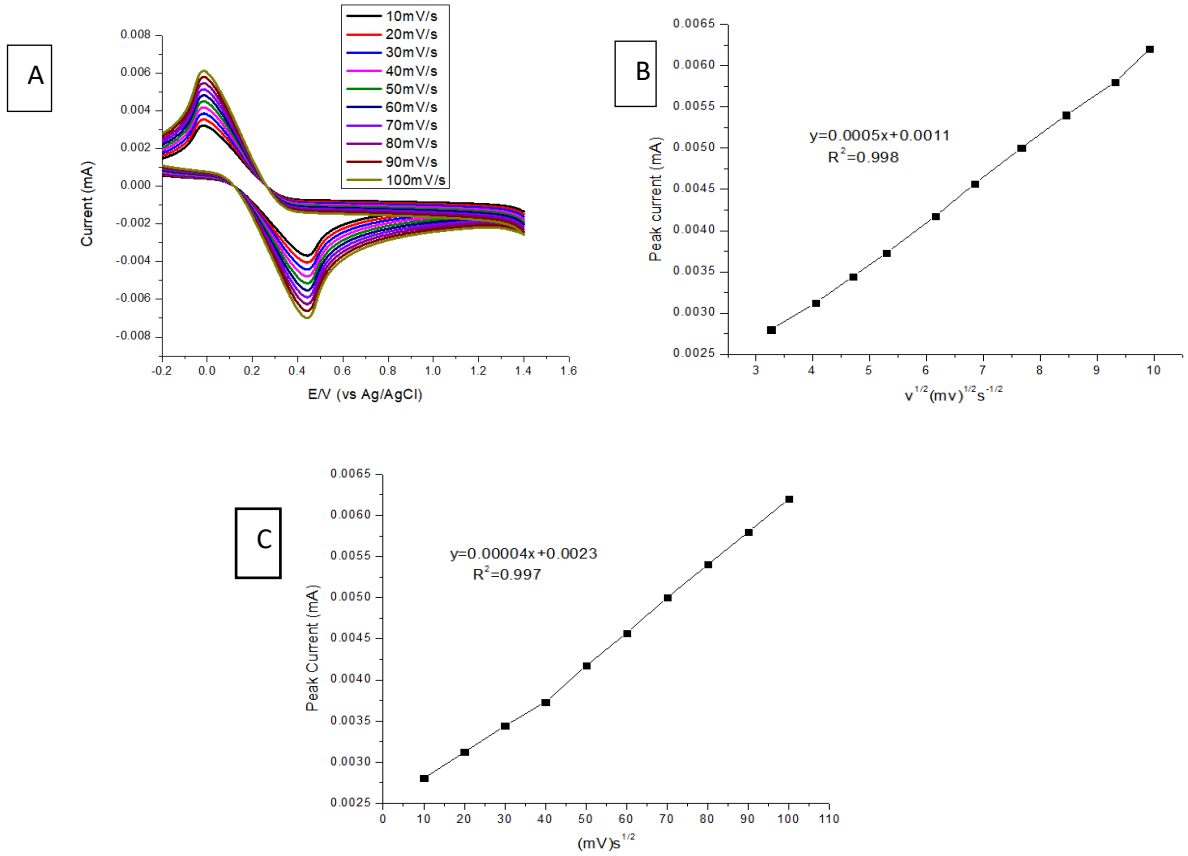


Figure 4.26. (A) Cyclic voltammogram showing the effects of different scan rates (10 to 100 mV/s) on peak current of 3%$Co_2TiO_4$-MWCNTs-TETA/GCE composite and the corresponding (B) relationship between peak current vs the square root of scan rate and (C) the relationship between peak current and the scan rate, in a phosphate buffer solution (0.1 mM, pH 7.5) containing 5 mM $[Fe(CN)_6]^{-3/-4}$.

The redox couple, $[Fe(CN)_6]^{-3/-4}$ was used to investigate the electrochemical properties of 3%$Co_2TiO_4$-MWCNTs-TETA, using cyclic voltammetry as shown in figure 4.27. An appendix 1 and 2 shows the corresponding electrochemical analysis for 5% $Co_3O_4$-MWCNTs-TETA, and 5% $TiO_2$-MWCNTs-TETA, respectively. The results of modified electrodes show that the electrochemical property on redox couple has reversible behaviour with current increasing linearly with the square root of scan rate on all the modified electrodes. The graphs of the peak current vs the scan rate also shows that the scan rate is proportional to the scan rate with the $R^2$

value of 0.99 for all the modified biosensors. This indicates that the reaction at the surface of the electrode for redox couple is diffusion controlled [59]. Electrochemical parameters, (i.e., diffusion coefficient and surface coverage) were determined for all the modified biosensors as follows:

### 4.6.1. Diffusion coefficient

$$i_p = 2.69x10^5 n^{3/2} A C D^{1/2} v^{1/2} \quad (1)$$

The diffusion coefficient is one of the most significant variables in electrochemical reactions. It describes how quickly the analyte interact with the modified electrode for analysis and this is calculated using the Randles–Sevcik equation (1); where $i_p$ is the peak current (mA), n is the number of electron transfer, A is the surface area of the electrode which was calculated to be 0.07 $cm^2$, C is the concentration of the analyte in the electrolyte which is 5 mM $[Fe(CN)_6]^{-3/-4}$ in 0.1 mM phosphate buffer (PBS), and v is the scan rate (mV/s). The data analysis of 3% $Co_2TiO_4$-MWCNTs-TETA/GCE in figure 4.24(B) indicates that the slope of the graph is 0.0005 $mA/mVs^{-1/2}$ on the graph of peak current vs square root of scan rate and the calculated diffusion coefficient was $0.7x10^{-4}$ $cm^2/s$. Based on the data in appendices 1 and 2 the diffusion coefficient of 5% $Co_3O_4$-MWCNTs-TETA and 5% $TiO_2$-MWCNTs-TETA were calculated to be $0.4x10^{-4}$ $cm^2/s$, and $0.5x10^{-4}$ $cm^2/s$, respectively. All the modified electrodes were proven to be diffusion controlled and diffusivity increases with the rate of the reaction from 5% $Co_3O_4$-MWCNTs-TETA < 5% $TiO_2$-MWCNTs-TETA < 3% $Co_2TiO_4$-MWCNTs-TETA. Therefore, conclusion was confidently reached that 3%$Co_2TiO_4$-MWCNTs-TETA is the best electrode for analysis.

### 4.6.2. Surface coverage

$$i_p = \frac{n^2 F^2 A \Gamma v}{4RT} \quad (2)$$

In addition, using the slope of peak current vs scan rate, the surface coverage of electroactive species (Γ) can be determined. According to equation 2, where n is the number of electrons transfer, F is the Faraday constant, v is the scan rate, A is the surface area and R is the gas constant at a given temperature of 298.15 K. The surface coverage indicates the surface concentration of the adsorbed species that occurred for the reaction to take place. The higher the surface coverage the higher the reaction rate and these were calculated to be $15x10^{-5}$, $30x10^{-5}$, and $60x10^{-5}$ $\mu M/cm^2$ for 5%$Co_3O_4$-MWCNTs-TETA/GCE, 5%$TiO_2$-MWCNTs-TETA/GCE, and 3%$Co_2TiO_4$-MWCNTs-TETA/GCE, respectively.

### 4.7. Determination of sensitivity of the biosensor towards hydrogen peroxide

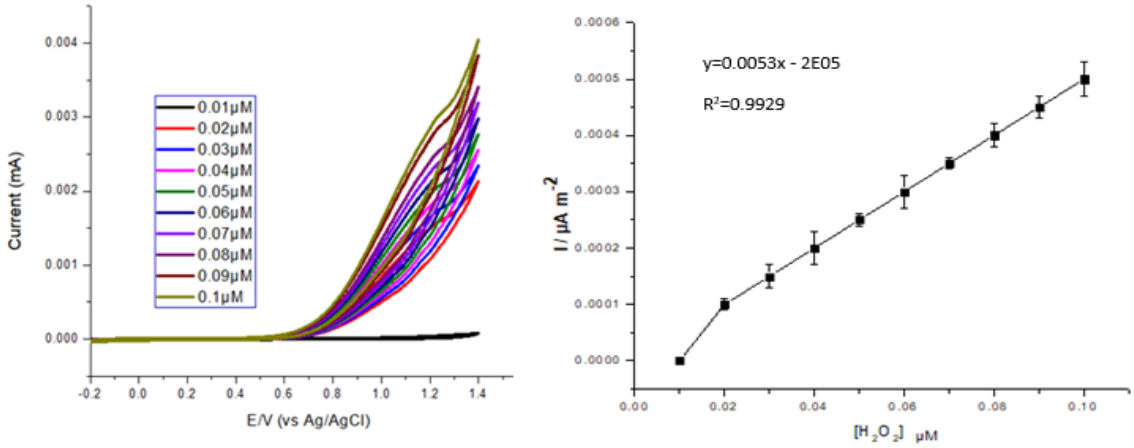


Figure 4.27: Sensitivity results towards hydrogen peroxide using XOD/3%Co3TiO4-MWCNTs-TETA/GCE

In order to determine the sensitivity of the prepared film electrode towards hypoxanthine. It is important to first check the prepared biosensor towards changes in response currents against increased hydrogen peroxide concentrations [64]. Xanthine oxidase catalyses hypoxanthine to xanthine with hydrogen peroxide as by product (refer to figure 1.1). If it can be proven through investigation that the biosensor is sensitive towards hydrogen peroxide, it will be quantifying that the

sensor it can be used for determination of hypoxanthine. Cyclic voltammetry experiments with varying concentrations of hydrogen peroxide in 0.1 mM phosphate buffer solution at pH 7.5 were conducted at a scan rate of 100 mV/s and the results are presented on figure 4.27. A linear increase was observed at increasing hydrogen peroxide concentrations between 0.01 µM and 0.1 mM. The data obtained showed that the electrode was sensitive to hydrogen peroxide and the current increases proportionally with the increase in concentration of hydrogen peroxide with $R^2$ value of 0.9929. This proved that the XOD/3%$Co_2TiO_4$-MWCNTs-TETA/GCE biosensor can be used for the determination of hypoxanthine.

### 4.8. Photocatalytic study of modified biosensor using cyclic voltammetry in 0.1 mM hypoxanthine solution

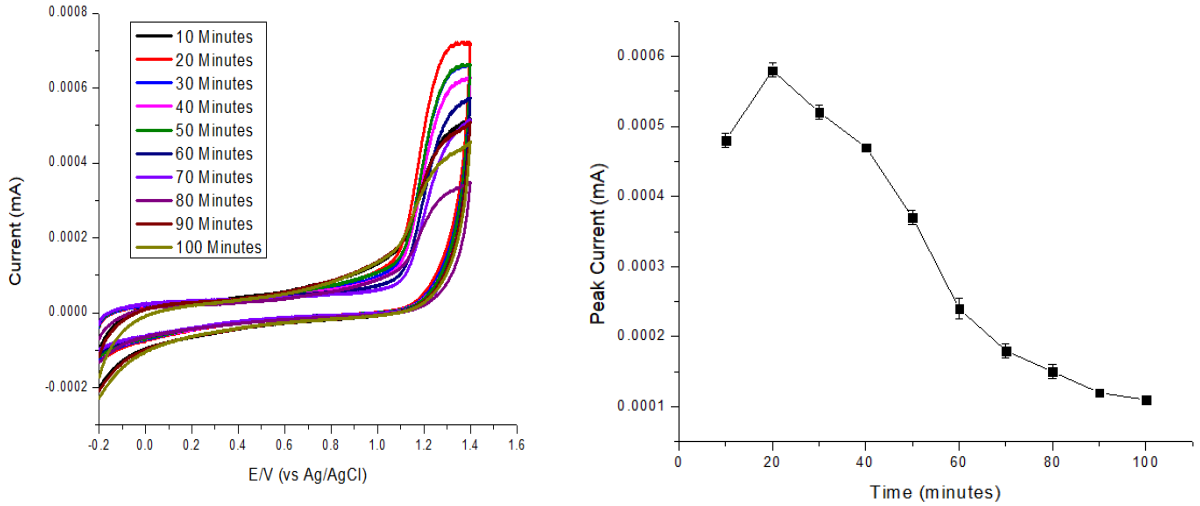


Figure 4.28. Effects of exposure to light on peak current of XOD/3%$Co_2TiO_4$-MWCNTs-TETA/GCE in a 0.05 M phosphate buffer solution containing 0.1 mM hypoxanthine.

The photocatalytic responses of the biosensors were studied using visible light at 10 minutes intervals as shown in figure 4.28. The biosensor of XOD/5%$TiO_2$-MWCNTs-TETA reached a maximum current response towards hypoxanthine detection after 40 minutes of exposure to light (see appendix 5A). The XOD/5%$Co_3O_4$-MWCNTs-TETA/GCE reached an optimum current response after 70 minutes of exposure to light (see appendix 5B). Interestingly the optimum current response was reached

within 20 minutes of exposure to light when using XOD/3%$Co_2TiO_4$-MWCNTs-TETA/GCE as shown in figure 4.28. This suggests an existence of some synergistic effects between titanium and cobalt which led to an increased rate of electron transfer. This is supported on FTIR, SEM, XRD, and TGA results.

## 4.9. Optimisations of the working conditions of the biosensor towards hypoxanthine detection

### 4.9.1 Effect of scan rate

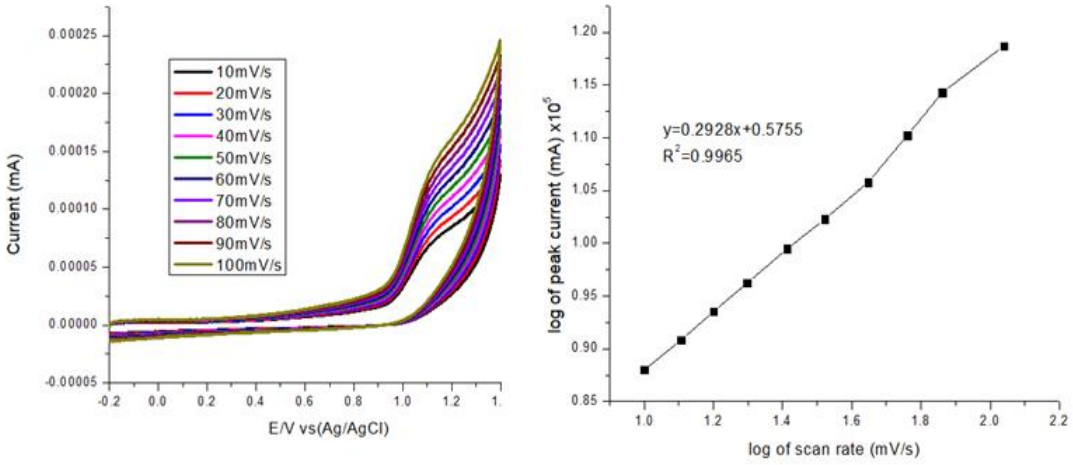


Figure 4.29: Effects of scan rate (10 to 100 mV/s) on current response of XOD/3% $Co_2TiO_4$-MWCNTs-TETA/GCE in a 0.1 M PB solution (pH 7.5) containing 0.1 mM Hx. (Graph of log scan rate vs log of peak current).

The electrochemical properties of the modified electrode were determined by investigating the effect of scan rate as shown in figure 4.29. The sensitivity of the electrode is affected by the potential sweep rate due to the kinetic reactions and the instrumental limitations [65]. The hypoxanthine detection peak current increased linearly with an increase in scan rate, and which suggests that this is the surface-controlled reaction, and the results agree with the thin layer electrochemical behaviour [70]. Furthermore, the graph of log (peak current) vs log scan rate was

found to be 0.9965 which implies the redox reactions of surface-bound composite and diffusion-controlled species. In conclusion, these results have proven that the XOD/3%$Co_2TiO_4$-MWCNTs-TETA/GCE are very good electrochemical materials to be incorporated with enzymes for the detection of hypoxanthine.

### 4.9.2. Effects of the enzyme (Xanthine oxidase) concentration

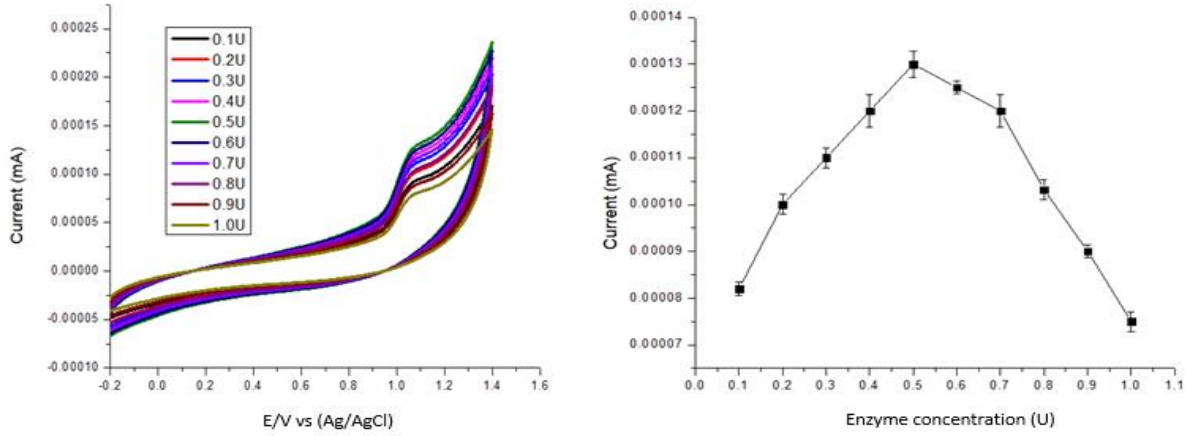


Figure 4.30: Effect of increasing the enzyme concentration (0.1U to 1.0U) on current response of XOD/3%$Co_2TiO_4$-MWCNTs-TETA/GCE in a 0.1 M PB solution (pH 7.5) containing 0.1 mM Hx.

Enzyme concentrations are often given in terms of units and not in mass concentration as observed in figure 4.30. Cyclic voltammograms for increasing concentrations of xanthine oxidase were recorded. It was observed that as the concentration of the enzyme increases the faradic current increased, which is due to the increased production of hydrogen peroxide [71]. However, as the concentration of enzyme increased the sudden decline in peak current was observed, which suggests that the limited quantity of the substrate concentration deactivates the enzyme [72]. The data indicates that an optimum current respond for the detection of hypoxanthine was reached at an enzyme concentration of 0.5U. These findings are, similar to the results reported elsewhere [73]. These results demonstrate these nanomaterials as good support material for immobilisation with enzyme for catalytic

detection of hypoxanthine. The presence of highly electroactive metal oxides and MWCNTs, which helps the enzyme facilitates and channels electrons.

### 4.9.3. Effects of pH

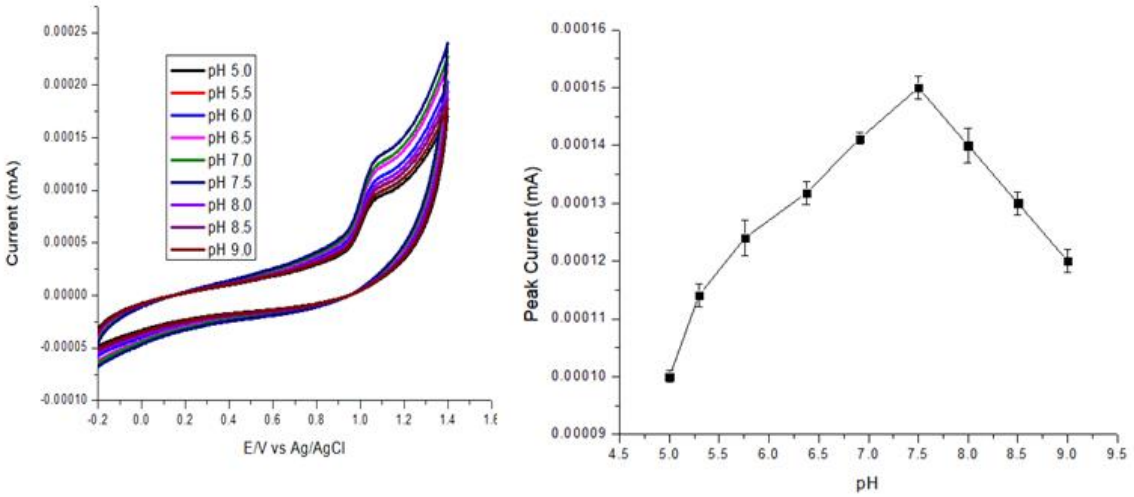


Figure 4 31. Effect of varying pH on peak current of XOD/3%$Co_2TiO_4$-MWCNTs-TETA/GCE in a 0.1 M PB solution (pH 7.5), towards the detection of 0.1 mM Hx.

Most biosensors are affected by the pH of the electrolyte in which the analysis takes place [74]. Therefore, it is important to determine the optimum pH of the biosensor to perform effectively. This was accomplished by preparing 0.1 mM hypoxanthine solution at different pH values ranging from 5 to 9 as shown in figure 4.31. The results indicated that the optimum pH of the biosensor was 7.5. After a thorough search on the literature, it was noted that the many studies have reported similar results [75-77].

### 4.9.4. Effect of varying temperature

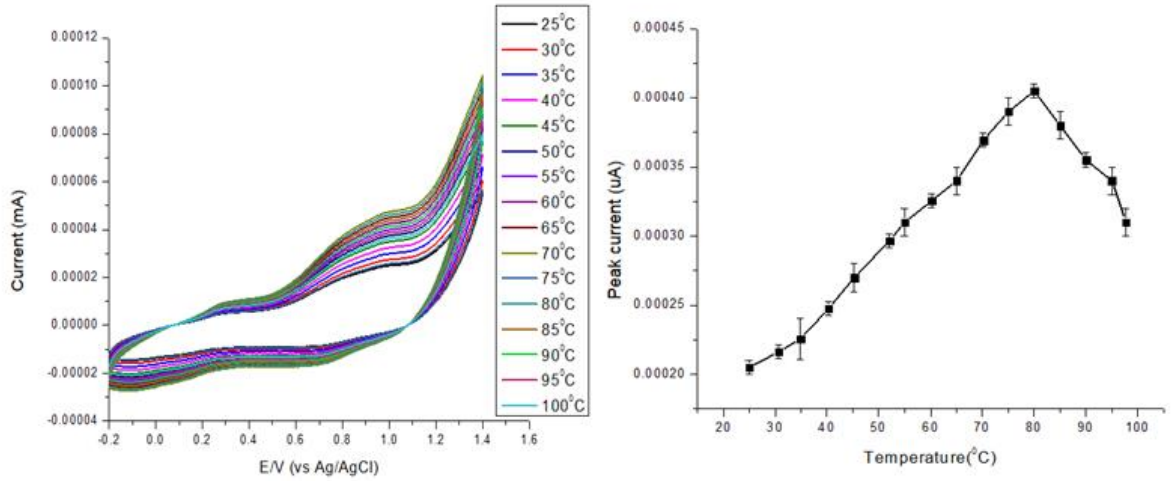


Figure 4 32. The effect of temperature on current response of XOD/3%$Co_2TiO_4$-MWCNTs-TETA/GCE in a 0.1 M PB solution (pH 7.5) towards the detection of 0.1 mM Hx.

Temperature is the critical factor in determining the overall performance of the biosensor. Very high temperatures can denature most enzymes and the immobilisation of the enzyme with nanomaterials like MWCNTs can change the optimum temperature of the enzyme [78]. Therefore, it is necessary to study the effects of temperature on the activity of enzyme and this was accomplished by preparing 0.1 mM of hypoxanthine using a water bath with temperature starting from 25 ˚C to 100 °C. The results presented in figure 4.32 above shows that the optimum temperature of the biosensor is 80 °C. However, an 80 °C is a very high temperature at which the maximum response current is observed since enzymes are protein, the protein structure of the enzyme is denatured and loses its activity at high temperatures. Therefore, working at high temperatures in long-term working conditions will disrupt the enzyme structure, subsequent studies were conducted at 25 ± 1 °C. In literature, the optimum temperatures were found at 55 °C, and 65 °C, and 70°C [79-81], respectively. However, they also indicated to better analyse at room temperature to avoid denaturing the enzyme at high temperatures for long term analysis.

### 4.9.5. Effect of interferences

#### 4.9.5.1. Cyclic voltammograms of interfering agents with hypoxanthine

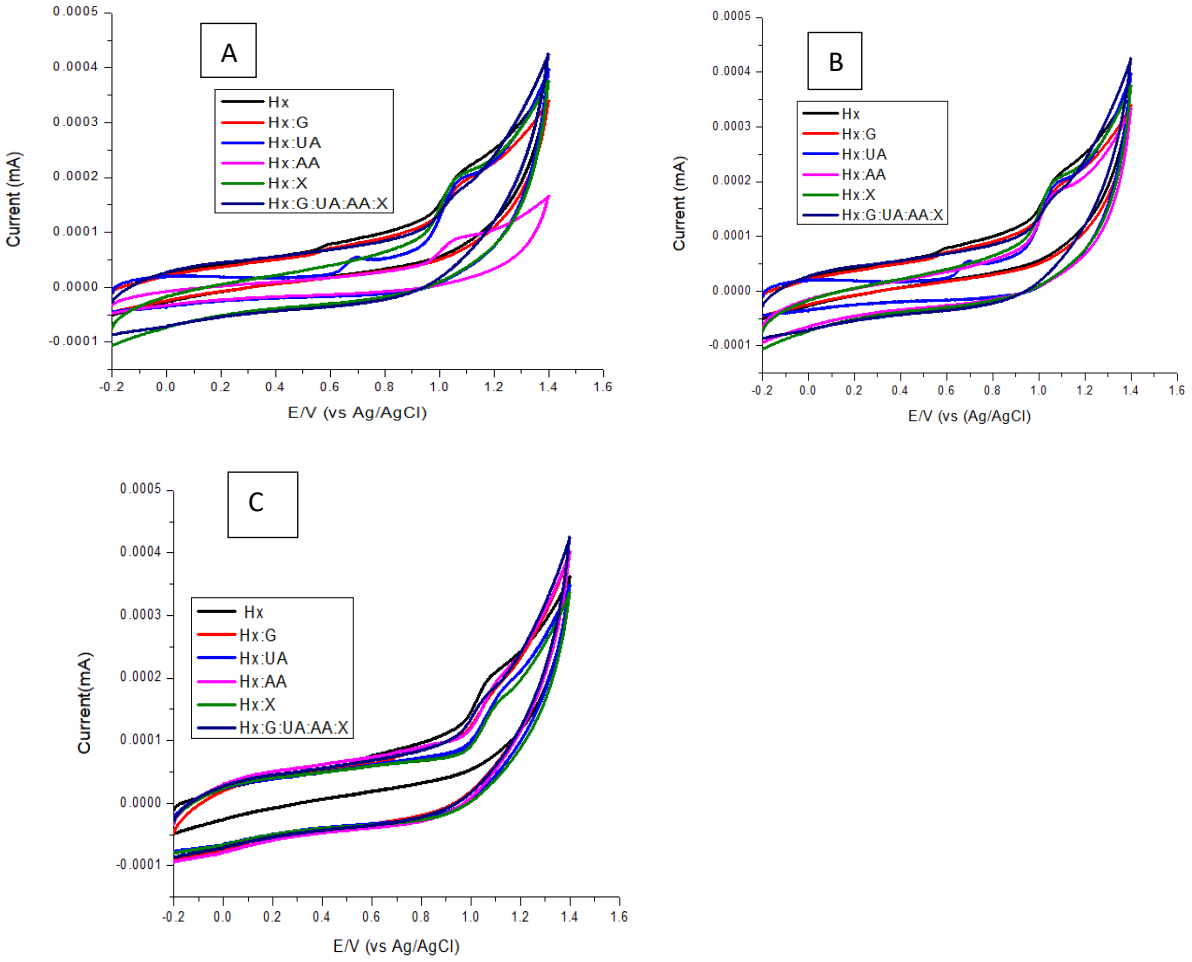


Figure 4.33. Cyclic voltammograms showing the peak current changes of the biosensor's response to a mixture of Hx and interferences (0.1 mM of hypoxanthine (Hx) and 0.1 mM of interferences i.e., Ascorbic acid (AA), Uric acid (UA), glucose (G) and xanthine (X)). (A) analysis using XOD/5%$TiO_2$-MWCNTs-TETA/GCE, (B) XOD/3%$Co_2TiO_4$-MWCNTs-TETA/GCE, and (C) XOD/3%$Co_2TiO_4$-MWCNTs-TETA/GCE (light activated) in a 0.1 M PB solution (pH 7.5).

In real samples analysis, there are biomolecules that tend to interfere with the analysis of hypoxanthine. These are biomolecules of similar structure as that of hypoxanthine [82-85]. To determine the qualities of the proposed biosensor against

interferences, a full investigation of the interfering species was undertaken. The peak current changes of biosensor response are shown by cyclic voltammogram in figure 4.33 and the peak profiles indicates that the biosensor has the ability to detect the presence of hypoxanthine (i.e., highly selective towards hypoxanthine) in the presence of most interfering species. This is clearly presented in bar graph in figure 4.34., which shows very low interfering values for most of the biosensors. However, the highest interfering species with 60% (current drop) is that of Ascorbic acid while using XOD/5%$TiO_2$-MWCNTs-TETA/GCE (refer to figure 4.33 A) monometallic biosensor. However, when using XOD/3%$Co_2TiO_4$-MWCNTs-TETA (see figure 4.33 B) bimetallic biosensor the results show a drastic improvement with only 5% current drop by ascorbic acid. This suggests that metallic interaction between cobalt and titanium has an effect on the improvement of the sensitivity of the biosensor. However, when light was shone for 20 min on XOD/3%$Co_2TiO_4$-MWCNTs-TETA/GCE the selectivity towards hypoxanthine decreased. Interestingly to note, the biosensor specificity increased, as indicated by the presence of only one peak current (hypoxanthine) on the cyclic voltammogram (Figure 4. 29C).

### 4.9.5.1. Bar graph showing interferences results

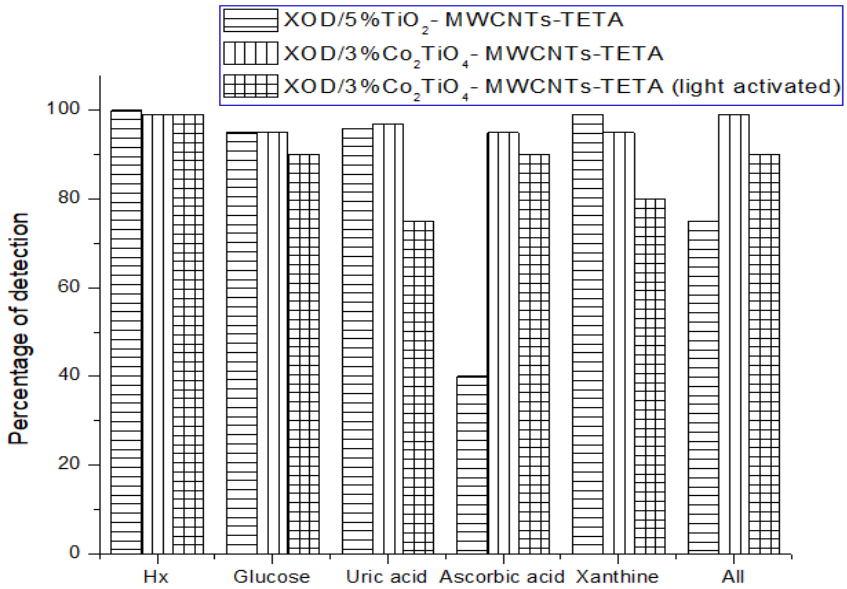


Figure 4.34: Bar graph showing detection of hypoxanthine using three different biosensors with interfering agents.

## 4.10. Determination of the detection limit of the modified biosensors

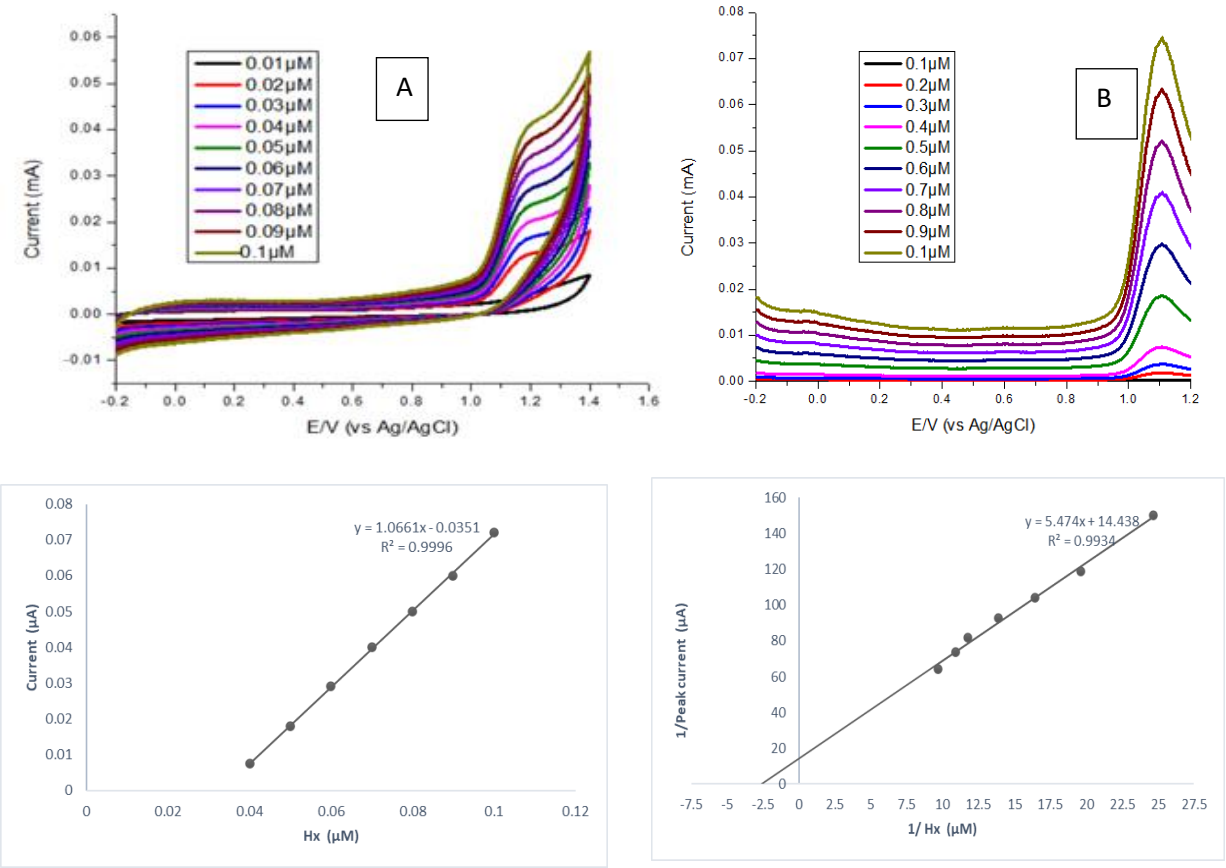


Figure 4.35. (A) CV, (B) DPV profiles/responses of XOD/3%$Co_2TiO_4$-MWCNTs-TETA/GCE in a 0.1 M PB solution (pH 7.5) containing different concentration of Hx (0.01 to 0.1 µM) and (C) Linear relationship of peak currents and different concentration of Hx at a potential of 1.1 V.

Determination of detection limit for hypoxanthine (hx) was thoroughly investigated using modified biosensors. CV and DPV analysis were undertaken using XOD-3%$Co_2TiO_4$-MWCNTs-TETA/GCE, XOD/5%$Co_3O_4$-MWCNTs-TETA/GCE, XOD/5%$TiO_2$-MWCNTs-TETA/GCE, and. (Refer to figure 4.35, appendices 3 and 4 respectively. All biosensors indicated a linear relationship between current and concentration of hypoxanthine.

Based on the Lineweaver Burk plot in figure 4.35D, the enzyme parameters, km and $V_{max}$ were calculated to be 0.379 µM and 0.06 mA/µM for XOD/3%$Co_2TiO_4$-MWCNTs-TETA/GCE. The value of the km is reasonably low, which means high affinity of the enzyme towards hypoxanthine. This also confirmed by increased current peaks observed on both the CV and the DPV which are higher on all the bimetallic biosensors of titanium and cobalt nanocomposite. The detection limits were calculated based on the relationship LoD = 3.3 $\delta$/m where $\delta$ is the relative standard deviation of the intercept of the y-coordinates from the line of best fit, and m the slope of the same line. The data indicates that the detection limit of the proposed biosensor was 0.16 nM. The research by Hu *et al*. [74] have recorded at detection limit of 3.93 µM when using the use of amino-functionalised metal organic framework nanosheet with peroxidase and fluorescence.

Similar calculations were done using 5%$Co_3O_4$-MWCNTs-TETA, and 5%$TiO_2$-MWCNTs-TETA and they were found to be 0.02 µM, and 0.002 µM respectively. The lowest detection limit of the enzyme with the nanomaterials was found to be excellent on bimetallic biosensor as compared to monometallic biosensors.

## 4.11. Operational and long-term stability of the biosensor

### 4.11.1. Operational stability

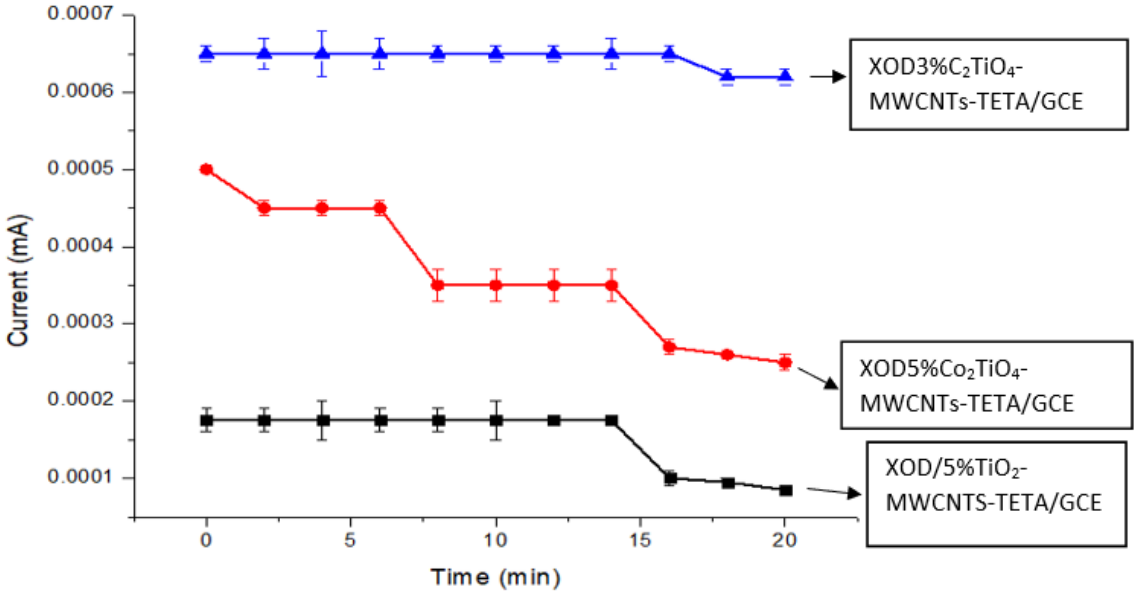


Figure 4.36. The operational stability of the biosensor modified with different metal oxides composition in 0,1 mM hypoxanthine solution.

Existing literature showed that most biosensors even though they are highly sensitive, they lack stability [87-90]. Therefore, investigation on the stability of the biosensor was conducted by carrying out an experiment at a constant pH, and temperature, in a solution containing 0.1 mM hypoxanthine. The cyclic voltammetry experiments were analysed at 2 minutes intervals to check the operational stability of the biosensor. The data in figure 4.36 shows that the biosensors modified with only one metal oxide lacked stability as compared to biosensors modified with bimetallic compounds. This shows that the metallic bond between titanium and cobalt has an effect on increasing the stability of the biosensors. Furthermore, the 3% loading of cobalt in XOD/3%$Co_2TiO_4$-MWCNTs-TETA/GCE showed increased stability, when compared to 5% cobalt loading. This is further supported by SEM results which showed fine distribution of the nanomaterials on 3%$Co_2TiO_4$-MWCNTs-TETA

nanocomposite as compared to 5%$Co_2TiO_4$-MWCNTs-TETA. Additional results tested for stability of the electrodes with different modifications is shown on appendix 11

### 4.11.2. Effects of storage on the stability of the developed biosensor

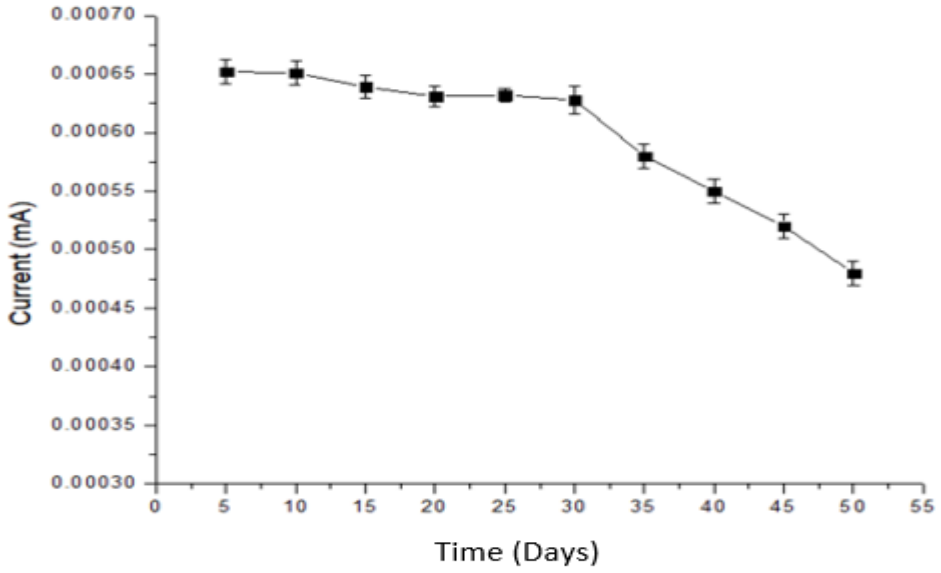


Figure 4.37: Effects of storage on the stability of XOD/3%$Co_2TiO_4$-MWCNTs-TETA/GCE towards the detection of 0.1 mM Hx in a PB solution (0.1 M, pH 7.5).

To investigate the storage stability of biosensor, experiments were conducted for 50 days at constant pH of 7.5, at room temperature in a solution containing 0.1 mM hypoxanthine. The results are shown in figure 4.37 relative standard deviation was calculated to be 10.7% and the biosensor after 50 days retained 73.4% of its initial performance. The performance of the proposed biosensor, XOD/3%$Co_2TiO_4$-MWCNTs-TETA/GCE showed very good stability on long term studies.

**Table 4.1: Comparisons of the electrode modifications reported on the literature**

| Electrode type | Linear range | LoD | Retained stability (long term studies) | Ref |
|---|---|---|---|---|
| 1,3,6,8-pyrene tetra sulfonic acid sodium salt functionalised nitrogen-doped graphene composite (XOD/PyTS–NG/GCE) | 8–200 μM | 0.231 μM | 86.4% after 15 days | 92 |
| carboxymethylcellulose-modified graphene oxide with platinum nanoparticles-decorated PAMAM-MNP hybrid nanomaterial (XOD/MNP-PAMAM-PtNP/rGO-CMC/GCE) | 50 nM–12 μM | 0.013 μM | 94% after 7 days | 93 |
| water-soluble carboxymethyl cellulose-nano-rod clay mineral palygorskite-nitrogen doped graphene (XOD/CMC-Pal-NG/GCE) | 0.6 -55 μM | 0.4 μM | - | 94 |
| amino-functionalized metal organic framework (XOD/NH2-Cu-MOF-GCE) | 10–2000 μM | 3.93 μM | - | 95 |
| poly(L-aspartic acid)-multi-walled carbon nanotube (XOD/Poly(L-Asp)/MWCNT/GCE) | 0.005–50.0 μM | $3.5\times10^{-4}$ μM | 80% after 20 days | 96 |
| ceria oxide nanoparticles (CeNPs/GCE | 597-800 μM | 15 μM | 86% after 14 days | 97 |
| 3%Cobalt titanium oxide- amine fuctionalised-multiwalled carbon nanotubes-triethylenetetramine (XOD/3%$Co_2TiO_4$-MWCNTs-TETA/GCE | 0.04-500 μM | 0.16 nM | 73.4% after 50 days | This work |

## 7.12. Analysis of fish stored at 25, 5 and -15 ºC for 7 days using cyclic and differential pulse voltammetry

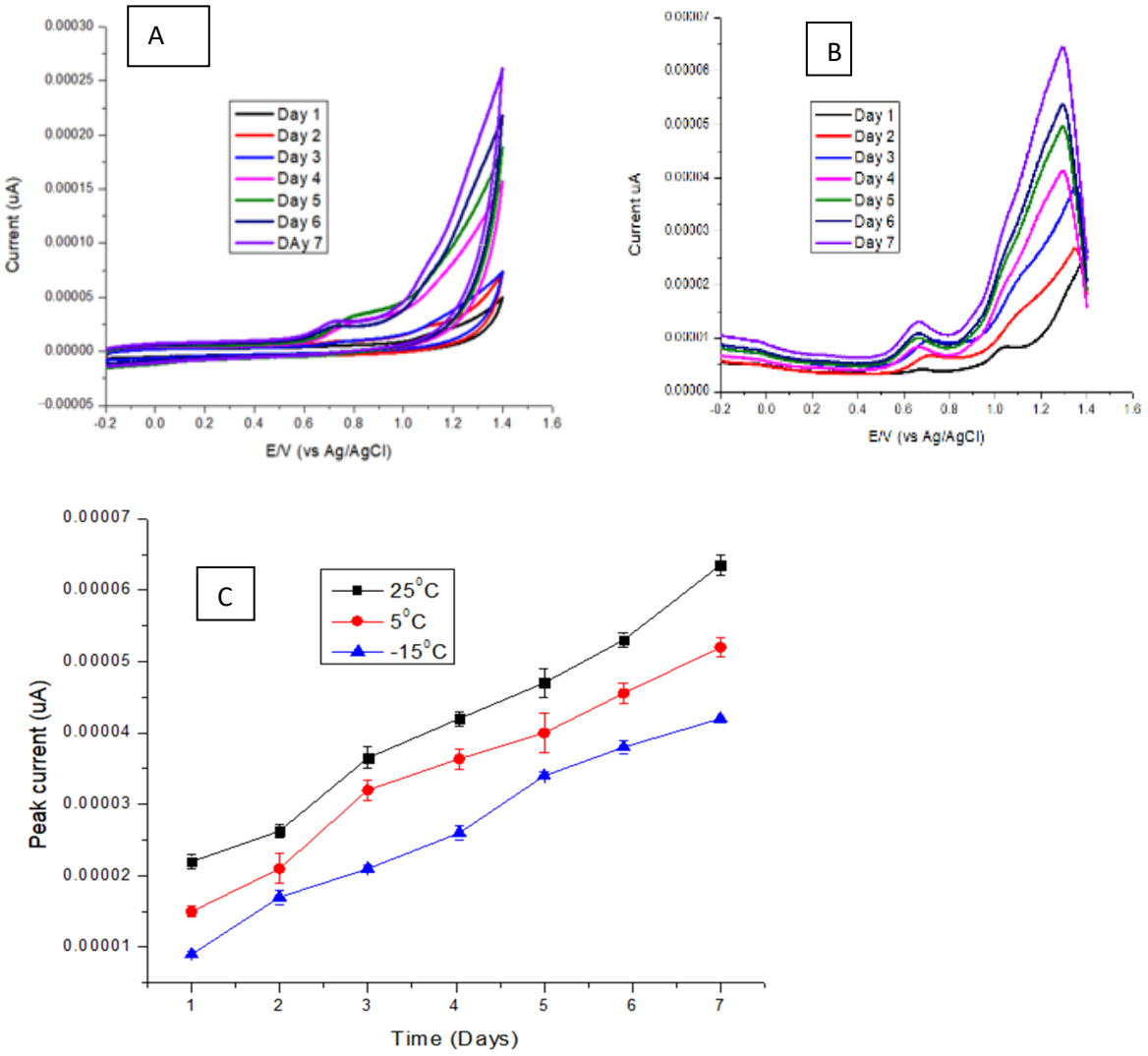


Figure 4.38. (A) CV and (B) DPV analysis of fish meat samples at different temperatures (25, 5 and -15 ºC) for 7 days using XOD/3%$Co_2TiO_4$-MWCNTs-TETA/GCE in a 0.1 M PB solution (pH 7.5). (C) The graph of peak current (at 1.2 V) of the differential pulse voltammetry against time (days) at three different temperatures.

The data in figure 4.38 shows the results obtained for meat analysis of fish stored at 25 $^0$C. The cyclic voltammogram and differential pulse voltammogram indicates that the hypoxanthine peak concentration increases from day 1 to day 7. The drastic

increase in hypoxanthine is also affected by the temperature where the meat is stored [98].

The results on meat analysis also inlcude analysis at 5 $^{o}$C (see appendix 8) The results show that the hypoxanthine peak is still increases on meat stored at 5 $^{o}$C. It is reported that mostly fish meat is preferably stored at -15 $^{o}$C to preserve the nutritional value of the meat [99]. However, on the analysis of hypoxanthine at this temperature the results (see appendix 9) show that from day 1 and 2 of the detection of hypoxanthine is very low. That suggests that fish meat stored at this temperature its quality is preserved. However, the results show that from day 3 to 7 its hypoxanthine concentration starts to gradually increase. Interesting to note, the rate at which hypoxanthine concentration is increases at -15 $^{0}$C is still less as compared to the results obtained at 25 $^{0}$C, and 5 $^{0}$C. Hence, a -15 $^{0}$C is a preferred storage temperature [100].

Figure 4.33 (C) shows summery of all results obtained at different temperatures. Higher temperature storage corresponds with high level of hypoxanthine. And low temperatures storage corresponds with low level of hypoxanthine. It is noteworthy to mention that the concentration of hypoxanthine increases with time regardless of the storage temperature. Whether frozen nor left at room temperature the fish meat deteriorates with time. However, it is recommended for meat to be frozen to delay the deterioration process.

### 4.13. Concluding remarks

In summary this work reports on the fabrication and application of a sensitive and highly stable biosensor for the determination of hypoxanthine. The presence of metal oxides and amine doped MWCNTs (with enhancement using light) have provided a suitable matrix for the immobilisation of the enzyme and for the detection of hypoxanthine. The biosensor has shown low interfering values with high stability and reusability and its lowest detection limit is 0.16 nM. The application of the biosensor was determined in fish meat bought at local supermarkets, and excellent results were obtained in relation to the freshness of the fishes at different temperatures. As such those evaluations suggested that the biosensor was a reliable analytical tool for

the determination of freshness of fish meat. The suggested platform in this work can also be applied for other meat analysis.

## 4.14. REFERENCES


[1] Salam, M. A., & Burk, R. (2017). Synthesis and characterization of multi-walled carbon nanotubes modified with octadecylamine and polyethylene glycol. *Arabian Journal of Chemistry*,*10*,. https://doi.org/10.1016/j.arabjc.2012.12.028

[2] Elkashef, M., Wang, K., & Abou-Zeid, M. N. (2016). Acid-treated carbon nanotubes and their effects on mortar strength. *Frontiers of Structural and Civil Engineering*, *10*(2), 180–188. https://doi.org/10.1007/s11709-015-0325-7

[3] Wang, T., Song, B., Qiao, K., Huang, Y., & Wang, L. (2018). Effect of dimensions and agglomerations of carbon nanotubes on synchronous enhancement of mechanical and damping properties of epoxy nanocomposites. *Nanomaterials*, *8*(12), 1–19. https://doi.org/10.3390/nano8120996

[4] Soleimani, M., Ghahraman Afshar, M., & Sedghi, A. (2013). Amino-Functionalization of Multiwall Carbon Nanotubes and Its Use for Solid Phase Extraction of Mercury Ions from Fish Sample. *ISRN Nanotechnology*, *2013*, 1–8. https://doi.org/10.1155/2013/674289

[5] Kashyap, A., Singh, N. P., Arora, S., Singh, V., & Gupta, V. K. (2020). Effect of amino-functionalization of MWCNTs on the mechanical and thermal properties of MWCNTs/epoxy composites. *Bulletin of Materials Science*, *43*(1). https://doi.org/10.1007/s12034-019-2012-0

[6] Jnido, G., Ohms, G., & Viöl, W. (2019). Deposition of TiO2 thin films on wood substrate by an air atmospheric pressure plasma jet. *Coatings*, *9*(7).

https://doi.org/10.3390/coatings9070441

[7] Chellappa, M., Anjaneyulu, U., Manivasagam, G., & Vijayalakshmi, U. (2015). Preparation and evaluation of the cytotoxic nature of TiO2 nanoparticles by direct contact method. *International Journal of Nanomedicine*, *10*, 31–41. https://doi.org/10.2147/IJN.S79978

[8] Sahoo, S., & Satpati, A. K. (2017). Electrochemical capacitance properties of cobalt oxide entangled over MWCNT and cobalt oxide AC composites. *Journal of Electroanalytical Chemistry*, 416–424. https://doi.org/10.1016/j.jelechem..08.022

[9] Madhi, A., Shirkavand Hadavand, B., & Amoozadeh, A. (2018). UV-curable urethane acrylate zirconium oxide nanocomposites: Synthesis, study on viscoelastic properties and thermal behavior. *Journal of Composite Materials*, *52*(21), 2973–2982. https://doi.org/10.1177/0021998318756173

[10] Stella, C., Soundararajan, N., & Ramachandran, K. (2014). Structural, optical, dielectric and magnetic properties of Mn 1-xCoxO2 nanowires. *Superlattices and Microstructures*, *71*(July), 203–210. https://doi.org/10.1016/j.spmi.2014.03.044

[11] Zheng, M., Zhang, H., Gong, X., Xu, R., Xiao, Y., Dong, H., Liu, X., & Liu, Y. (2013). A simple additive-free approach for the synthesis of uniform manganese monoxide nanorods with large specific surface area. *Nanoscale Research Letters*, *8*(1), 1–7. https://doi.org/10.1186/1556-276X-8-166

[12] Ghosh, D., Bhandari, S., & Khastgir, D. (2016). Synthesis of MnO2 nanoparticles and their effective utilization as UV protectors for outdoor high voltage polymeric insulators used in power transmission lines. *Physical Chemistry Chemical Physics*, *18*(48), 32876–32890. https://doi.org/10.1039/C6CP06611A

[13] Soldatova, A. V., Balakrishnan, G., Oyerinde, O. F., Romano, C. A., Tebo, B.

M., & Spiro, T. G. (2019). Biogenic and Synthetic MnO2 Nanoparticles: Size and Growth Probed with Absorption and Raman Spectroscopies and Dynamic Light Scattering. *Environmental Science and Technology*, *53*(8), 4185–4197. https://doi.org/10.1021/acs.est.8b05806

[14] Chan, Z. M., Kitchaev, D. A., Weker, J. N., Schnedermann, C., Lim, K., Ceder, G., Tumas, W., Toney, M. F., & Nocera, D. G. (2018). Electrochemical trapping of metastable Mn3+ ions for activation of MnO2 oxygen evolution catalysts. *Proceedings of the National Academy of Sciences of the United States of America*, *115*(23), E5261–E5268. https://doi.org/10.1073/pnas.1722235115

[15] Pudukudy, M., & Yaakob, Z. (2016). Synthesis, Characterization, and Photocatalytic Performance of Mesoporous α -Mn 2 O 3 Microspheres Prepared via a Precipitation Route *Journal of Nanoparticles*,https://doi.org/10.1155/2016/8037013

[16] Abbas, H., & Nasser, S. A. (1996). Hydroxyl as a defect of the manganese dioxide lattice and its applications to the dry cell battery. *Journal of Power Sources*, *58*(1), 15–21. https://doi.org/10.1016/0378-7753(95)02770-X

[17] Eslam A.A. Aboelazm, Gomaa A.M. Ali, K. F. C. (2018). Cobalt Oxide Supercapacitor Electrode Recovered from Spent Lithium-Ion Battery. Chemistry of Advanced Materials, 3(4), 67–74

[18] Bahari, H. R., Sidek, H. A. A., Adikan, F. R. M., Yunus, W. M. M., & Halimah, M. K. (2012). Infrared study of Er3+/Yb3+ co-doped GeO2-PbO-Bi2O3 glass. *International Journal of Molecular Sciences*, *13*(7), 8609–8614. https://doi.org/10.3390/ijms13078609

[19] Inamuddin, Shakeel, N., Imran Ahamed, M., Kanchi, S., & Abbas Kashmery, H. (2020). Green synthesis of ZnO nanoparticles decorated on polyindole functionalized-MCNTs and used as anode material for enzymatic biofuel cell applications. *Scientific Reports*, *10*(1), 1–10. https://doi.org/10.1038/s41598-020-61831-4

[20] Manoj, V., Karthika, M., Praveen Kumar, S. R., Boomadevi, S., Jeyadheepan, K., Karn, R. K., John Bosco Balaguru, R., & Pandiyan, K. (2014). Synthesis of zno nanoparticles using carboxymethyl cellulose hydrogel. In *Asian Journal of Applied Sciences* (Vol. 7, Issue 8, pp. 798–803). https://doi.org/10.3923/ajaps.2014.798.803

[21] Silva, W. M., Ribeiro, H., Seara, L. M., Calado, H. D. R., Ferlauto, A. S., Paniago, R. M., Leite, C. F., & Silva, G. G. (2012). Surface properties of oxidized and aminated multi-walled carbon nanotubes. *Journal of the Brazilian Chemical Society*, *23*(6), 1078–1086. https://doi.org/10.1590/S0103-50532012000600012

[22] Yibeltal, A. W., Beyene, B. B., Admassie, S., Taddesse, A. M., Dar, B., Program, M. S., Box, P. O., Ababa, A., & Dawa, D. (2020)*., 138,*. *34*(1), 55–66

[23] Lavand, A. B., & Malghe, Y. S. (2015). Synthesis, characterization and visible light photocatalytic activity of nitrogen-doped zinc oxide nanospheres. *Journal of Asian Ceramic Societies*, *3*(3), 305–310. https://doi.org/10.1016/j.jascer.2015.06.002

[24] Thamaphat, K., Limsuwan, P., & Ngotawornchai, B. (2008). *Phase Characterization of TiO 2 Powder by XRD and TEM*. *361*, 357–361

[25] . Shitole, K. D., Nainani, R. K., & Thakur, P. (2013). Preparation, characterisation and photocatalytic applications of TiO 2-MWCNTs composite. *Defence Science Journal*, *63*(4), 435–441. https://doi.org/10.14429/dsj.63.4870
.

[26] Jun, L. Y., Mubarak, N. M., Yon, L. S., Bing, C. H., Khalid, M., & Abdullah, E. C. (2018). Comparative study of acid functionalization of carbon nanotube via ultrasonic and reflux mechanism. *Journal of environmental chemical engineering*, *6*(5), 5889-5896..

[27] Lendzion-bielun, Z., Narkiewicz, U., & Arabczyk, W. (2013). *Cobalt-based*

*Catalysts for Ammonia Decomposition*. *June*. https://doi.org/10.3390/ma6062400

[28] S. Y. Vaselnia, M. K. Aminian, and R. D. Banadaki, “Experimental and theoretical study on the structural , electronic , and optical properties within DFT + U , F xc kernel for LRC model , and BSE approaches . Part I : CoTiO 3 and Co 2 TiO 4 pigments,” *Powder Technol.*, vol. 390, pp. 50–61, 2021, doi: 10.1016/j.powtec.2021.05.070.

[29] Rujiwatra C, “Co-Ti-O Complex Oxides : Hydrothermal Synthesis , Phase Characterization , Color Analysis and Catalytic Activity Assessment,” vol. 42, no. 4, pp. 857–867, 2015.

[30] C. J. Venegas., “Co 2 TiO 4 / Reduced Graphene Oxide Nanohybrids for Electrochemical Sensing Applications,” pp. 1–18

[31] M. Ramezani and S. M. Hosseinpour-mashkani, “Controlled Synthesis , Characterization , and Photocatalytic Application of Co 2 TiO 4 Nanoparticles,” vol. 46, no. 2, pp. 1371–1377, 2017, doi: 10.1007/s11664-016-5129-6.

[32] Chudoba, D., Łudzik, K., Jażdżewska, M., & Wołoszczuk, S. (2020). Kinetic and equilibrium studies of doxorubicin adsorption onto carbon nanotubes. *International Journal of Molecular Sciences*, *21*(21), 1–24. https://doi.org/10.3390/ijms21218230

[33] Tan, J. M., Bullo, S., Fakurazi, S., & Hussein, M. Z. (2020). Preparation, characterisation and biological evaluation of biopolymer-coated multi-walled carbon nanotubes for sustained-delivery of silibinin. *Scientific Reports*, *10*(1), 1–15. https://doi.org/10.1038/s41598-020-73963-8

[34] Jang, J., Miran, W., & Lee, D. S. (2018). Amino-functionalized multi-walled

carbon nanotubes for removal of cesium from aqueous solution. *Journal of Radioanalytical and Nuclear Chemistry*, *316*(2), 691–701. https://doi.org/10.1007/s10967-018-5812-6

[35] Borai, E. H., M. M.E. Breky, M. S. Sayed, and M. M. Abo-Aly. 2015. “Synthesis, Characterization and Application of Titanium Oxide Nanocomposites for Removal of Radioactive Cesium, Cobalt and Europium Ions.” *Journal of Colloid and Interface Science* 450: 17–25. https://doi.org/10.1016/j.jcis.2015.02.062.

[36] Tao, L., Shengjun, L., Bowen, Z., Bei, W., Dayong, N., Zeng, C., Ying, Y., Ning, W., & Weifeng, Z. (2015). Supercapacitor electrode with a homogeneously Co3O4-coated multiwalled carbon nanotube for a high capacitance. *Nanoscale Research Letters*, *10*(1). https://doi.org/10.1186/s11671-015-0915-2

[37] Massoumi, B., Jaymand, M., Samadi, R., & Entezami, A. A. (2014). In situ chemical oxidative graft polymerization of thiophene derivatives from multi-walled carbon nanotubes. *Journal of Polymer Research*, *21*(5). https://doi.org/10.1007/s10965-014-0442-3

[38] Malikov, E., Muradov, M., Kukovecz, A., & Kónya, Z. (2014). Oxidation of multiwalled carbon nanotubes using different oxidation agents like nitric acid and potassium permanganate. *News of Baku University*, *4*(January), 49–59.

[39] Špitalský, Z., Krontiras, C. A., Georga, S. N., & Galiotis, C. (2009). Effect of oxidation treatment of multiwalled carbon nanotubes on the mechanical and electrical properties of their epoxy composites. *Composites Part A: Applied Science and Manufacturing*, 778–783. https://doi.org/10.1016/j.

[40] Maleki, A., Hamesadeghi, U., Daraei, H., Hayati, B., Najafi, F., McKay, G., & Rezaee, R. (2017). Amine functionalized multi-walled carbon nanotubes: Single and binary systems for high capacity dye removal. *Chemical Engineering Journal*, *313*(May 2018), 826–835. https://doi.org/10.1016/j.

[41] Jang, J., Miran, W., & Lee, D. S. (2018). Amino-functionalized multi-walled carbon nanotubes for removal of cesium from aqueous solution. *Journal of Radioanalytical and Nuclear Chemistry*, 691–701. https://doi.org/10.1007/s10967-018-5812-6

[42] Lin, Y. H., Weng, C. H., Srivastav, A. L., Lin, Y. T., & Tzeng, J. H. (2015). Facile Synthesis and Characterization of N-Doped TiO2 Photocatalyst and Its Visible-Light Activity for Photo-Oxidation of Ethylene. *Journal of Nanomaterials*, *2015*(December). https://doi.org/10.1155/2015/807394

[43] Al-Taweel, S. S., & Saud, H. R. (2016). New route for synthesis of pure anatase TiO2 nanoparticles via utrasound-assisted sol-gel method. *Journal of Chemical and Pharmaceutical Research*, *8*(2), 620–626.

[44] Huang, B. S., Tseng, H. H., & Wey, M. Y. (2009). Comparison of visible-light-driven routes of anion-doped TiO2 and composite photocatalyst. *Journal of the Ceramic Society of Japan*, *117*, 753–758. https://doi.org/10.2109/jcersj2.117.753

[45] Shi, J. L., Gao, J. H., Lin, Z. X., & Yan, D. S. (1993). Effect of agglomerates in ZrO2 powder compacts on microstructural development. *Journal of Materials Science*, *28*(2), 342–348. https://doi.org/10.1007/BF00357805

[46] Vasylkiv, O., & Sakka, Y. (2001). Synthesis and Colloidal Processing of Zirconia Nanopowder. *Journal of the American Ceramic Society*, *84*(11), 2489–2494. https://doi.org/10.1111/j.1151-2916.2001.tb01041.x

[47] Lephuthing, S. S., Okoro, A. M., Lesufi, M., Ige, O. O., & Olubambi, P. A. (2018). Effect of milling parameters on the dispersion characteristics of multi-walled carbon nanotubes in transition metal oxides. *IOP Conference Series: Materials Science and Engineering*, *430*(1), 0–7. https://doi.org/10.1088/1757-

899X/430/1/012002

[48] Dey, S., & Praveen Kumar, V. V. (2020). The performance of highly active manganese oxide catalysts for ambient conditions carbon monoxide oxidation. *Current Research in Green and Sustainable Chemistry*, *3*(July), 100012. https://doi.org/10.1016/j.crgsc.2020.100012

[49] Leong, Z. Y., & Yang, H. Y. (2019). A Study of MnO 2 with Different Crystalline Forms for Pseudocapacitive Desalination. *ACS Applied Materials and Interfaces*, *11*(14), 13176–13184. https://doi.org/10.1021/acsami.8b20880

[50] Sellers, M. C. K., Castle, B. M., & Marsh, C. P. (2013). Three-dimensional manganese dioxide-functionalized carbon nanotube electrodes for electrochemical supercapacitors. *Journal of Solid State Electrochemistry*, *17*(1), 175–182. https://doi.org/10.1007/s10008-012-1863-8

[51] Hafeez, M., Shaheen, R., Akram, B., Zain-Ul-Abdin, Haq, S., Mahsud, S., Ali, S., & Khan, R. T. (2020). Green synthesis of cobalt oxide nanoparticles for potential biological applications. *Materials Research Express*, *7*(2). https://doi.org/10.1088/2053-1591/ab70dd

[52] Farhadi, S., Javanmard, M., & Nadri, G. (2016). Characterization of cobalt oxide nanoparticles prepared by the thermal decomposition of [Co(NH3)5(H2O)](NO3)3 complex and study of their photocatalytic activity. *Acta Chimica Slovenica*, *63*(2), 335–343. https://doi.org/10.17344/acsi.2016.2305

[53] Mansouri, B., Maleki, A., Johari, S. A., & Reshahmanish, N. (2015). Effects of cobalt oxide nanoparticles and cobalt ions on gill histopathology of zebrafish (Danio rerio). *AACL Bioflux*, *8*(3), 438–444

[54] Fernández-Loyola, R., Muthuvel, M., Hernández-Maldonado, A. B., Menchaca-Rivera, J. A., Perez-Robles, J. F., Solorza-Feria, O., & Botte, G. G. (2021). Nanocomposites of multi-walled carbon nanotubes with encapsulated cobalt.

*CeramicsInternational*,*47*-54https://doi.org/10.1016/j.

[55] Domingos, R. F., Rafiei, Z., Monteiro, C. E., Khan, M. A. K., & Wilkinson, K. J. (2013). Agglomeration and dissolution of zinc oxide nanoparticles: Role of pH, ionic strength and fulvic acid. *Environmental Chemistry*, *10*(4), 306–312. https://doi.org/10.1071/EN12202

[56] Méndez-Lozano, N., Apátiga-Castro, M., Manzano-Ramírez, A., Rivera-Muñoz, E. M., Velázquez-Castillo, R., Alberto-González, C., & Zamora-Antuñano, M. (2020). Morphological study of $TiO_2$ thin films doped with cobalt by Metal Organic Chemical Vapor Deposition. *Results in Physics*, *16*(December 2019), 102891. https://doi.org/10.1016/j.rinp.2019.102891

[57] Sutrave, D. S. (2018). Properties of Stacked Cobalt: Ruthenium Oxide Thin Film. *International Journal for Research in Applied Science and Engineering Technology*, *7*(1), 437–441. https://doi.org/10.22214/ijraset.2019.1076

[58] Cao, Y., Qiu, J., & Smith, P. (1995). Effect of solvents and co-solvents on the processibility of polyaniline: I. solubility and conductivity studies. *Synthetic Metals*, *69*(1–3), 187–190. https://doi.org/10.1016/0379-6779(94)02412-R

[59] Forati-Nezhad, M., Mir Mohamad Sadeghi, G., Yaghmaie, F., & Alimohammadi, F. (2015). Affecting the morphology of silver deposition on carbon nanotube surface: From nanoparticles to dendritic (tree-like) nanostructures. *Materials Science and Engineering C*, *46*(January 2015), 232–238. https://doi.org/10.1016/j.msec.2014.10.039

[60] Liu, C.-X., & Choi, J.-W. (2012). Improved Dispersion of Carbon Nanotubes in Polymers at High Concentrations. *Nanomaterials*, *2*(4), 329–347. https://doi.org/10.3390/nano2040329

[61] Duan, X., Wei, W., Wang, S., & Ni, B. J. (2019). Recent advances in transition metal-based electrocatalysts for alkaline hydrogen evolution. *Journal of Materials Chemistry A*, *7*(25), 14971–15005. https://doi.org/10.1039/c9ta03220g

[62] Karimi-Maleh, H., Kumar, B. G., Rajendran, S., Qin, J., Vadivel, S., Durgalakshmi, D., Gracia, F., Soto-Moscoso, M., Orooji, Y., & Karimi, F. (2020). Tuning of metal oxides photocatalytic performance using Ag nanoparticles integration. *Journal of Molecular Liquids*, *314*, 113588. https://doi.org/10.1016/j.molliq.2020.113588

[63] Leary, R., & Westwood, A. (2011). Carbonaceous nanomaterials for the enhancement of TiO2 photocatalysis. *Carbon*, *49*(3), 741–772. https://doi.org/10.1016/j.carbon.2010.10.010

[64] Pesci, F. M., Wang, G., Klug, D. R., Li, Y., & Cowan, A. J. (2013). Efficient suppression of electron–hole recombination in oxygen-deficient hydrogen-treated TiO2 nanowires for photoelectrochemical water splitting. *The Journal of Physical Chemistry C*, *117*(48), 25837-25844.

.

[65] Moreno, A. M., Bloom, D., Singh, P., Fantry, J., Gorton, S., & Mhadeshwar, A. (2013). A Novel Enzymatic Technology for Removal of Hydrogen Sulfide from Biogas. In *New and Future Developments in Catalysis: Batteries, Hydrogen Storage and Fuel Cells*. Elsevier B.V. https://doi.org/10.1016/B978-0-444-53880-2.00002-8

[66] Mooltongchun, M., & Teepoo, S. (2019). A Simple and Cost-effective Microfluidic Paper-Based Biosensor Analytical Device and its Application for Hypoxanthine Detection in Meat Samples. *Food Analytical Methods*, *12*(12), 2690–2698. https://doi.org/10.1007/s12161-019-01626-0

[67] Sharma, N. K., Thakur, S., Thakur, N., Savitri, & Bhalla, T. C. (2016). Thermostable Xanthine Oxidase Activity from Bacillus pumilus RL-2d Isolated from

Manikaran Thermal Spring: Production and Characterization. *Indian Journal of Microbiology*, *56*(1), 88–98. https://doi.org/10.1007/s12088-015-0547-3

[68] Egwim, E. C., Vunchi, M. A., & Egwim, P. O. (2005). Comparism of xanthine oxidase activities in cow and goat milks. *Biokemistri*, *17*(1), 1–6. https://doi.org/10.4314/biokem.v17i1.32581

[69] Görgülü, M., Çete, S., Arslan, H., & Yaşar, A. (2013). Preparing a new biosensor for hypoxanthine determination by immobilization of xanthine oxidase and uricase in polypyrrole-polyvinyl sulphonate film. *Artificial Cells, Nanomedicine and Biotechnology*, *41*(5), 327–331. https://doi.org/10.3109/21691401.2012.744993

[70] Yang, W., Xu, W., Wang, Y., Chen, D., Wang, X., Cao, Y., Wu, Q., Tu, J., & Zhen, C. (2020). Photoelectrochemical Glucose Biosensor Based on the Heterogeneous Facets of Nanocrystalline TiO 2 /Au/Glucose Oxidase Films . *ACS Applied Nano Materials*, *3*(3), 2723–2732. https://doi.org/10.1021/acsanm.0c00086

[71] Erol, E., Yildirim, E., & Cete, S. (2020). Construction of biosensor for hypoxanthine determination by immobilization of xanthine oxidase and uricase in polypyrrole-paratoluenesulfonate film. *Journal of Solid State Electrochemistry*, *24*(7), 1695–1707. https://doi.org/10.1007/s10008-020-04715-x

[72] Ozturk, G., German, J. B., & de Moura Bell, J. M. L. N. (2019). Effects of industrial heat treatments on the kinetics of inactivation of antimicrobial bovine milk xanthine oxidase. *Npj Science of Food*, *3*(1). https://doi.org/10.1038/s41538-019-0046-8

[73] Fernandes, P. (2016). Enzymes in fish and seafood processing. *Frontiers in Bioengineering and Biotechnology*, 1–14. https://doi.org/10.3389/fbioe.2016.00059

[74] Hu, Shuisheng, Jingjing Yan, Xueming Huang, Longhua Guo, Zhenyu Lin, Fang

Luo, Bin Qiu, Kwok Yin Wong, and Guonan Chen. 2018. “A Sensing Platform for Hypoxanthine Detection Based on Amino-Functionalized Metal Organic Framework Nanosheet with Peroxidase Mimic and Fluorescence Properties.” *Sensors and Actuators, B: Chemical* 267 (May): 312–19. https://doi.org/10.1016/j.snb.2018.04.055

[75] Li, T., Ren, L., Wang, D., Song, M., Li, Q., & Li, J. (2019). Optimization of extraction conditions and determination of purine content in marine fish during boiling. *PeerJ*, *2019*(5), 1–23. https://doi.org/10.7717/peerj.6690

[76] Dolmacı, N., Çete, S., Arslan, F., Yaşar, A., Servet, Ç., Arslan, F., & Ya, A. (2012). *An amperometric biosensor for fish freshness detection from xanthine oxidase immobilized in polypyrrole-polyvinylsulphonate film An amperometr i c b i osensor for f i sh freshness detect i on from xanth i ne ox i dase i mmob i l i zed i n polypyrrole-poly*. *1199*. https://doi.org/10.3109/10731199.2011.646410

[77] Narang, J., Malhotra, N., Singhal, C., & Pundir, C. S. (2017). Evaluation of Freshness of Fishes Using MWCNT / TiO 2 Nanobiocomposites Based Biosensor. *Food Analytical Methods*, 522–528. https://doi.org/10.1007/s12161-016-0594-3

[78] Luo, A., Lian, Q., An, Z., Li, Z., Guo, Y., Zhang, D., Xue, Z., Zhou, X., & Lu, X. (2015). Simultaneous determination of uric acid , xanthine and hypoxanthine based on sulfonic groups functionalized nitrogen-doped graphene. *JEAC*, *756*, 22–29. https://doi.org/10.1016/j.jelechem.2015.08.008

[79] Li, T., Ren, L., Wang, D., Song, M., Li, Q., & Li, J. (2019). Optimization of extraction conditions and determination of purine content in marine fish during boiling. *PeerJ*, *2019*(5), 1–23. https://doi.org/10.7717/peerj.6690

[80] Görgülü, M., Çete, S., Arslan, H., Yaşar, A., Görgülü, M., Çete, S., Arslan, H., & Yaşar, A. (2013). *Preparing a new biosensor for hypoxanthine determination by immobilization of xanthine oxidase and uricase in polypyrrole-polyvinyl sulphonate film Preparing a new biosensor for hypoxanthine determination by immobilization of*

*xanthine oxidase and uricase* . *1401*. https://doi.org/10.3109/21691401.2012.744993

[81]. Sampels, S. (2015). The Effects of Storage and Preservation Technologies on the Quality of Fish Products: A Review. *Journal of Food Processing and Preservation*, *39*(6), 1206–1215. https://doi.org/10.1111/jfpp.12337

[82] Yildirim, E., & Cete, S. (2020). Construction of biosensor for hypoxanthine determination by immobilization of xanthine oxidase and uricase in polypyrrole-paratoluenesulfonate film. *Journal of Solid State Electrochemistry*, *24*(7), 1695–1707. https://doi.org/10.1007/s10008-020-04715-

[83] Chen, Jiamin, Yi Lu, Fen Yan, Yuanzi Wu, Da Huang, and Zuquan Weng. (2020). "A Fluorescent Biosensor Based on Catalytic Activity of Platinum Nanoparticles for Freshness Evaluation of Aquatic Products." *Food Chemistry* 310 https://doi.org/10.1016/j.foodchem.2019.125922

[84]. Villalonga R, Diez P, Gamella M, Reviejo J, Pingarrón. J.M., (2011) Electroanalysis nanostructure and performance of carbon nanotubes in the electrochemical for setection of hypoxanthine by enzymatic reactions, *Digest Journal of Nanomaterial and Biostructure,* volume 9, 23:1790–1796, pp 1331-1338.

[85] Amit, S. K., Uddin, M. M., Rahman, R., Islam, S. M. R., & Khan, M. S. (2017). A review on mechanisms and commercial aspects of food preservation and processing. *Agriculture and Food Security*, *6*(1), 1–22. https://doi.org/10.1186/s40066-017-0130-8

[86] Dawson, P., Al-Jeddawi, W., & Remington, N. (2018). Effect of Freezing on the Shelf Life of Salmon. *International Journal of Food Science*, *2018*. https://doi.org/10.1155/2018/1686121

[87] Khan, M. Z. H., Ahommed, M. S., & Daizy, M. (2020). Detection of xanthine in food samples with an electrochemical biosensor based on PEDOT:PSS and functionalized gold nanoparticles. *RSC Advances*, *10*(59), 36147–36154.

https://doi.org/10.1039/d0ra06806c

[88] Liao, L., Xing, Y., Xiong, X., Gan, L., Hu, L., Zhao, F., Tong, Y., & Deng, S. (2020). An electrochemical biosensor for hypoxanthine detection in vitreous humor: A potential tool for estimating the post-mortem interval in forensic cases. *MicrochemicalJournal*,*155*(February),104760.https://doi.org/10.1016/j.microc.2020.104760

[89] Seki, T., Orita, Y., Yamaji, K., & Shinoda, A. (1997). Simultaneous determination of creatinine, hypoxanthine and uric acid in biological samples by column-switching liquid chromatography with ultraviolet detection. In *Journal of pharmaceutical and biomedical analysis* (Vol. 15). https://doi.org/10.1016/S0731-7085(97)00011-3

[90] Chen, W., Lin, X. H., Lei, Y., & Liu, A. L. (2019). An electrochemical biosensor for sensitive detection of nicotine-induced dopamine secreted by PC12 cells. *Journal of Electroanalytical Chemistry*, *832*(October 2018), 217–224. https://doi.org/10.1016/j.jelechem.2018.10.018

[91] Azura, N., Said, M., & Ogurtsov, V. I. (2014). *25.)Electrochemical biosensor based on microfabricated electrode electrochemical biosensor based on for life sciences applications A dissertation submitted for the degree of Doctor of Philosophy National University of Ireland April 2014 Supervisors Dr . V*. *April*. https://doi.org/10.13140/RG.2.2.11066.49603

[92] Luo, A., Lian, Q., An, Z., Li, Z., Guo, Y., Zhang, D., Xue, Z., Zhou, X., & Lu, X. (2015). Simultaneous determination of uric acid , xanthine and hypoxanthine based on sulfonic groups functionalized nitrogen-doped graphene. *JEAC*, *756*, 22–29. https://doi.org/10.1016/j.jelechem.2015.08.008

[93] Borisova, B, Alfredo S, Sandra J, Miriam, M, Pedro S, Concepción, P, José M. Pingarrón, J, and Reynaldo Villalonga. (2016). “Reduced Graphene Oxide-Carboxymethylcellulose Layered with Platinum Nanoparticles/PAMAM

Dendrimer/Magnetic Nanoparticles Hybrids. Application to the Preparation of Enzyme Electrochemical Biosensors." *Sensors and Actuators, B: Chemical* 232: 84–90. https://doi.org/10.1016/j.snb.2016.02.106.

[94] Wen, Y, Juan C, Lanjiao, X, Xiaoning, L, Ling B, Yingdong, L, and Mingfang L. (2017). "Simultaneous Analysis of Uric Acid, Xanthine and Hypoxanthine Using Voltammetric Sensor Based on Nanocomposite of Palygorskite and Nitrogen Doped Graphene." *Journal of Electroanalytical Chemistry* 805 (159–70. https://doi.org/10.1016/j.jelechem.2017.09.053.

[95] Hu, S, Jingjing, Y, Xueming, H, Longhua, G, Zhenyu, L, Fang Luo, and Bin Q., (2018). "A Sensing Platform for Hypoxanthine Detection Based on Amino-Functionalized Metal Organic Framework Nanosheet with Peroxidase Mimic and Fluorescence Properties." *Sensors and Actuators, B: Chemical* 267: 312–19. https://doi.org/10.1016/j.snb.2018.04.055.

[96] Yazdanparast, S, Ali, B, Saleheh, A, and Masoud, R. (2019). "Enzyme-Based Ultrasensitive Electrochemical Biosensor Using Poly(L-Aspartic Acid)/MWCNT Bio-Nanocomposite for Xanthine Detection: A Meat Freshness Marker." *Microchemical Journal* 149 (May): 104000. https://doi.org/10.1016/j.microc.2019.104000.

[97] Mustafa, F, Ali, O, and Silvana A,. (2021). "Cerium Oxide-Based Hypoxanthine Biosensor for Fish Spoilage Monitoring." *Sensors and Actuators, B: Chemical* 332 129435. https://doi.org/10.1016/j.snb.2021.129435.

[98] Chen, J, Yi, L, Fen, Y, Yuanzi, W, and Zuquan, W. (2020). "A Fluorescent Biosensor Based on Catalytic Activity of Platinum Nanoparticles for Freshness Evaluation of Aquatic Products." *Food Chemistry* 310). https://doi.org/10.1016/j.foodchem.2019.125922

[99] Amit, S. K., Uddin, M. M., Rahman, R., Islam, S. M. R., & Khan, M. S. (2017). A review on mechanisms and commercial aspects of food preservation and

processing. *Agriculture and Food Security*, *6*(1), 1–22. https://doi.org/10.1186/s40066-017-0130-8

[100] Getu, A., & Misganaw, K. (2015). Post-harvesting and Major Related Problems of Fish Production. *Fisheries and Aquaculture Journal*, *06*(04). https://doi.org/10.4172/2150-3508.1000154

# CHAPTER 5

# 5. Conclusions and Recommendations

## 5.1 Conclusion

The sol gel method was successfully done to prepare the metal oxides. The *in-situ* method of functionalisation of MWCNTs was also successfully employed. The FTIR spectroscopy confirmed the functionalisation of acid-treated and amino doped MWCNTs by the presence of functional groups such as carboxyl (COOH), hydroxyl (OH) and amino ($NH_2$) groups. Comparative study was conducted for all the prepared metal oxides. It was found that the best two metal oxides are $TiO_2$ and $Co_3O_4$ as confirmed by the cyclic voltammetry. These metal oxides were then analysed on the XRD. It was found that $TiO_2$ has a strong diffraction peak at $25^0$ and broad peak at $45^0$, indicating that the titania nanoparticles are in the anatase phase, which had (101), and (211) planes respectively. While the XRD results for cobalt oxide demonstrate nanocomposite formation, which contained CoO and $Co_3O_4$ phases on cobalt oxide structures. The XRD analysis have shown a mixture of phases synthesised through by the sol gel method for the bimetallic nanocomposite which were $Co_2TiO_4$ and $Co_2TiO_3$. It is reported that the unit-cell parameters of $Co_2TiO_4$ could depend on the sintering conditions, such as temperature and pressure, and stoichiometry of the nanoparticles. From the results, it cannot be concluded that the synthesis of a single phase of $Co_2TiO_4$ is unlikely under the sol gel method. However, stoichiometry and synthetic temperature should be considered thoroughly during their synthesis. Only one published paper has reported the synthesis of pure $Co_2TiO_4$ by co-precipitation, followed by calcination at high temperature. Interestingly to note on the nanocomposite of 3% $Co_2TiO_4$-MWCNTs-TETA, the major phase obtained is $Co_2TiO_4$. These could show MWCNTs as good support materials for the synthesis of $Co_2TiO_4$.

The SEM revealed the morphological results of the functionalised MWCNTs that differed from that of the raw MWCNTs, which were highly agglomerated. It was also discovered that acid treatments on the MWCNTs deteriorate the tubes, while the

amino functionalisation decrease agglomeration with less damage done to the MWCNTs. The TGA results shows that MWCNTs alone are highly thermally stable with decomposition starting at 600 $^{0}$C. However, upon acid and amino functionalisation, the MWCNTs starts decomposing at low temperatures around 230 $^{0}$C. This is caused by heat treatment and acids that damage the tubes during functionalisation.

Nevertheless, the is strong evidence that as the MWCNTs are functionalised further with not only acids, but also amino-containing agents, the electroconductivity, surface area, and stability of the MWCNTs tend to increase confirmed by differential pulse and cyclic voltammetric techniques). Furthermore, the study has also shown an important discovery that increasing the organic length of the amino-containing agents when functionalising the MWCNTs, tends to increase the electroconductivity of the material, i.e, from hydrazine to triethylenetetramine (TETA) increase in electroconductivity was observed. This study has proven that the amino functionalisation of MWCNTs gives out excellent characteristics of the MWCNTs, which are hindered when they are not functionalised or slightly hindered when they are functionalised with acids only. The present study has brought new knowledge of taking the advantage of photocatalytic characteristics of the metal oxides and MWCNTs through using them to increase the specificity, sensitivity, and stability of the produced biosensor. MWCNTs have shown to be good support nanomaterials for deposition of metal oxides as they shift the maximum absorbance of the metal oxides to a higher wavelength, that is redshift of maximum absorbance was observed, indicating that less energy may be required for the excitation of electrons.

The surface modification of the glassy carbon electrode (GCE) is known to alter its characteristics including stability, repeatability, wide linearity range, low detection limit and sensitivity, resulting in its improved performance. In this study, the modified electrode, namely, XOD/3%$Co_2TiO_4$-MWCNTs-TETA/GCE showed excellent results as compared with electrodes which consisted of only one metal oxide in their nanocomposites. The modified electrode has good working characteristics like sensitivity, repeatability, low detection limit of 0.16 nM and wide linearity range from 0.004 to 500 µM. Thus, an outstanding approach towards the development of XOD/3%$Co_2TiO_4$-MWCNTs-TETA/GCE for determination of hypoxanthine in fish

meat is first of its kind to be reported in this study. The use of doping the MWCNTs with metal oxides showed a drastic improvement in the sensitivity, specificity, and electroconductivity of the biosensor.

Before this study many biosensors suffered interferences with the ascorbic acid. This study has solved that problem by combing two highly electroconductive metal oxides, which are titanium and cobalt oxides. This bimetallic modified biosensor showed drastic improvement in the interference with ascorbic acid and other studied biomolecules. Many different percentage composition biosensors were prepared and tested. However, the 3% $Co_2TiO_4$-MWCNTs modified biosensor in the presence of TETA and xanthine oxidase (XOD) was selected to be used in fish meat analysis. It was chosen because of its highly electroconductive, stable, sensitive, and specific, which were better as compared with those of other tested modified biosensors in this study. Important findings of this part were that even though fish meat is deep-frozen at -15 $^0$C, it is still vulnerable to an increase in hypoxanthine concentration and degradation as time passes by. Therefore, it can be concluded that fish storage might not depend solely on deep freezing for conserving meat, especially for longer periods. The developed XOD/3%$Co_2TiO_4$-MWCNTs-TETA modified biosensor showed excellent properties and has a good potential to be used in fish meat analysis.

### 5.2 Recommendations

The findings of this research lay foundation for the future studies to consider other types of meat including poultry, red meat, and pork to investigate their deterioration rate and their degree of spoilage based on hypoxanthine concentration. Since it was found that deep freezing does not entirely protect the fish meat from deteriorating, it remains important to consider other methods that can be combined with deep freezing to protect the nutritional information of meat like protective coverage of meat and coating with anti-spoilage agents in the future. Furthermore, to understand the mechanism of the modified biosensor with metal oxides at an atomic level, it is important to further study these nanomaterials using the X-ray photoelectron spectroscopy (XPS) to have a clear understanding of factors affecting the

electrochemical behaviour and the conductivity of these nanomaterials. It will be also beneficial to consider studying these nanomaterials using the Raman spectroscopy to elucidate the intramolecular bonds given by the effects of functionalising the MWCNTs to confirm their increased stability and specificity. Additionally, Brunauer-Emmett-Teller (BET) can be used to determine the exact surface area of the nanocomposites.

## 5.4 Appendices

### 5.4.1. Equations and calculations

**(a) Diffusion coefficient of XOD/3%$Co_2TiO_4$-MWCNTs-GCE was calculated as follows**

$$i_p = 2.69x10^5 n^{3/2} A C D^{1/2} v^{1/2}$$

$$0.0005\ mA/mVs^{-1} = 2.69x10^5 (1)^{3/2} (0.07\ cm^2)\ (5\ mM)\ (D)^{1/2}$$

$$D^{1/2} = \frac{0.0005\ mA/mVs^{-1}}{2.69x10^5 (1)^{\frac{3}{2}} (0.07\ cm^2)(5\ mM)}$$

$$D = \sqrt{\frac{0.0005\ mA/mVs^{-1}}{2.69x10^5 (1)^{\frac{3}{2}} (0.07\ cm^2)(5\ mM)}}$$

$D = 0.7x10^{-4}\ cm^2/s$

**(b) Surface coverage of XOD/3%$Co_2TiO_4$-MWCNTs-GCE was calculated as follows**

$$i_p = \frac{n^2F^2A\Gamma v}{4RT}$$

$$\Gamma = \frac{Slope(4RT)}{n^2F^2A}$$

$$\Gamma = \frac{\frac{0.00004mA}{mV/s}(4x8.3145\frac{J}{mol}\cdot K)x298.15K)}{1^2(96.5\ KJ/mol\ )^2(0.07\ cm^2)}$$

$\Gamma$= 60 x $10^{-5}$ mol/$cm^2$

**(c) Limit of detection (LoD) of XOD/3%$Co_2TiO_4$-MWCNTs-GCE was calculated as follows**

LoD = 3.3δ/m

$$= 3.3x\ (\frac{5.1x10^{-5}\mu A}{1.0661\ \mu A/\mu M})$$

=0.00016 µM

=0.16 nM

* Similar calculations were done for other electrodes

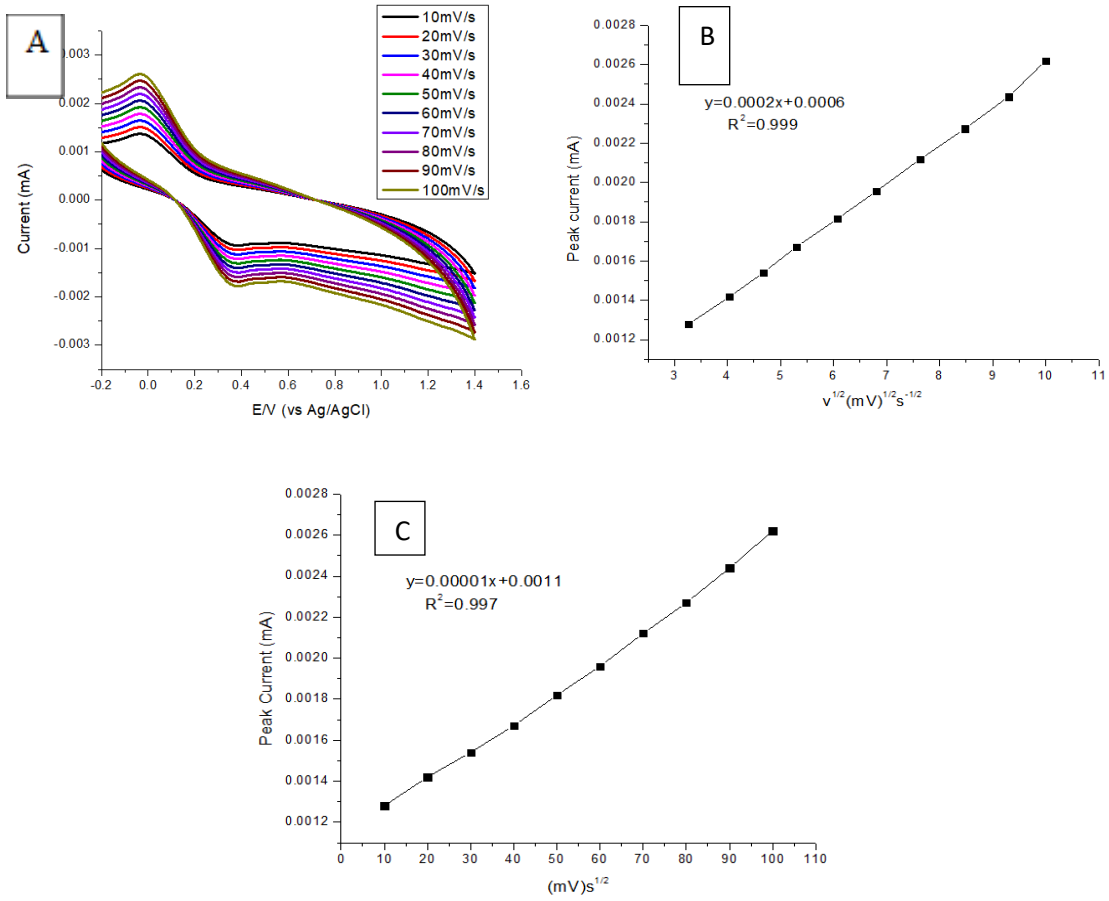


Appendix 1: Cyclic voltammograms at different scan rates from 10 to 100 mV/s represented by graphs A and B show the relationship between the peak current and the square root of the scan rate, and graph C presents the relationship between peak current and scan rate. This is for 5% $Co_3O_4$-MWCNTs-TETA composites.

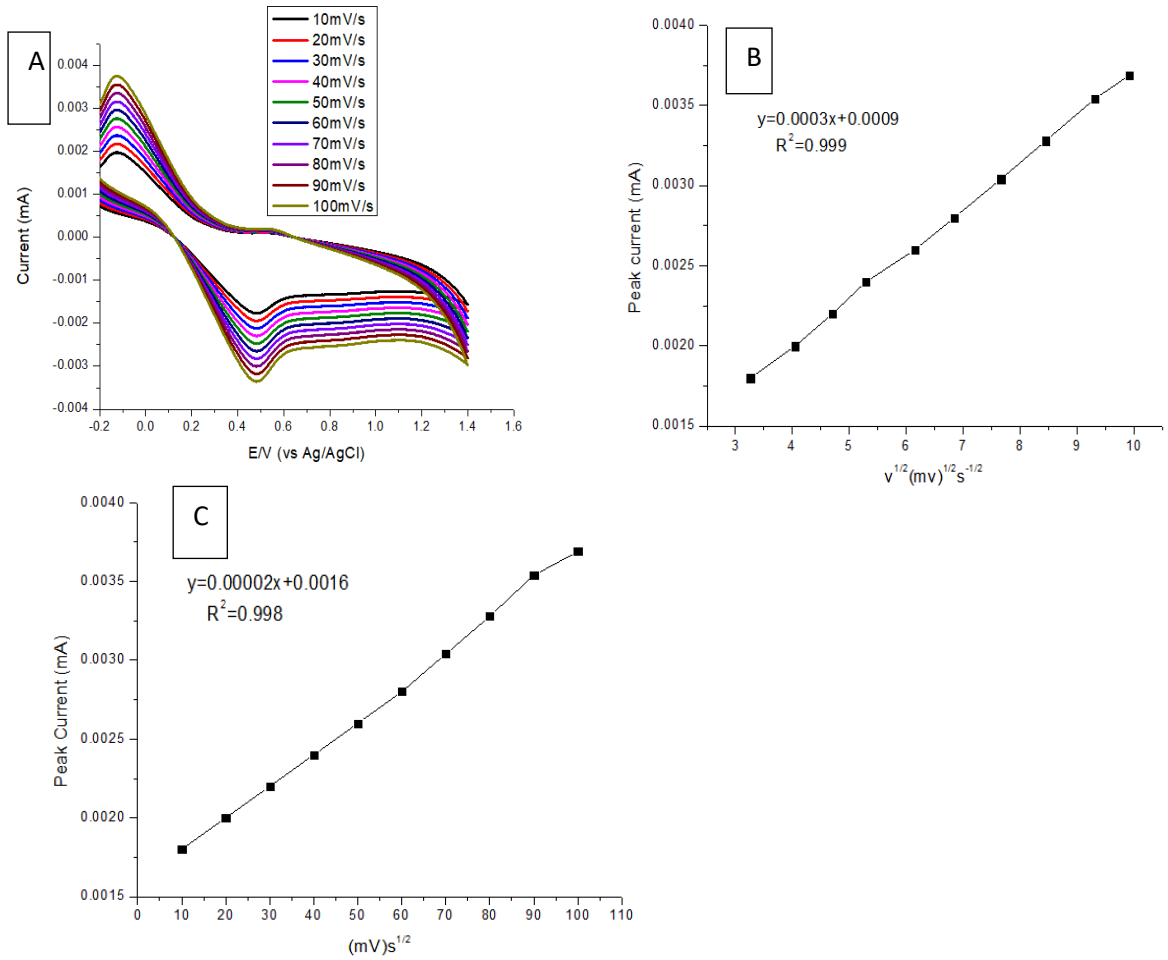


Appendix 2: Cyclic voltammogram obtained using 5%$TiO_2$-MWCNTs-TETA electrode differentiating scan rates from 10 to 100mV/s represented by graphs A and B represents the relationship between peak current and the square root of scan rates and graph C represents the relationship between peak current and the scan rate.

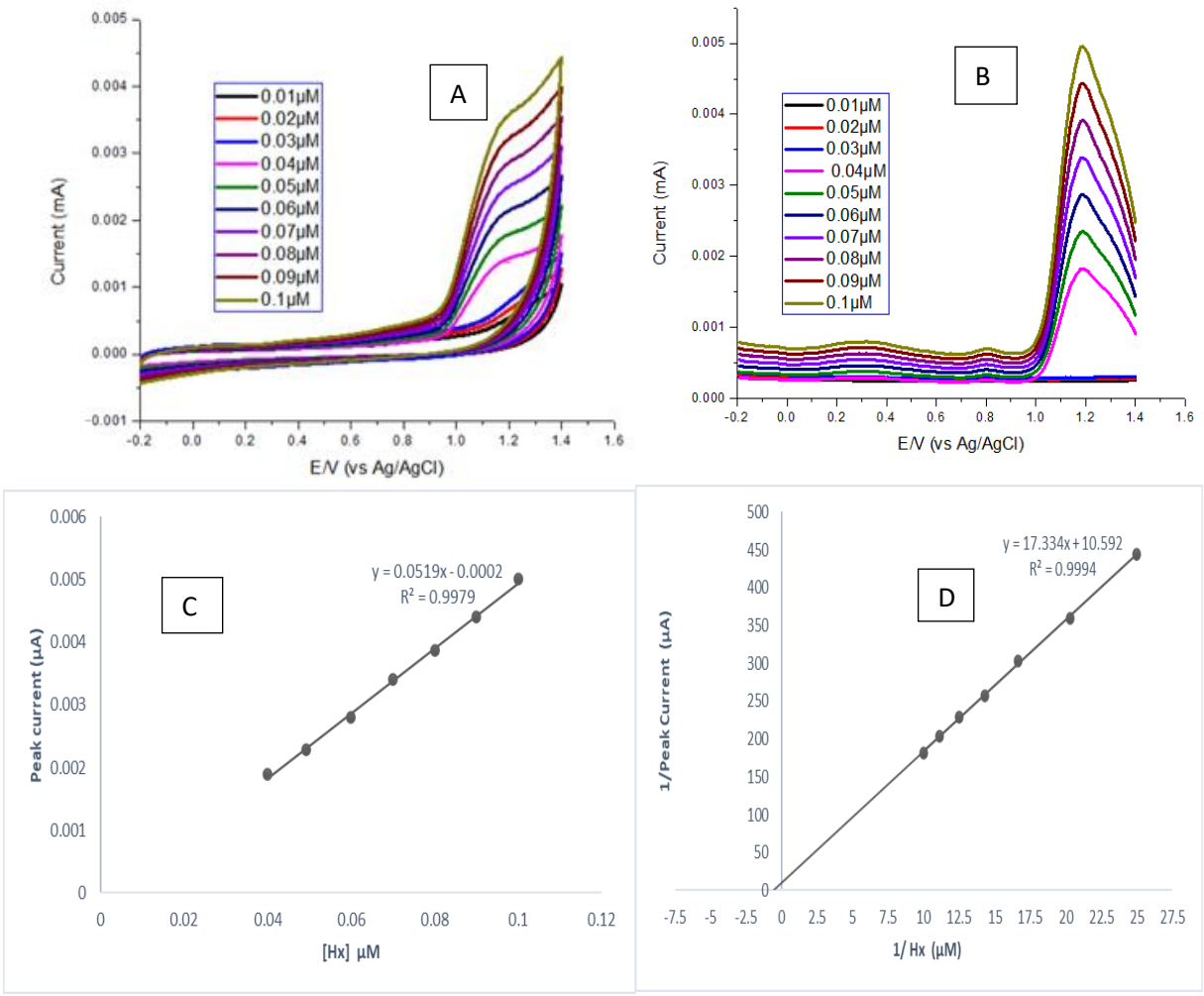


Appendix 3. Cyclic voltammograms (A) of hypoxanthine detection, differential pulse voltammograms (B) for detection of hypoxanthine, Calibration curve for detection of hypoxanthine (C), and Lineweaver Burk plot (D) using XOD/5%$Co_3O_4$-MWCNTs-TETA/GCE.

.

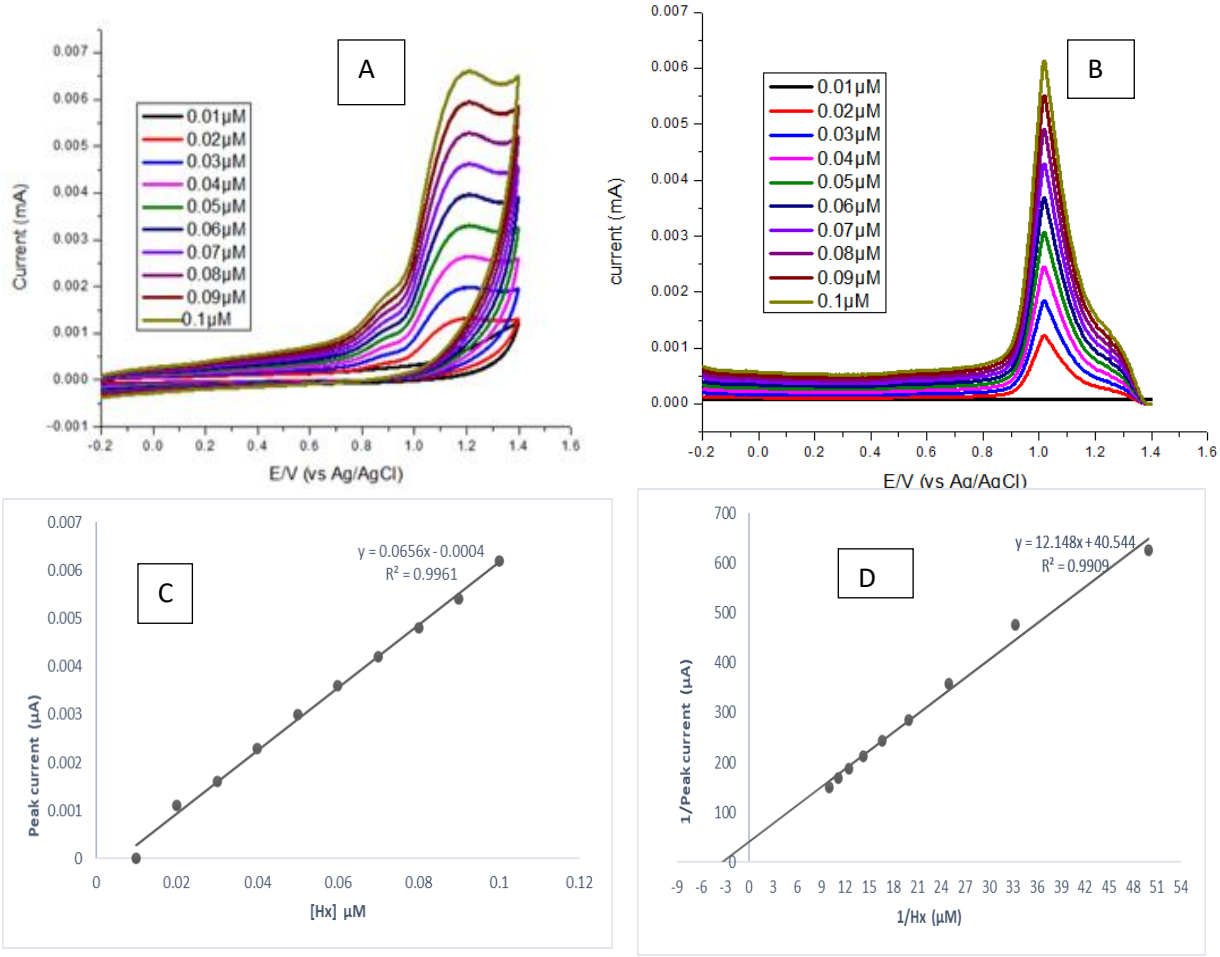


Appendix 4. Cyclic voltammograms (A) of hypoxanthine detection, differential pulse voltammograms (B) for detection of hypoxanthine, Calibration curve for detection of hypoxanthine (C), and Lineweaver Burk plot (D) using XOD/5% $TiO_2$-MWCNTs-TETA/GCE

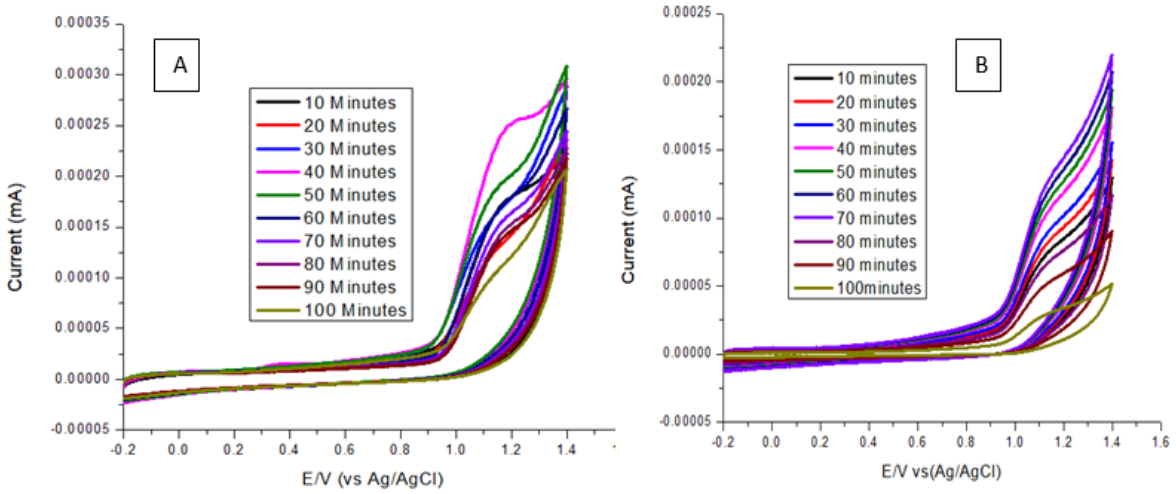


Appendix 5: Cyclic voltammograms for catalytic detection of hypoxanthine in 0.1 mM hypoxanthine solution containing phosphate buffer (5 mM) at pH 7.5. Effects of exposure to light on peak current for (A) 5%$TiO_2$-MWCNTs-TETA and (B) 5%$Co_3O_4$-MWCNTs-TETA in a 0.05 M PB solution containing 40 µM Hx.

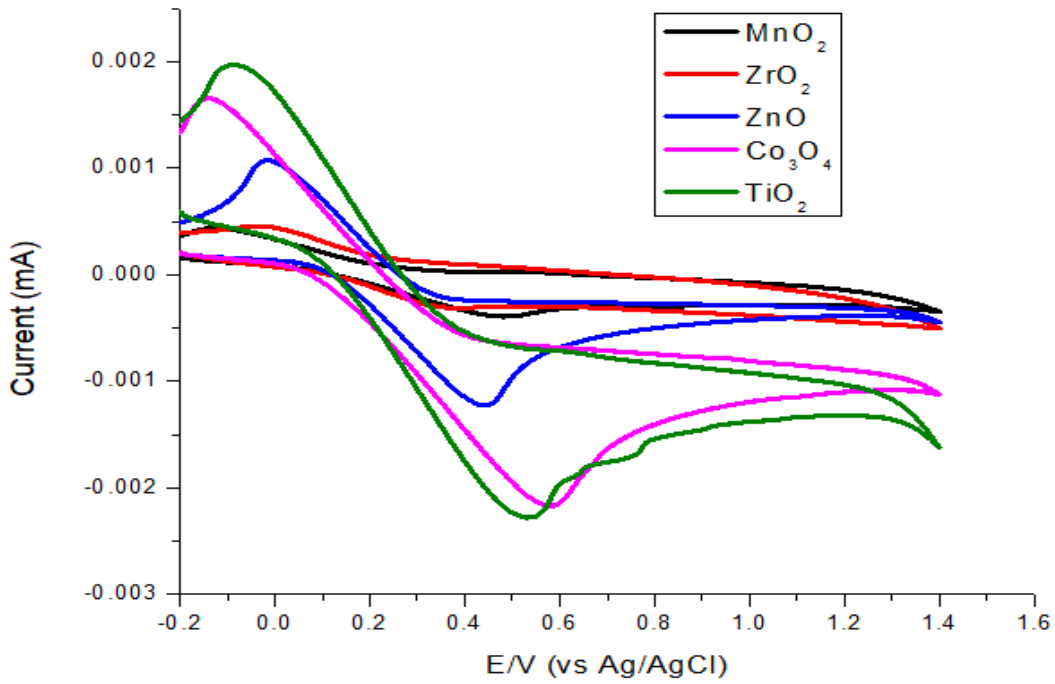


Appendix 6: Cyclic voltammograms representing comparative results of all metal oxides

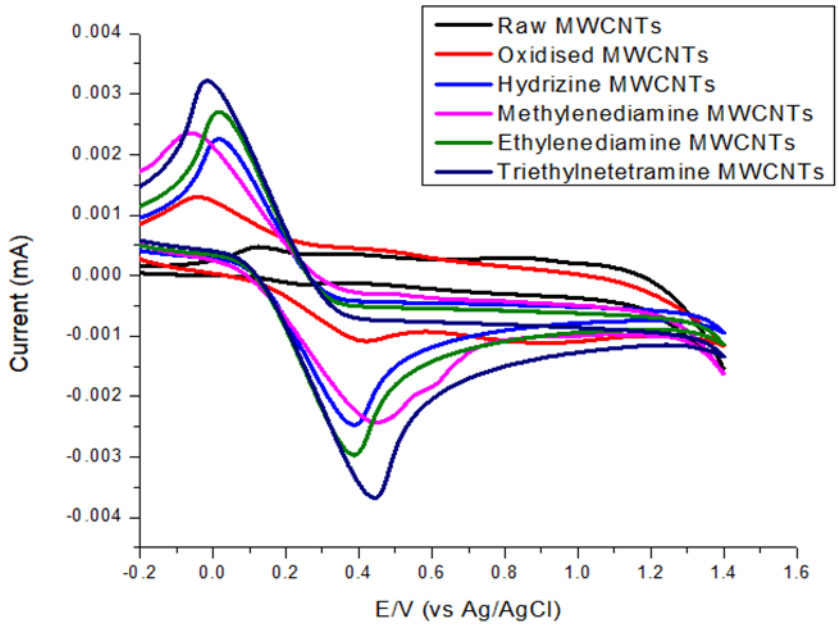


Appendix 7: Cyclic voltammograms of comparative study of all modified MWCNTs in 5 mM ferrocyanide solution

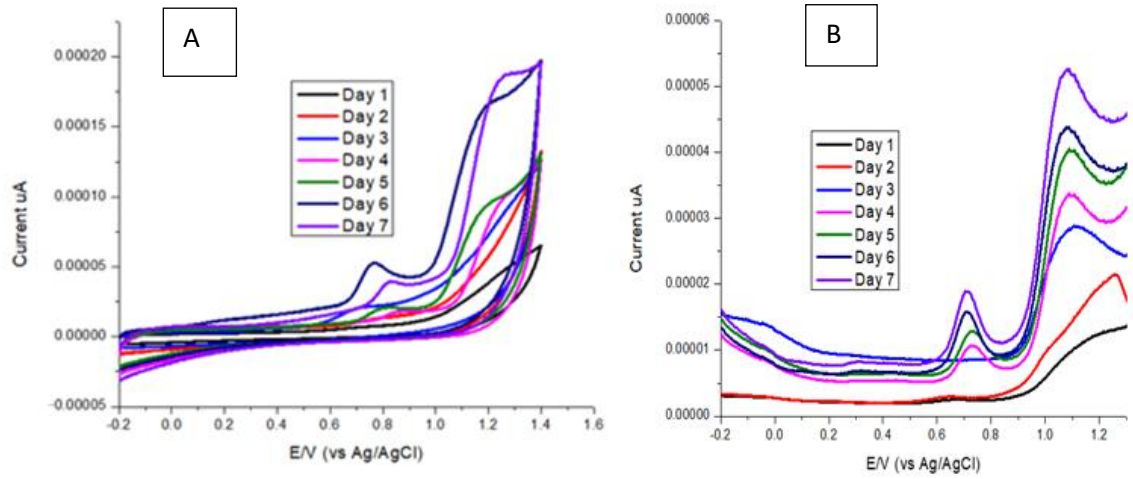


Appendix 8: Cyclic voltammograms (A), and differential pulse voltammograms (B) of fish meat analysis stored at 5 $^{0}$C studied using XOD/3%Co2TiO4-MWCNTs-TETA

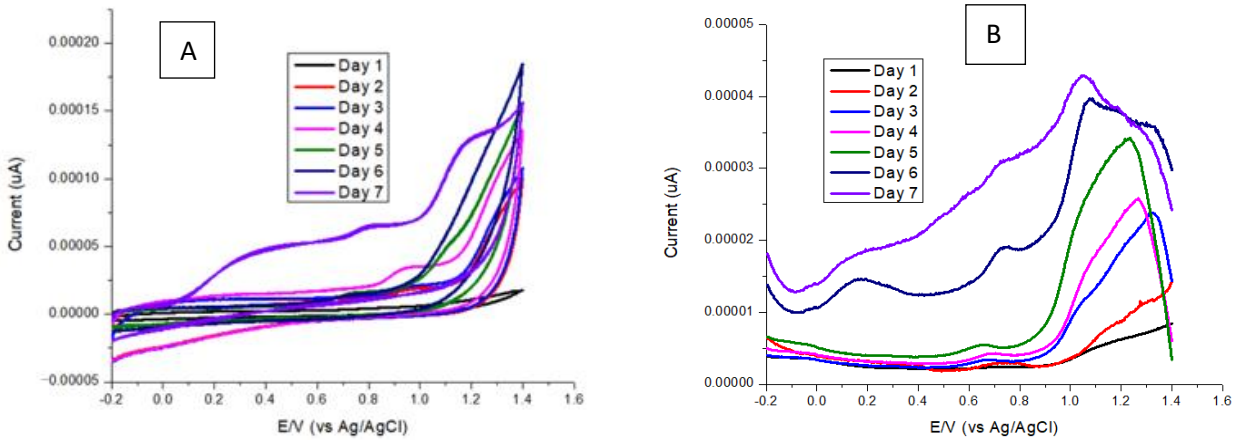


Appendix 9: Cyclic voltammograms (A), and differential pulse voltammograms (B) of fish meat analysis stored at -15 $^{0}$C

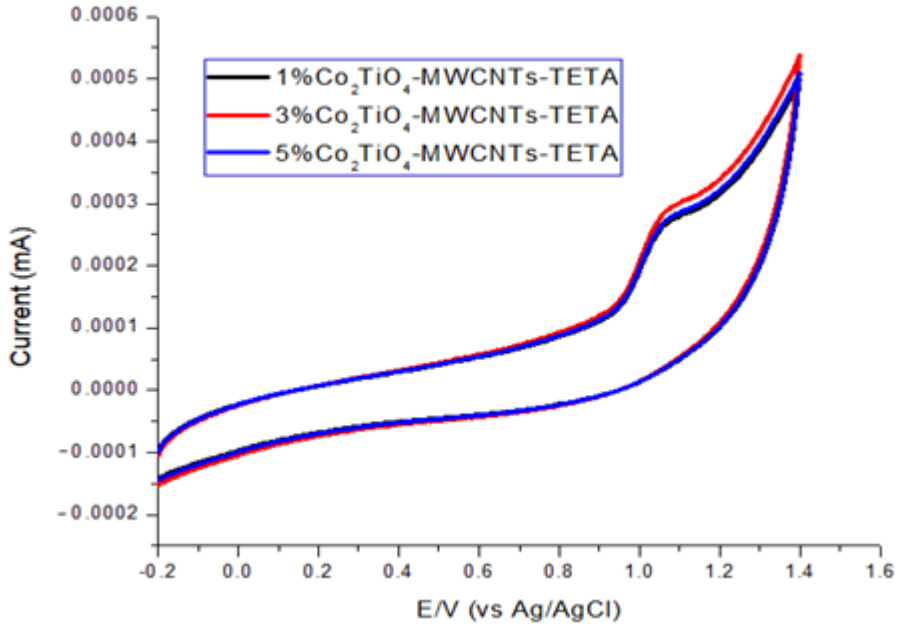


Appendix 10: Cyclic voltammogram showing the effects of cobalt loading on current response of XOD/$Co_2TiO_4$-MWCNTs-TETA/GCE in a phosphate buffer solution (0.1 M, pH 7.5) containing in 0,1 mM hypoxanthine.

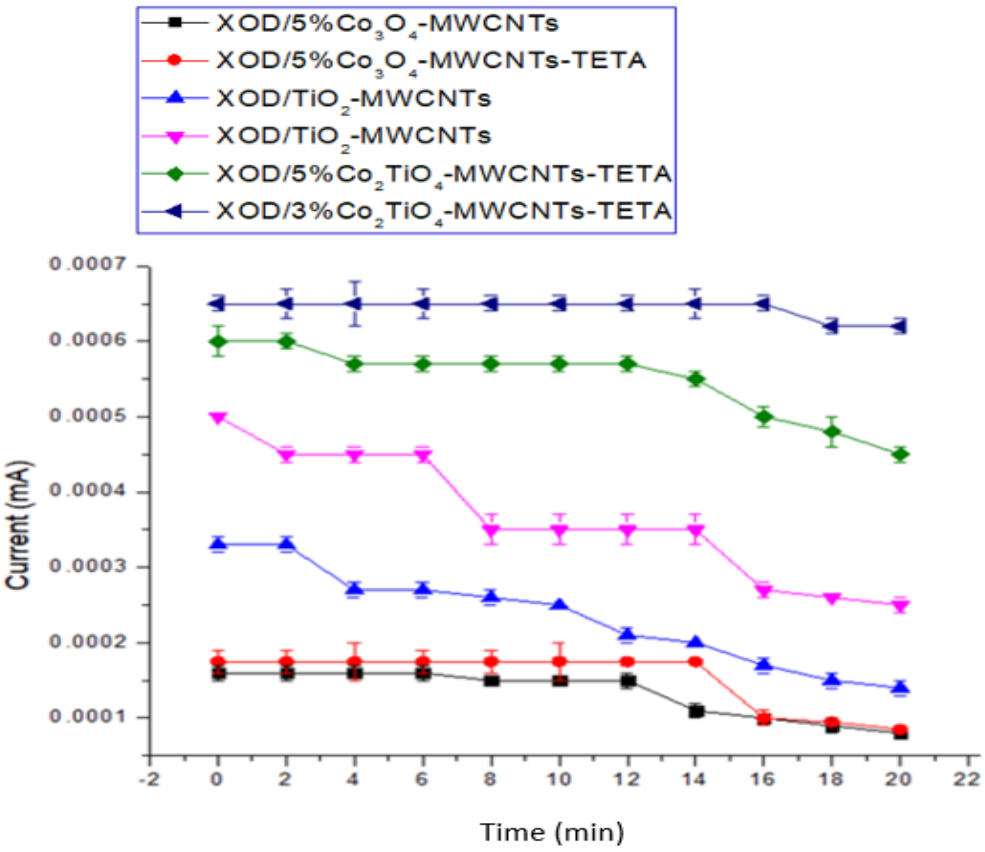


Appendix 11: Presents operational stability of modified electrodes using cyclic voltammetry with repetitive cycles at 2 minutes interval in 0.1 mM hypoxanthine solution. All electrodes were modified with 0.5 U of xanthine oxidase (XOD).

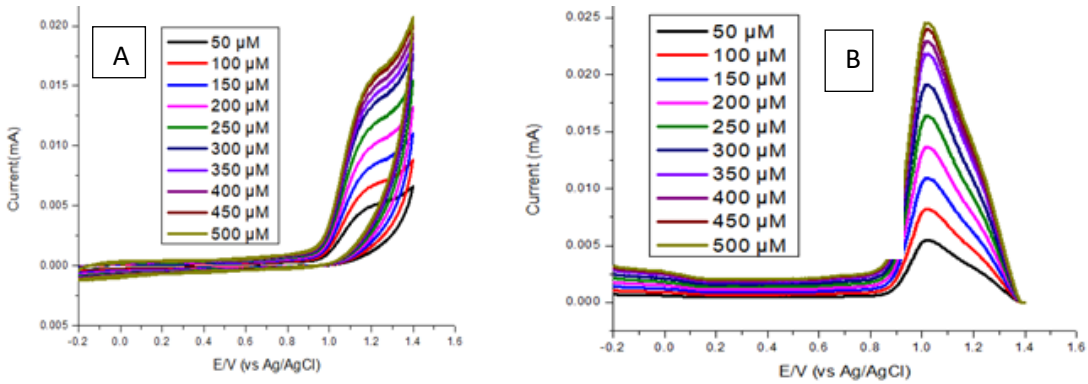


Appendix 12: cyclic Voltammograms (A), differential pulse voltammograms (B) at high concentrations level of hypoxanthine using XOD/3%$Co_2TiO_4$-MWCNTs-TETA/GCE.